Effect of Ternary Solutes on the Evolution of Structure and Gel Formation in Amphiphilic Copolymer Solutions

by

Norman Anthony Kang Meznarich

A dissertation submitted in partial fulfillment
of the requirements for the degree of
Doctor of Philosophy
(Materials Science and Engineering)
in The University of Michigan
2012

Doctoral Committee:

Professor Brian J. Love, Chair
Professor John W. Halloran
Professor Ronald G. Larson
Assistant Professor Anish Tuteja

Acknowledgements

I sincerely thank my advisor, Brian Love, for his mentorship and friendship throughout my graduate schooling. His guidance and support have been instrumental in my academic development.

I also thank the numerous mentors, teachers, colleagues, and friends with whom I have had the pleasure of interacting and working with throughout the efforts culminating in this dissertation. It is without doubt that their presence has made this endeavor a wholly enjoyable and unforgettable experience. I am honored by the opportunity to develop as a scientist and an engineer, and as others have helped me in the past, I will seek to repay the debt of gratitude to others as I move forward towards the future.

Lastly I thank my family for their support and encouragement as I have made my way along this academic journey. The road has been long and arguably the true voyage is only just beginning, and I am truly glad to be able to share it with them.

Table of Contents

Acknowledgements ii
List of Figures iv
List of Tables x
Abstract xi
Chapter 1 Background and Motivation 1
1.1 Overview of Pluronic surfactants 1
1.2 Micellization and gelation of Pluronic surfactants 4
1.3 Applications of Pluronic gel systems 9
1.4 Motivation 10
Chapter 2 Rheometric Characterization of F127 Gelation 15
2.1 Introduction 15
2.2 Materials and methods 16
2.3 Results 22
2.4 Discussion 28
2.5 Chapter summary 31
Chapter 3 Structural Study of F127 Gel Formation 33
3.1 Introduction 33
3.2 Materials and methods 34
3.3 Results 43
3.4 Discussion 58
3.5 Chapter summary 68
Chapter 4 Thermophysical Properties of Pluronic Micellization 70
4.1 Introduction 70
4.2 Materials and methods 71
4.3 Results 75
4.4 Discussion 87
4.5 Chapter Summary 93
Chapter 5 Summary and Future Work 94
5.1 Summary 94
5.2 Future work 99
References 101

List of Figures

Figure 1.1 Pluronic grid. The first letter of each Pluronic surfactant, as well as the colors, indicate the phase of the pure surfactant at room temperature. Surfactants are liquids (L) in the blue region, pastes (P) in the green region, and solids (F) in the pink region. 3

Figure 1.2 Synthesis of Pluronic surfactants. The subscripts a and b in the reaction schematic represent variable repeat lengths of the monomeric blocks, which vary in length for different formulations of Pluronic surfactants. Figure reproduced from[1] .. 4

Figure 1.3 Temperature-dependent micellization and gelation of Pluronic surfactants 5

Figure 1.4 Phase diagrams of the four Pluronic surfactants. Clockwise from upper left the phase diagrams are for Pluronic L121, L122, F127, and P123. Increasing temperature is depicted on the *y*-axis and increasing concentration is depicted on the *x*-axis. Figure reproduced from[8]. 7

Figure 1.5 Pluronic surfactant gel formation. The bolded boxes and percentages indicate the minimum concentration required to form gels. F127 has the best gel-forming abilities of all the available Pluronic surfactants. Figure reproduced from Schmolka[1]. 8

Figure 1.6 Chemical structures of the additives used in this study. Molecular weights are as follows: methylparaben = 152 g/mol, dexamethasone = 392 g/mol, cisplatin = 301 g/mol, magnesium citrate = 214 g/mol. 12

Figure 2.1 Rheometer setup. A humidity cover (not shown) was used during the experimental runs in order to minimize sample evaporation. 17

Figure 2.2 Power law analysis of rheometry data. The linearly increasing viscosity values (white circles) are fitted with a linear trendline, which is extrapolated backwards to where it intercepts the initial viscosity value as measured using a frequency sweep. This intersection (arrow) indicates the time at which the gelation

bas begun. For clarity, the pre-gelation data has been excluded (as was done for the analysis). Figure reproduced from [55]. 20
Figure 2.3 Boltzmann sigmoid curve showing relevant fitting parameters. 21
Figure 2.4 Viscosity vs. Temperature for a 20% F127 solution heated at different rates. Heating rate influences gelation time. For clarity, the number of data points shown has been reduced. Figure reproduced from[55]. 22
Figure 2.5 Viscosity vs. time for 20% F127 at three heating rates. The black line shows the corresponding log-Boltzmann sigmoid fit applied to the data. For clarity, the number of data points was reduced for the 1°C/min and 10°C/min heating rates. Figure reproduced from[55]. 24
Figure 2.6 Difference in T_{gel} as a result of added methylparaben for 15-30% F127. Figure reproduced from[55]. Absolute values of T_{gel} are listed in Table 2.1. 27
Figure 2.7 Comparison of the characteristic gelation time Δt as a function of F127 concentration under a heating rate of 0.1°C/min. Figure reproduced from[55]. 28
Figure 3.1 Typical transmission SAXS configuration. Focused x-ray beam originates from the left of the image, passes through the sample, and proceed on to the detector (off-screen on the right). Tubes of cooled nitrogen gas (white tubes) enter the sample stage, which also contains a heating element. This image was taken at the Advanced Photon Source 5-ID beamline. 36
Figure 3.2 Static vs. dynamic SAXS tests. The top plot shows the stepwise temperature increases used in the static temperature experiments. The bottom plot shows the continuously changing temperature in the dynamic experiments. The width of the capture events illustrates that the capture times used in the static experiments were much longer than those used for the dynamic experiments, necessitating the constant temperature. 40
Figure 3.3 Intensity vs. *q* plots for 20-30% F127 solutions. Figure adapted from[66]. 46
Figure 3.4 Intensity vs. *q* plots for 20-30% F127 solutions containing MP (1% wt/v). Figure adapted from[66]. 47
Figure 3.5 Intensity vs. *q* plots for 20-30% F127 solutions containing DX (1% wt/v). Figure adapted from[66]. 48

Figure 3.6 Transition from an fcc structure to a bcc structure at high temperatures for a 30% F127 solution. The lines from bottom to top show the sample at 80°C, at 80°C after additional incubation, and finally an increase to 90°C. Arrows indicate the (200), (220), and (310) peaks of the bcc phase. The two large peaks flanking 0.7 nm^{-1} in the 80°C lines are the (220) and (311) peaks of the fcc structure. Figure adapted from[66]. 50
Figure 3.7 Dynamic temperature test of 30PL (a) and 30MP (b) samples heated at a rate of 1°C/min through their gel transition temperatures: 15-35°C for 30PL and 10-30°C for 30MP, respectively. The appearance of the ordered phase is more abrupt in 30PL vs. 30MP. Figure reproduced from[66]. 51
Figure 3.8 2D scattering patterns of 30PL (a, b) and 30MP (c, d) samples at both 30 and 60°C. Diffraction spots that appear (a) do not move as the temperature is further increased (circled examples); however new spots appear as additional crystalline domains are nucleated. Figure reproduced from[66].....52
Figure 3.9 Hydrodynamic radius (R_h) as a function of scattering angle. The filled circles indicate neat 1% F127 solutions and the open circles indicate 1% F127 solutions with 0.1% added MP. Figure reproduced from[55].....53
Figure 3.10 Normalized probability intensity as a function of R_h reported for two representative 1% F127 samples, one containing MP (open circles) and one without (filled circles). The sample containing MP has a decreased polydispersity. Figure reproduced from[55].....54
Figure 3.11 Intensity vs. *q* plots for 20-30% F127 solutions containing magnesium citrate (1% wt/v). 56
Figure 3.12 Intensity vs. *q* plots for 25-30% F127 solutions containing cisplatin (1% wt/v).....57
Figure 3.13 Intensity vs. *q* plot for a 30% F127 solution containing propylparaben (1% wt/v). Control solution of 30% F127 is shown in (b).....58
Figure 4.1 Pluronic grid showing commercially available varieties of Pluronic surfactants. Circled items indicate surfactants used in this study.....72
Figure 4.2 Representative DSC micellization endotherm. The labels depict the values measured from each thermogram. The onset temperature is the intersection of the

baseline and the maximum slope of the initial portion of the peak. The peak temperature is the maximum deflection from the baseline, and the enthalpy is the total area between the curve and the baseline (shaded). 75
Figure 4.3 DSC thermograms for F127 concentrations ranging from 10 to 50 wt%, in increments of 10%. The numbers 1-5 indicate the curves associated with 10, 20, 30, 40, and 50% F127, respectively. The three circles indicate small secondary endothermic peaks visible for 30, 40 and 50% F127, this is associated with F127 gelation, where the micelles have arranged into crystalline lattices. 76
Figure 4.4 10% wt/v Pluronic surfactant series comparing increasing PEO content while keeping PPO block length constant. From numbers 1-3 the surfactants used are L121, P123 and F127, respectively. The curves have been aligned so the initial baseline is consistent for all samples. 78
Figure 4.5 10% wt/v Pluronic surfactant series comparing increasing PEO content while keeping PPO block length constant. From numbers 1-4 the surfactants used are L101, P104, P105 and F108, respectively. The curves have been aligned so the initial baseline is consistent for all samples. 78
Figure 4.6 10% wt/v Pluronic Surfactant series comparing increasing PEO content while keeping PPO block length constant. From numbers 1-3 the surfactants used are L121, L101, and L61, respectively. (*) It is not entirely clear if surfactant 3 has a resolvable peak. The curves have been aligned so the initial baseline is consistent for all samples. 79
Figure 4.7 10% wt/v Pluronic surfactant series comparing increasing PPO central block length, while keeping a proportionally constant amount of PEO. From numbers 1-4 the surfactants used are P105, P85, P65 and L35, respectively. The curves have been aligned so the initial baseline is consistent for all samples. 79
Figure 4.8 10% wt/v Pluronic surfactant series comparing increasing PPO central block length, while keeping a proportionally constant amount of PEO. From numbers 1-4 the surfactants used are F127, F108, F68 and F38, respectively. The curves have been aligned so the initial baseline is consistent for all samples. 80
Figure 4.9 10% wt/v Pluronic surfactant series comparing constant molecular weight, while varying the PEO/PPO ratio. From numbers 1-3 the surfactants used are L121,

P85 and F38, respectively. The curves have been aligned so the initial baseline is consistent for all samples.....80
Figure 4.10 10% F127 with progressively increasing amounts (from 0 to 1%) of added MP. The arrow indicates the direction of increasing MP concentration. Each overlaid curve has an additional 0.1% MP added. As increasing amounts of MP are added to the solution, the micellization endotherm is progressively suppressed, and the peak shifts slightly lower in temperature. The curves have been aligned so the initial baseline is consistent for all samples.....82
Figure 4.11 Onset temperature, peak temperature, and enthalpy measured for a series of 10% F127 solutions containing increasing amounts of MP. 82
Figure 4.12 10% F127 with progressively increasing amounts (from 0 to 1%) of added PP. The arrow indicates the direction of increasing PP. Each overlaid curve has an additional 0.2% PP added. As increasing amounts of PP are added, the micellization endotherm is again similarly suppressed, as was the case for added MP. The curves have been aligned so the initial baseline is consistent for all samples. 83
Figure 4.13 10% wt/v Pluronic F68 with progressively increasing amounts (from 0 to 1%) of added MP. The arrow indicates the direction of increasing MP. Each overlaid curve has an additional 0.5% MP added. As increasing amounts of MP are added, the micellization endotherm is suppressed, as was the case for F127. It should be noted, however, that for the 1% added MP curve, the solution was already saturated with MP and thus the actual concentration was somewhere between 0.5% and 1% MP. The curves have been aligned so the initial baseline is consistent for all samples. 85
Figure 4.14 10% wt/v Pluronic F108 with progressively increasing amounts (from 0 to 1%) of added MP. The arrow indicates the direction of increasing MP. Each overlaid curve has an additional 0.5% MP added. As increasing amounts of MP are added, the micellization endotherm is suppressed, as was the case for F127. The curves have been aligned so the initial baseline is consistent for all samples.....85
Figure 4.15 10% wt/v Pluronic P123 with progressively increasing amounts (from 0 to 1%) of added MP. The arrow indicates the direction of increasing MP. Each overlaid curve has an additional 0.5% MP added. As increasing amounts of MP are

added, the micellization endotherm is suppressed, as was the case for F127. The curves have been aligned so the initial baseline is consistent for all samples. 86
Figure 4.16 Onset and peak temperatures for Pluronic F127, P123, and F68 with increasing amounts of added methylparaben. The F68 solution was already saturated prior to 1% added MP. 86
Figure 4.17 Enthalpy of micellization for Pluronic F127, P123, and F68 with increasing amounts of added methylparaben. The F68 solution was already saturated prior to 1% added MP. 87

List of Tables

Table 2.1 Gel temperature as determined by power law analysis. The asterisk indicates data collected using a smaller gap dimension of approximately 0.6 mm since the tests run at larger gap dimensions resulted in a lack of identifiable gelation. Table reproduced from[55]. 23

Table 2.2 Log-Boltzmann analysis used to determine gel time. Values with asterisks indicate data collected using a smaller gap dimension of approximately 0.6mm. Table reproduced from[55] 25

Table 3.1 Summary of expected peaks and relative peak positions for the fcc and bcc crystal structures. Bolded entries are planes with identical ratios in both crystal structures. 42

Table 3.2 Identified peak positions (in units of nm^{-1}) and identified phase at 40°C. (*) Indicates that no peak was found at this temperature but visible at higher temperatures. Table reproduced from[66]. 49

Table 3.3 Identified peak positions (in units of nm^{-1}) and identified phase at 70°C. Superscripts indicate [1]fcc peaks and [2]bcc peaks, based on their position relative to the fundamental peak. Table reproduced from[66]. 49

Table 3.4 Peak positions and calculated ratios for selected datasets at 70°C from the 12-BM beamline. [1]Indicates a possible gyroid phase in the 30PL sample. [2]Possible gyroid phase or bcc (211) peak based on the bcc peak positions listed in Table 3.1. 55

Table 4.1 List of Pluronic surfactants used. Nominal chemical formulae for each are $(PEO)_x(PPO)_y(PEO)_x$. Data compiled from[12,86-91]. 73

Abstract

Aqueous solutions of polyoxyethylene-polyoxypropylene-polyoxyethylene (PEO-PPO-PEO) amphiphilic triblock copolymers (commercially known as Pluronic surfactants) undergo reversible and temperature-dependent micellization and arrangement into cubic ordered lattices known as “micelle gels”. The macroscopic behavior of the ordering is a transition from a liquid to a gel. While the phase behavior and gel structure of pure Pluronic surfactant solutions have been well studied, less is known about the effects of added ternary solutes. In this dissertation, a comprehensive investigation into the effects of the added pharmaceutical methylparaben on solutions of F127 ranging from 10 to 30 wt% was conducted in order to better understand the behavior of F127 in multicomponent pharmaceutical formulations. The viscoelastic properties of F127 gel formation were studied using rheometry, where heating rates of 0.1, 1, and 10 degrees C/min were also used to probe the kinetics of the gel transition. In solutions containing methylparaben, F127 gelation occurred at up to 15 degrees C lower temperatures and was accelerated by a factor of three to four. Small angle x-ray scattering (SAXS) was used to characterize the structure of the ordered domains, and how they were affected by the presence of dissolved pharmaceuticals. It was found that ordered domain formation changed from heterogeneous nucleation and growth to possible homogeneous nucleation and growth. A roughly 2% reduction in the cubic lattice parameter was also observed for solutions containing methylparaben. Differential scanning calorimetry (DSC) experiments were performed on a series of different Pluronic surfactants in order to

characterize the micellization behavior as a function of PPO center block length and PEO/PPO ratio. Added methylparaben suppressed the micellization endotherm, the degree of suppression depending linearly on the amount of added methylparaben, as well as the length of the PPO center block and PEO/PPO ratio. This dissertation yielded a thorough characterization of the changes in micellization and gelation behavior in F127 gels as a result of added pharmaceuticals. Previously unobserved behavior such as the onset of ordered domain formation in F127 gels was observed, and a greater understanding of the interactions between amphiphilic copolymer solutions and dissolved solutes was achieved.

Chapter 1

Background and Motivation

1.1 Overview of Pluronic surfactants

Polyethylene oxide-polypropylene oxide-polyethylene oxide (PEO-PPO-PEO) triblock copolymers are a subset of amphiphilic block polymers known commercially as Pluronic surfactants. A variety of Pluronic surfactants are readily available, with differing block and arm lengths. These can be arranged on what is known as the Pluronic grid (Figure 1.1). On the lateral axis, moving further to the right indicates an increasing weight percentage of the hydrophilic arms (PEO). Moving up on the vertical axis indicates increasing length of the hydrophobic center block (PPO). Each surfactant is indicated by a formula code, which comprises of three segments. The leading character indicates the physical form of the Pluronic surfactant at room temperature: L for liquids, P for pastes, and F for flakes (solids). The second character (or central two characters, in the case that the code is four characters long) indicates the length PPO block. Multiplying this number by 300 gives the approximate molecular weight of the PPO center block. The final digit indicates the mass fraction (as 1/10 the weight percentage) of the molecule that is comprised of PEO. For example, the Pluronic surfactant with code F108 is a flaked solid ("F") at room temperature with a PPO mass of approximately 3000 g/mol ("10" times 300), and is 80% by weight PEO ("8" times 10). The total

molecular weight of F108 would thus be approximately 15,000 g/mol. The nominal chemical formula for F108 is $PEO_{132}PPO_{50}PEO_{132}$.

Synthesis of Pluronic block copolymers, described by Schmolka[1], is achieved using a propylene glycol initiator which is lengthened by sequential addition of propylene oxide monomer units. This reaction is catalyzed by a basic catalyst and run under elevated temperature and pressure, until the desired molecular weight is achieved. Following this, ethylene oxide is sequentially added to both ends of the PPO center block until the desired mass ratio is achieved. Figure 1.2 illustrates the synthesis reaction. Commercial preparations of Pluronic surfactants often contain impurities of the PPO homopolymer, and di- and triblock copolymers with different molecular weights and PEO/PPO mass ratio than the desired product[2,3]. These impurities can be removed using gel permeation chromatography (GPC) to selectively filter for polymer chains of the right molecular weight [2,4].

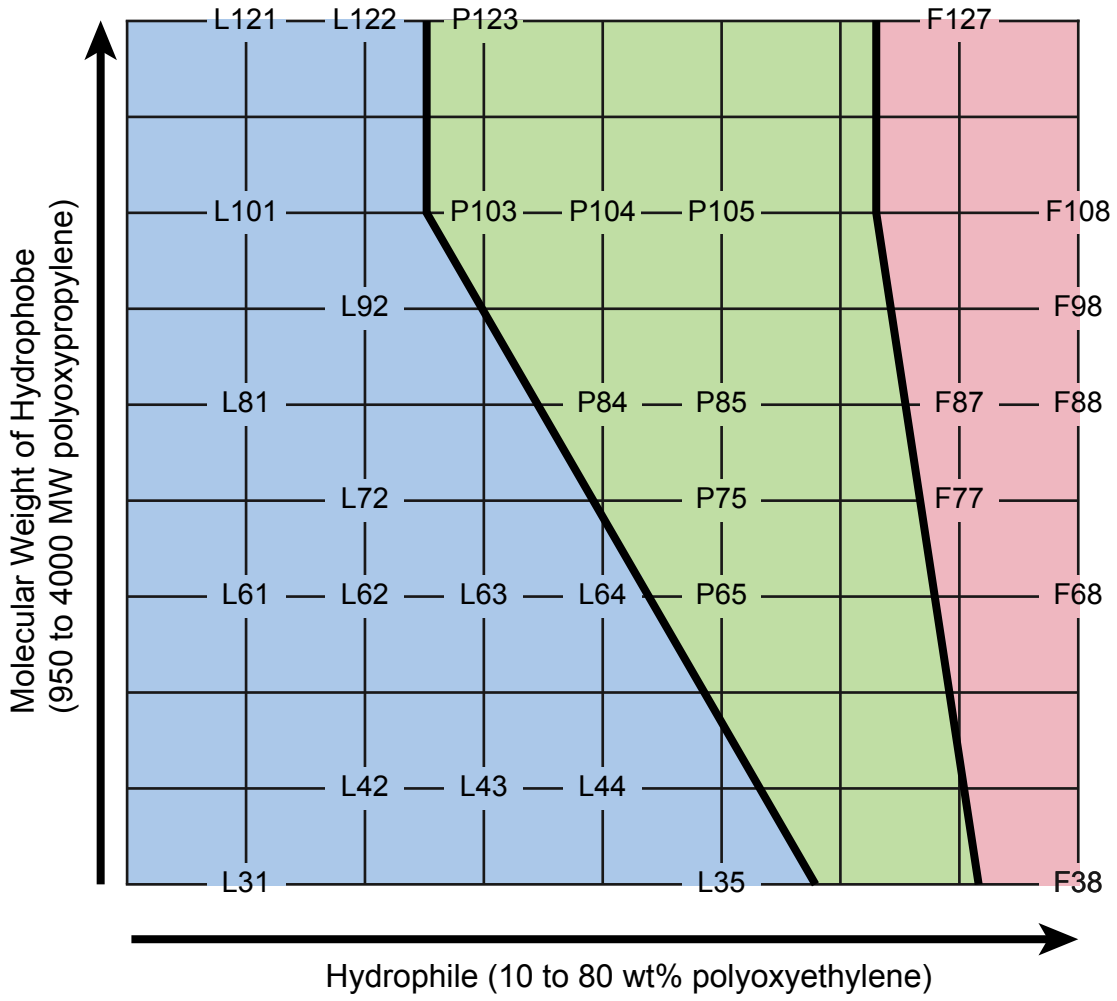

Figure 1.1 Pluronic grid. The first letter of each Pluronic surfactant, as well as the colors, indicate the phase of the pure surfactant at room temperature. Surfactants are liquids (L) in the blue region, pastes (P) in the green region, and solids (F) in the pink region.

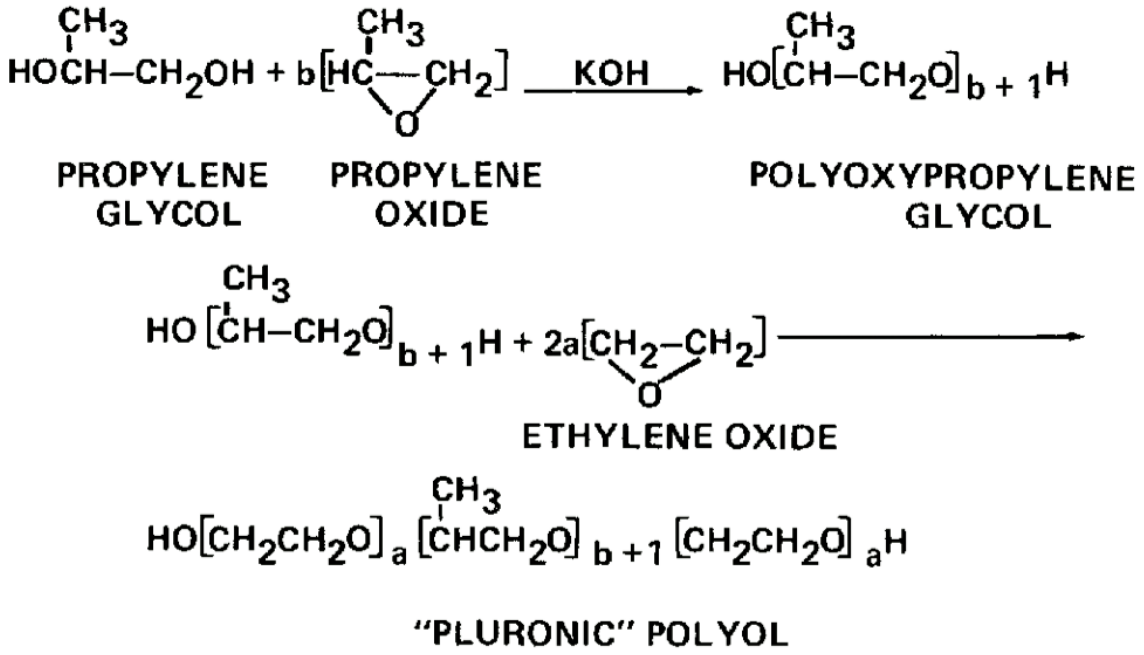

Figure 1.2 Synthesis of Pluronic surfactants. The subscripts a and b in the reaction schematic represent variable repeat lengths of the monomeric blocks, which vary in length for different formulations of Pluronic surfactants. Figure reproduced from[1].

1.2 Micellization and gelation of Pluronic surfactants

Dispersed solutions of Pluronic surfactants, like many amphiphiles, will undergo self-assembly, known as micellization. Micellization can be achieved by varying concentration at a given temperature (the critical value of which is defined as the critical micelle concentration or *cmc*) or by varying temperature for a given concentration (the critical temperature being defined as the critical micelle temperature or *cmt*). A schematic of this process is illustrated in Figure 1.3. As the solution crosses the *cmt*, micelles will form and an equilibrium balance of micelles and dispersed polymer chains will be established[5,6]. The driving force for micellization is entropic in nature, owing to the hydrophobic effect[7], where hydrophobic molecules associate with one another in

order to dissipate the "water cages" of ordered water molecules that form around each hydrophobic molecule. Studies have shown that micelle formation in most Pluronic surfactants results in spherical micelles[8,9], however, wormlike micelles have been observed to exist[10,11].

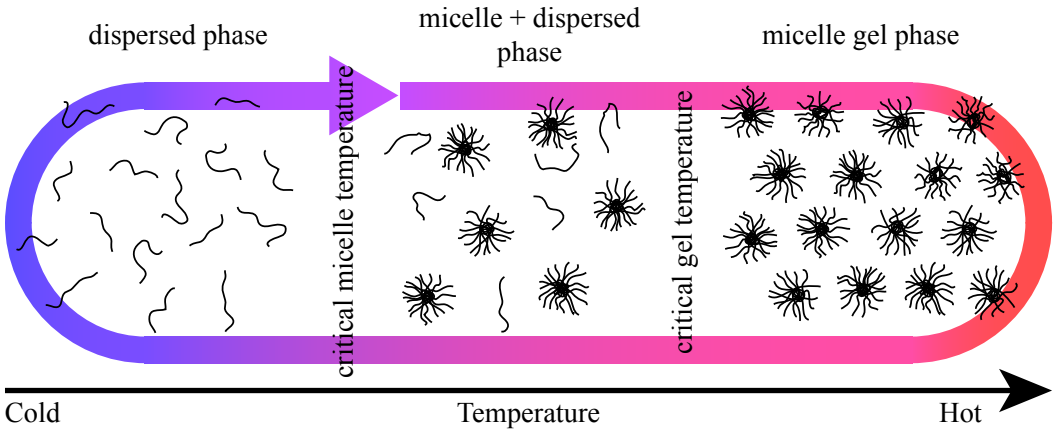

Figure 1.3 Temperature-dependent micellization and gelation of Pluronic surfactants

Gel formation in solutions of Pluronic surfactants is driven by an increase in the size (aggregation number) of Pluronic micelles, and their subsequent ordering into liquid crystalline lattices[8,12,13]. The arrangement into crystalline lattices is the result of two factors: an increasing volume fraction occupied by micelles and the repulsive force between micelles. As the volume fraction of micelles increases (which occurs via both new micelle formation and Ostwald ripening from neighboring micelles[14]), and increasing repulsive interactions between nearby micelles occurs, the micelles form ordered phases in order to maximize their distance from one another, much like atoms in a crystalline lattice.

The majority of the ordered phases consist of cubic packing arrangements of spherical micelles, however, at very high Pluronic concentrations (in the vicinity of pure polymer), lamellar phases were commonly identified. Additionally, Pluronic surfactants with a low PEO content by weight (<15%) also formed lamellar phases. As the weight percent of PEO in the molecular formula increases (~25%), hexagonal ordered phases are formed. Finally, for most Pluronics with higher PEO content (>25%), cubic phases are observed[8]. Scattering studies on these ordered phases typically demonstrate scattering rings, indicating that many randomly oriented ordered domains exist in the solution[9,15,16]. The application of shear, however, leads to substantially enhanced ordering of the micelles, and single-crystal like scattering behavior has been observed[17-19].

The micellization and gelation behavior of Pluronic surfactants have been studied extensively[5,12,13,20-22]. The phase behavior for many Pluronic surfactants have been probed[8,16]. Different Pluronic surfactants have been shown to exhibit varying phase behavior, some displaying complex phase characteristics, while others having relatively simple behavior. Figure 1.4 shows the phase diagrams for four different Pluronic surfactants, each with increasing PEO content. The phase behavior for F127 only has three major phase regions with a thin two-phase region at the interface between the isotropic phase and the cubic phase (the aforementioned equilibrium regime where micelles and dispersed unimers exist), whereas P123 has a more complicated phase diagram, including an order-to-order transition between the cubic and hexagonal phases and an extended multiphase region.

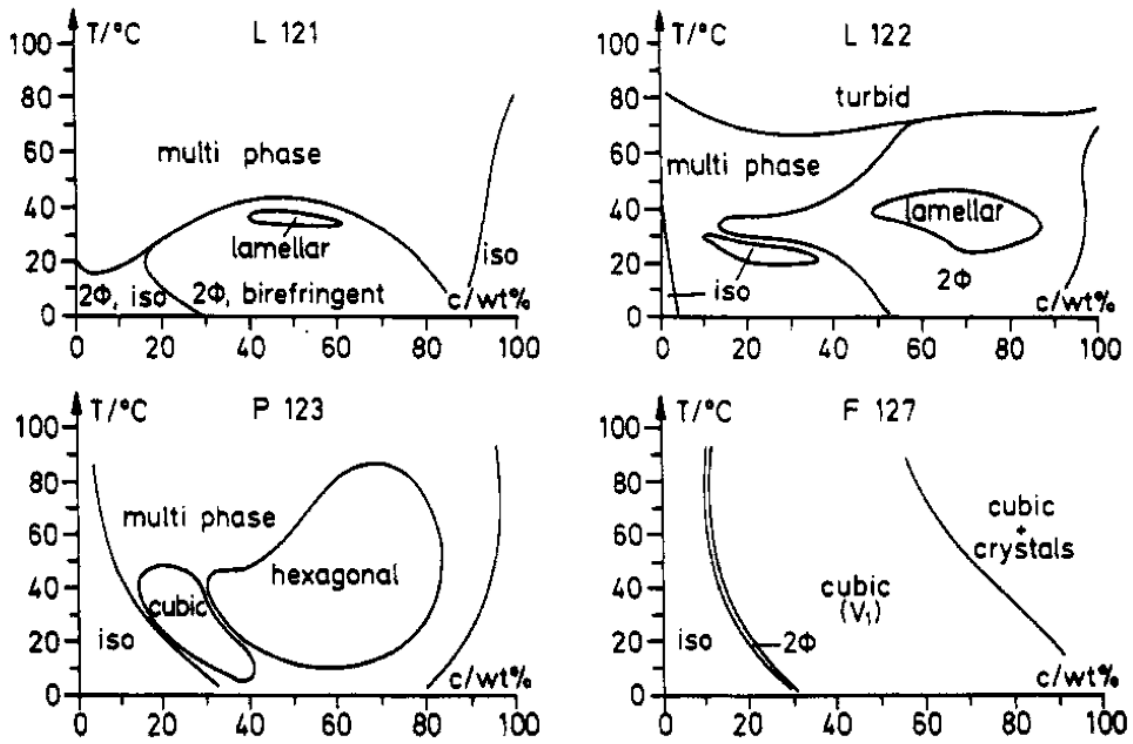

Figure 1.4 Phase diagrams of the four Pluronic surfactants. Clockwise from upper left the phase diagrams are for Pluronic L121, L122, F127, and P123. Increasing temperature is depicted on the *y*-axis and increasing concentration is depicted on the *x*-axis. Figure reproduced from[8].

Pluronic "micelle gels" differ from most conventional polymer hydrogels. Conventional gel formation is typically achieved via covalent bond formation between adjacent polymer chains (crosslinking), or physical entanglement of multiple chains, resulting in a mechanically robust tangled network[23]. In a micelle gel, the lattice ordering of individual micelles offers mechanical stability[24]. Because there is no covalent bond formation in micelle gels, and the micellization behavior of Pluronic surfactants is driven by temperature (for a fixed concentration solution), the gelation process is reversible.

Not all Pluronic surfactants are capable of producing gels, however. Figure 1.5 illustrates the relative gel forming abilities of the Pluronic surfactants and their relative positions on the Pluronic grid[1]. Pluronic F127 is the best for gel formation, with

concentrations of around 20% being sufficient for gel formation, whereas other Pluronic surfactants require substantially higher concentration solutions, and about half of the available surfactants are not able to form a gel no matter the concentration used.

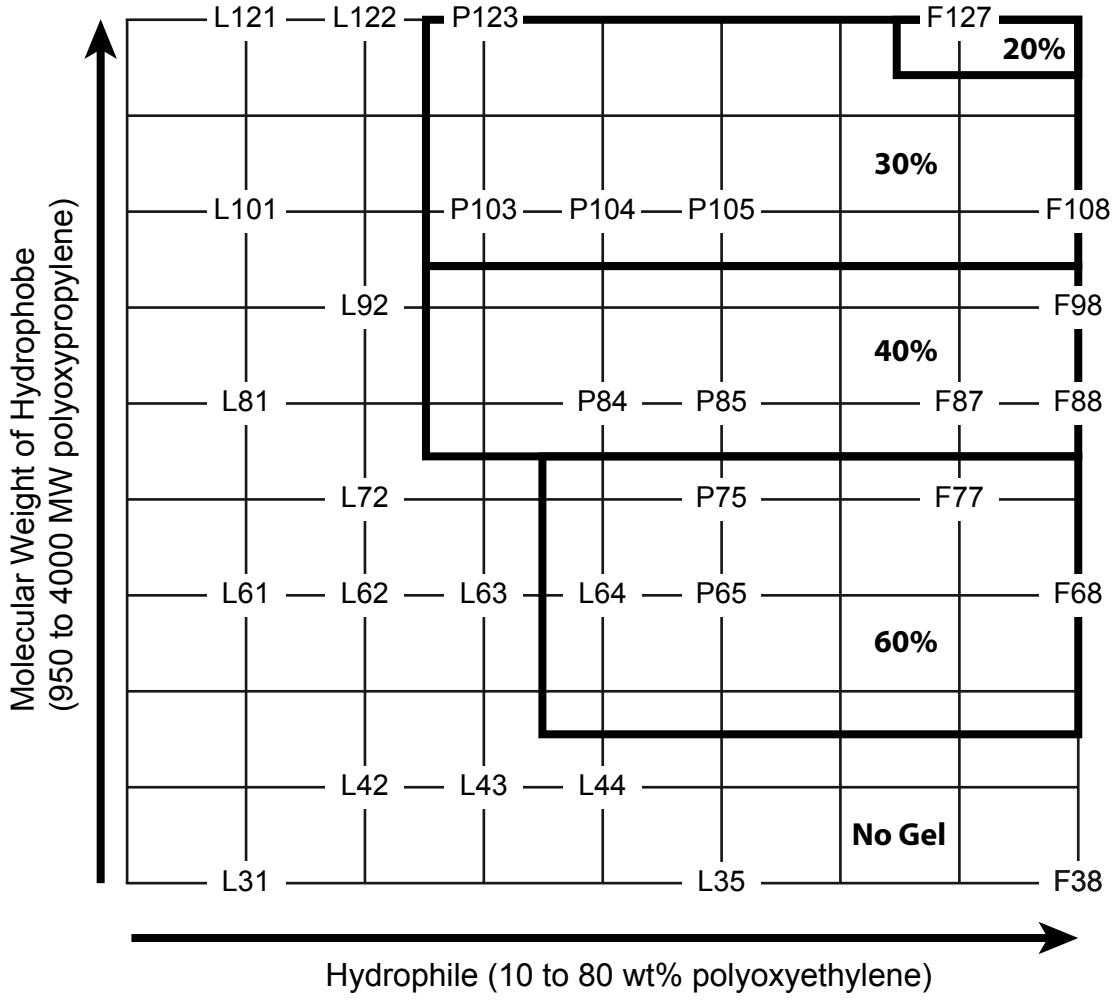

Figure 1.5 Pluronic surfactant gel formation. The bolded boxes and percentages indicate the minimum concentration required to form gels. F127 has the best gel-forming abilities of all the available Pluronic surfactants. Figure reproduced from Schmolka[1].

1.3 Applications of Pluronic gel systems

Pluronic surfactants have found multiple industrial applications, performing in roles as detergents, stabilizers, emulsifiers, lubricators, etc[12,25]. Several attributes of the Pluronic gels also make them particularly attractive for use in biomedical applications. The high biocompatibility of Pluronic surfactants also makes them safe for direct interaction with host tissues with minimum concern for cytotoxicity[1]. The reverse thermal gelation properties makes Pluronic gels particularly suited for in-vivo delivery of pharmaceutical or therapeutic agents. Pluronic gels combine the convenient delivery mechanism of a solution-based formulation with the enhanced release characteristics or enhanced mechanical properties of a gel-based formulation. Compared to more conventional gels, which are liquid at high temperatures and solids or gels at low temperatures, Pluronic gels can be delivered as a cool liquid and will form a gel upon warming to body temperature. This delivery strategy is more favorable than delivering a heated fluid (which would gel upon cooling to body temperature), as contact with heated fluids may be damaging to surrounding tissues or skin, and may cause discomfort to patients. Additionally, the elevated temperatures required to maintain solutions in the melted state may also be damaging to physiologically sensitive therapeutics such as enzymes or proteins, which may become denatured by the heat.

1.3.a. Clinical applications of Pluronic hydrogels

There has been a substantial amount of prior research studying the potential for Pluronic hydrogels in clinical applications. Multiple delivery strategies have been utilized: transdermal or percutaneous delivery[26-28], oral or buccal delivery[29,30], ophthalmic delivery[31], rectal delivery[32], intraperitoneal injections[33] etc. There is also evidence that

formulations of F127 can facilitate transport of molecules across bilipid membranes[34], including having potential as a gene delivery agent[3,35]. Other applications for F127 use have also included topical applications such as wound and burn healing[36,37], or using F127 as a temporary embolic material[38].

Kabanov *et al.*[39] prepared a review article detailing the use of F127 formulations in antitumor therapy where it was found that F127 delivery of anticancer therapeutics played a role in sensitizing tumors to the treatment, thereby increasing their efficacy. Escobar-Chavez *et al.*[40] also conducted a comprehensive review, compiling recent efforts on the application of F127 gels in pharmaceutical formulations.

1.4 Motivation

As described previously in this chapter, the thermodynamics of micelle and gel formation is relatively well known for a variety of Pluronic surfactants. Kinetic or transient effects, however, have been given somewhat less attention. Given the large potential to encounter non-equilibrium transition conditions in real-world applications, this gap in the literature represents a key area in which more work needs to be done. If there are significant transient factors in the formation or properties of Pluronic gels, these factors need to be studied and accounted for in order to achieve maximum optimization of Pluronic formulations for a given application.

Relating to the addition of ternary components into these systems, there have been some studies that endeavor to determine changes in the gel behavior, however the solutes studied typically are of a general nature (salts, hydrocarbon chains, etc.) and rarely feature additives that would be of use in direct application. Early work by Vadnere, *et*

al.[7] showed that the presence of solutes could raise or lower the *cmt* of Pluronic solutions. Nagarajan[41,42] conducted studies the solubilization of hydrocarbon chains into Pluronic surfactants.

Regarding the significant body of work that already exists studying the use of F127 or other Pluronic surfactants as a delivery vehicle for therapeutics or pharmaceuticals, the majority of these studies focus on the efficacy and application of F127 formulations in pharmaceutical or therapeutic applications. Relatively little is known about how the presence of such additives affects the gel properties of Pluronic surfactants, or the mechanisms by which enhanced release or delivery profiles is achieved. Bentley *et al.*[43] conducted rheological studies on formulations of Pluronic F127 (also referred to in the literature as Poloxamer 407) with added lecithin. They measured an increase in the mechanical properties of F127 gels as a result of the added phospholipid. Ricci *et al*.[44] also conducted a rheological study of F127 hydrogels containing the pharmaceutical lidocaine hydrochloride. It was found that the addition of lidocaine decreased the viscosity of the hydrogels. Sharma *et al*.[45] surveyed the effects of added anti-inflammatory drugs on the thermoreversible gelation of F127 solutions and conducted some studies on the changes in the micelle properties and structures[46,47] as well. They found that the critical gel temperature was significantly lowered for solutions containing pharmaceutical additives. However, efforts such as these are relatively rare in the literature.

The aim of this dissertation work was to provide a more comprehensive study of the effects, both microscopic and macroscopic, on the gel formation and properties of Pluronic F127 gels. F127 will be used in particular, because it is the Pluronic surfactant

with the greatest gel-forming abilities. This will make it easiest to identify differences in gel behavior, since the range of available concentrations at which F127 solutions gel is greater than that of all the other available Pluronic surfactants.

The effects of ternary additives, specifically focusing on pharmaceuticals, will be studied given the preponderance of prior literature on utilizing F127 as a delivery agent for therapeutics. For this work, the primary pharmaceutical tested was methyl *p*-hydroxybenzoate (methylparaben or MP). Methylparaben is a small, mostly hydrophobic molecule that has antifungal and antibacterial properties[48]. The chemical structure of methylparaben is shown in Figure 1.6.

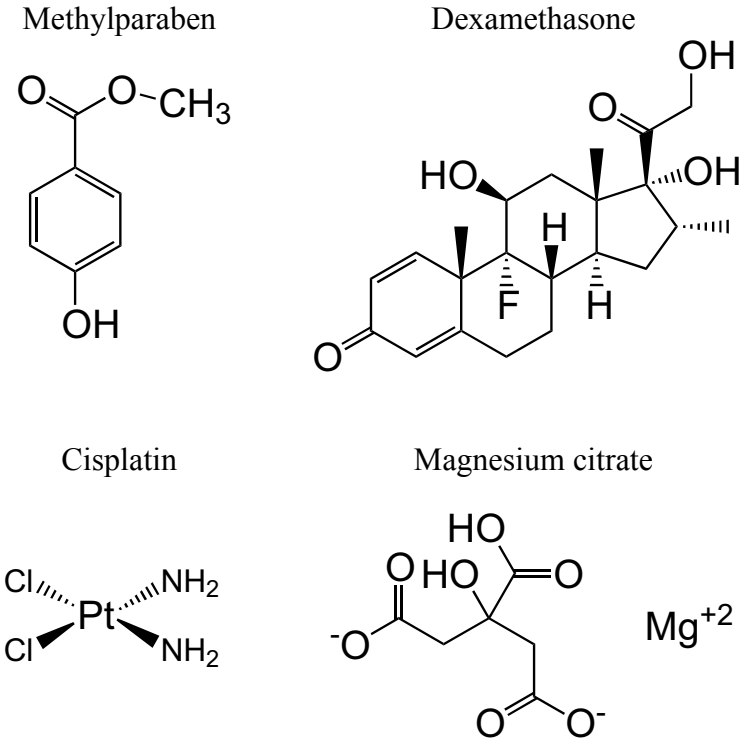

Figure 1.6 Chemical structures of the additives used in this study. Molecular weights are as follows: methylparaben = 152 g/mol, dexamethasone = 392 g/mol, cisplatin = 301 g/mol, magnesium citrate = 214 g/mol.

As many of the candidate pharmaceuticals exhibit hydrophobic characteristics, the selection of MP is an appropriate choice for use as a model. Additionally, its low cost and ready availability also contributed to its selection. Some prior literature also exists that involved studying the properties of F127 gels with added methylparaben [45-47] so that results could be compared to the existing literature.

In addition to the main focus on methylparaben, three additional additives were used in preliminary experiments designed to expand the range of tested solutes. These additives are dexamethasone, a common anti-inflammatory and immunosuppressant drug, and the chemotherapy agent *cis*-diamminedichloroplatinum(II) (cisplatin), a chemotherapy agent. Magnesium citrate was also tested in order to study the effects of added pharmaceuticals that were more hydrophilic in nature. The structures and molecular weights of these molecules are also listed in Figure 1.6.

Three main methods were used to complete this study: rheology, small angle x-ray scattering (SAXS), and differential scanning calorimetry (DSC). Rheology was used to study the macroscopic properties of the gel, the critical gel temperature (T_{gel}) and the viscoelastic properties. Structural studies on the micelle lattices were carried out using SAXS, and the energetics of micellization and gel formation were probed using DSC. Efforts were made to explore kinetic effects such as non-equilibrium heating rates, in order to determine if transient effects play a significant role in gel formation. By completing a thorough study of the effects of added MP on F127 gel formation, a more complete picture of the molecular interactions taking place will be developed, and this will hopefully ultimately lead to the development of more general understanding of ternary components and their interactions with amphiphilic copolymer micelles and gels.

Such knowledge would prove to be useful in the optimization of polymer formulations designed to be used in pharmaceutical or biomedical applications, and could possibly be extended to other disciplines as well.

Chapter 2

Rheometric Characterization of F127 Gelation

2.1 Introduction

Aqueous solutions of Pluronic F127 exhibit temperature-dependent micellization behavior, similar to that of other amphiphilic copolymer systems. High temperatures or high concentrations of these solutions are known to form hydrogels. The formation of these gels is attributed to the close packing and ordering of micelles. The quasiequilibrium phase boundaries of these systems have been studied extensively[6,8,13,49-51], but the kinetics of the gel formation are less well-known.

Additionally, the presence of dissolved solutes is known to affect the gel properties[10,15,52-54], but again, not much attention has been paid to the effects that these ternary additives have on the kinetics of the gel transition. This chapter covers a set of rheological experiments designed to study the effect of increasing heating rate on the gel formation of F127 solutions, as well as how the gelation behavior is affected by the presence of the added pharmaceutical methylparaben.

The experiments, results, and discussion covered in this chapter were submitted and published in the journal *Macromolecules*[55].

2.2 Materials and methods

2.2.a. Solution preparation

Pluronic F127 was obtained from Sigma-Aldrich (St. Louis, MO) and used as received. Solutions of Pluronic F127 were preparing according to the "cold method" method outlined by Schmolka[1]. Weighed amounts of F127 were added slowly to deionized water and stirred gently to avoid foaming. Once all the dry F127 was added, the solution was then kept at 4°C to dissolve quiescently. For the high concentration solutions (25% or greater), the solution was periodically stirred between cool incubations to facilitate dissolution of the F127 flakes.

Methylparaben (MP) was also obtained from Sigma-Aldrich and used as received. Solutions containing MP were prepared by first making a 10% F127 solution saturated with excess MP. Excess undissolved MP was removed by filtering the stock solution through a 0.45 μm vacuum filter. The final concentration of MP in this solution was approximately 2% wt/v. A saturated solution was used in order to maximize observable differences in rheological response owing to the presence of MP. After this saturated stock solution was made, aliquots were removed and weighed amounts of F127 were added to the aliquots until the desired final F127 concentration was achieved. This method of preparation, adopted from Sharma *et al*.[45] ensured that the amount of added MP was consistent for each concentration.

2.2.b. Rheometry

All rheometry experiments were conducted on a TA Instruments (New Castle, DE) ARES AR-2000 rheometer in dynamic oscillatory mode. A Peltier thermal stage accessory was attached to the rheometer motor in order to control the temperature and

heating rate of the solutions. Parallel plate geometry was used in each test, with the Peltier thermal stage serving as the lower surface, and a stainless steel upper tool (25mm diameter) for the upper surface. Figure 2.1 illustrates the experimental setup. For each experiment, approximately 0.5 mL of test solution was dispensed onto the thermal stage, and the upper tool lowered until contact between the solution and the upper surface was achieved. Following this, the upper tool was further lowered until the edges of the solution extended to the edge of the upper surface.

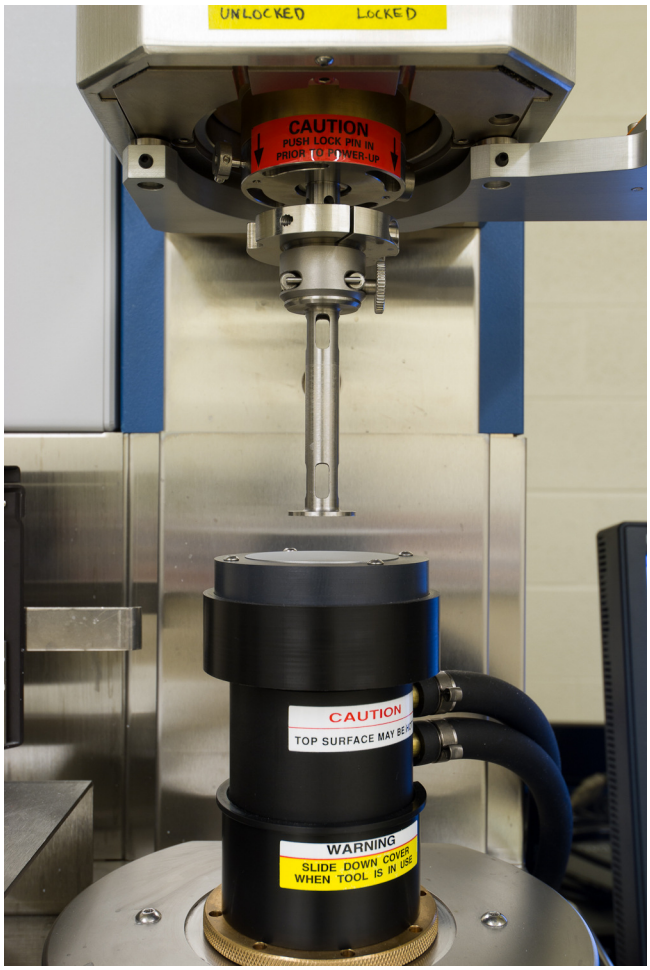

Figure 2.1 Rheometer setup. A humidity cover (not shown) was used during the experimental runs in order to minimize sample evaporation.

The resulting gap thickness was typically around 1 mm. To minimize the effects of sample evaporation, a humidity cover saturated with distilled water was put over the sample after loading.

The rheometer was operated in dynamic oscillatory mode with a frequency of 10 rad/s and an applied strain of 1%. Scout tests conducted using these parameters, as well as comparison to literature[6,51,56] ensured that these settings kept the solution in the linear viscoelastic range throughout the experiment. Data was collected at 0.1 Hz for the 0.1°C/min tests, and 1 Hz for the 1 and 10°C/min tests. Each experimental condition was repeated a minimum of three times, with the results being the average of the three repetitions.

Owing to the low viscosity of the solutions in the liquid phase at low temperatures, additional measurements were taken to provide a more reliable measure of the initial viscosity of the solutions prior to the gelation event. This was accomplished using a dynamic oscillatory frequency sweep performed at the starting temperature of the corresponding ramp test, covering a frequency range from 1 to 15 rad/s and an applied strain of 200%, with data points being recorded in 0.05 rad/s increments.

The temperature range used was typically between 15°C and 65°C. Higher concentrations of F127 were started at lower temperatures (as low as 5°C) in order to fully capture the liquid-to-gel transition, because the gel transition at the highest F127 concentrations occurs at or below 15°C. A total of three heating rates were tested: 0.1°C, 1°C, and 10°C/min. A typical thermal schedule was as follows: the solution was heated from the starting temperature at a steady heating rate to the final temperature, followed

by a 10-minute incubation at the final temperature to allow any temperature-lagging processes to complete.

For the 0.1°C/min tests, sample evaporation over the duration of the test made it impractical to conduct the entire heating ramp at 0.1°C/min, so an alternative schedule was utilized in which a 10°C range surrounding the gelation temperature was heated at 0.1°C/min; starting nominally 5°C below the transition temperature and ending nominally 5°C above the transition temperature. The rest of the heating ramp was conducted at 1°C/min. This reduced the total time for each 0.1°C/min experiment, so that sample evaporation would not negatively affect the high temperature results because the solution was heated so slowly.

2.2.c. Data analysis

Power law analysis was used to quantify the critical gel temperature, T_{gel}, by determining the point at which the complex viscosity η increased above the baseline level. In order to accomplish this, the raw rheometry data was plotted as log(η) vs. log(*t*) and the linearly increasing region isolated from the rest of the data. A linear trendline was fitted to this isolated data, and the trendline extrapolated backwards until it intersected a horizontal line defined by the initial viscosity as measured using the frequency sweep test data. The *x* value of the intersection, indicating the time at which the viscosity first began to rise above the baseline value, was correlated to the temperature of the system by referencing that time to the raw rheometry data. This temperature was taken to be the critical gel temperature (T_{gel}). Figure 2.2 shows this process applied to a sample dataset of 20% F127 heated at 1°C/min.

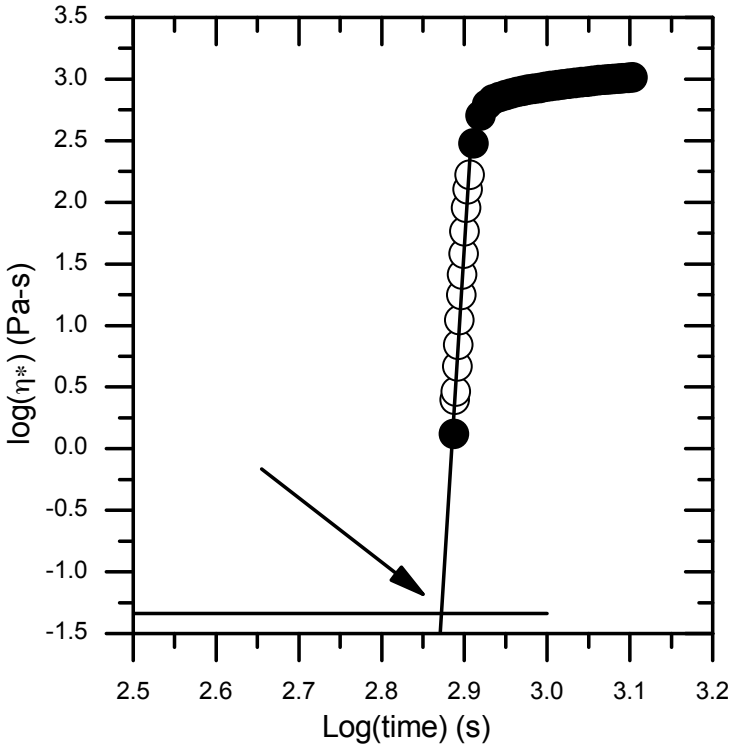

Figure 2.2 Power law analysis of rheometry data. The linearly increasing viscosity values (white circles) are fitted with a linear trendline, which is extrapolated backwards to where it intercepts the initial viscosity value as measured using a frequency sweep. This intersection (arrow) indicates the time at which the gelation bas begun. For clarity, the pre-gelation data has been excluded (as was done for the analysis). Figure reproduced from [55].

A log-Boltzmann sigmoid model was used in order to characterize the characteristic gelation time (Δt). Equation 2.1 describes the fitting model used, where t_0 denotes the inflection time, the time at which the complex viscosity has reached halfway between its initial and final values. Figure 2.3 illustrates a representative Boltzmann sigmoid curve and illustrates the four relevant fitting parameters: η_0, η_f, t_0, and Δt.

$$\log \eta^*(t) = \log(\eta_f) + \frac{\log(\eta_0) - \log(\eta_f)}{(1 + e^{\frac{t-t_0}{\Delta t}})}$$

Equation 2.1

The slope of the curve at t_0 is defined in Equation 2.2.

$$\frac{d\log(\eta_{t_0})}{dt} = \frac{\log(\eta_f) - \log(\eta_0)}{4\Delta t}$$

Equation 2.2

The value $4\Delta t$ can be interpreted as the total time elapsed between the onset and the completion of gelation. As such, it can be used to compare the rate at which differing formulations of F127 solutions gel. The smaller the value of $4\Delta t$ or (Δt), the faster the gelation.

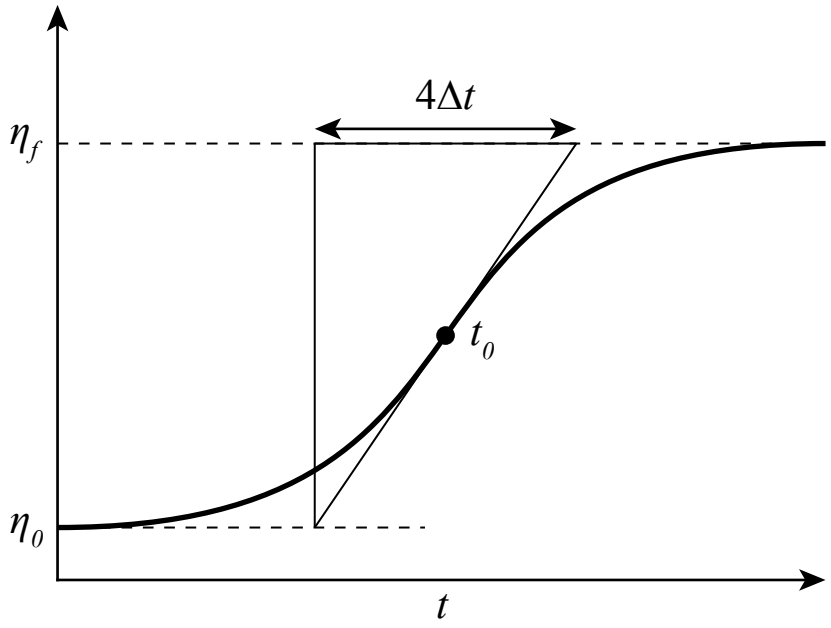

Figure 2.3 Boltzmann sigmoid curve showing relevant fitting parameters.

2.3 Results

2.3.a. Heating rate influences gelation temperature

Figure 2.4 illustrates the effect that heating rate has on gelation temperature. The data has been plotted as the complex viscosity vs. temperature, and it is clearly seen that at 0.1°C/min, the gelation occurs at a lower temperature than for the higher heating rates. Table 2.1 summarizes the identified T_{gel} as determined by power law analysis. The most pronounced changes in T_{gel} occurred at the lower F127 concentrations. Comparing T_{gel} to heating rate, the most pronounced differences occur between the 0.1°C/min and 1°C/min heating rates.

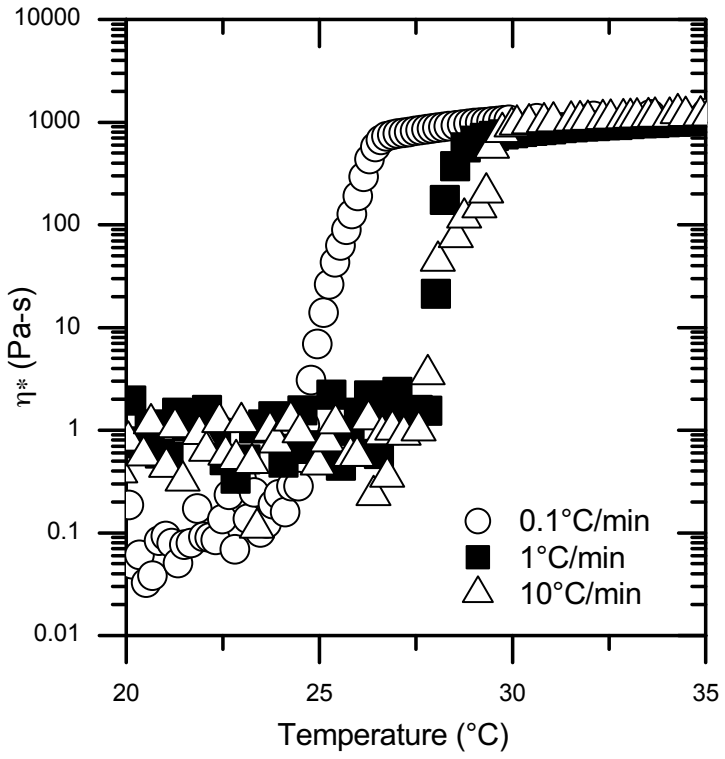

Figure 2.4 Viscosity vs. Temperature for a 20% F127 solution heated at different rates. Heating rate influences gelation time. For clarity, the number of data points shown has been reduced. Figure reproduced from[55].

F127 Concentration		0.1°C/min	1°C/min	10°C/min
Neat F127	10%	44.9 ±1.3	47.2 ±1.8*	58.5 ±1.8
	15%	30.0 ±0.1	31.5 ±0.3	50.5 ±0.4
	20%	23.9 ±0.1	27.5 ±0.3	26.6 ±0.4
	25%	19.8 ±0.1	22.2 ±0.1	20.0 ±0.3
	30%	17.0 ±0.1	19.3 ±0.0	19.3 ±0.7
F127 + MP	10%	46.9 ±1.6	33.6 ±1.0*	63.8 ±2.0
	15%	25.4 ±0.4	30.0 ±1.9	46.6 ±0.8
	20%	12.0 ±0.0	12.4 ±0.1	12.4 ±0.3
	25%	9.9 ±0.0	10.3 ±0.1	10.8 ±0.2
	30%	8.1 +0.1	8.3 +0.0	8.9 ±0.5

Table 2.1 Gel temperature as determined by power law analysis. The asterisk indicates data collected using a smaller gap dimension of approximately 0.6 mm since the tests run at larger gap dimensions resulted in a lack of identifiable gelation. Table reproduced from[55].

2.3.b. Heating rate influences gelation time

The gelation time Δt is also affected by the heating rate. Generally, faster heating rates and/or higher F127 concentration resulted in shorter gel times. Figure 2.5 shows a 20% F127 solution heated at different rates along with the fitted log-Boltzmann sigmoid curve overlaid on the raw data. At the highest concentrations and highest heating rates, the gel transition was on the order of a few seconds. Differences in Δt are minimized under these conditions; however, sampling rate limitations of the rheometer (1 Hz maximum) may be the limiting factor, masking differences in actual gel time. Table 2.2 summarizes the fitting values used in the log-Boltzmann sigmoid analysis.

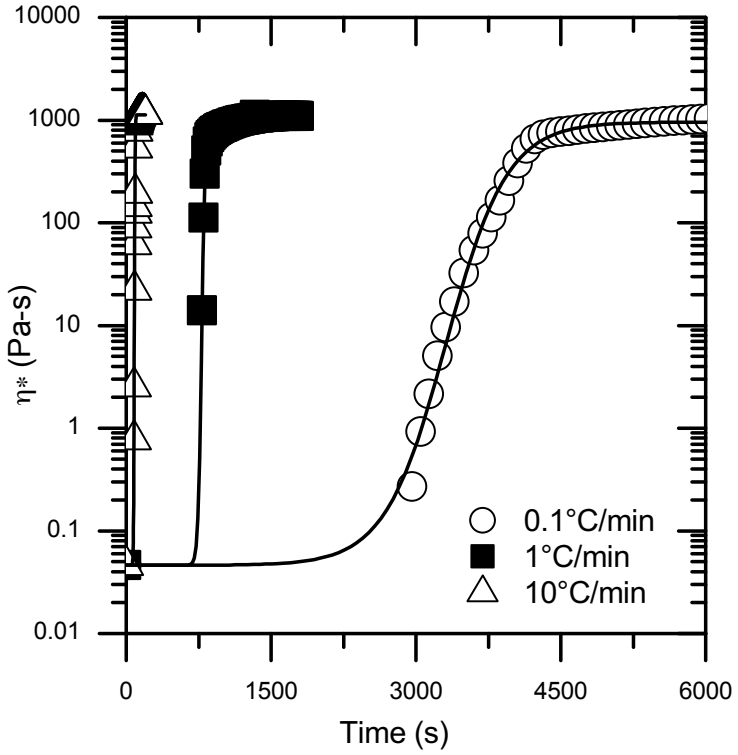

Figure 2.5 Viscosity vs. time for 20% F127 at three heating rates. The black line shows the corresponding log-Boltzmann sigmoid fit applied to the data. For clarity, the number of data points was reduced for the 1°C/min and 10°C/min heating rates. Figure reproduced from[55].

Heating Rate	F127 Concentration	$\log(\eta_0)$ Pa-s	$\log(\eta_f)$ Pa-s	t_0 (s)	Δt (s)
0.1°C/min	10%	-1.87	2.68 ±0.11	4983 ±732	283 ±29
	15%	-1.72	2.87 ±0.08	4217 ±29	333 ±58
	20%	-1.34	2.98 ±0.01	3308 ±11	325 ±19
	25%	-0.98	3.26 ±0.01	3142 ±6	89 ±9
	30%	-0.91	3.38 ±0.00	4774 ±25	109 ±1
	10% + MP	-1.91	2.25 ±0.09	6417 ±889	300 ±0
	15% + MP	-1.46	2.43 ±0.10	1310 ±340	233 ±58
	20% + MP	-0.80	3.12 ±0.01	1786 ±12	103 ±6
	25% + MP	-0.69	3.27 ±0.08	3447 ±12	105 ±24
	30% + MP	-0.50	3.37 ±0.01	2282 ±20	87 ±6
1°C/min	10%*	-1.87	2.25 ±0.05	2932 ±39	253 ±17
	15%	-1.72	1.67 ±0.02	1181 ±33	129 ±10
	20%	-1.34	3.00 ±0.01	783 ±5	18 ±1
	25%	-0.98	3.25 ±0.00	457 ±2	11 ±3
	30%	-0.91	3.37 ±0.01	874 ±3	6 ±2
	10% + MP*	-1.91	2.27 ±0.06	2178 ±28	244 ±9
	15% + MP	-1.46	2.05 ±0.00	1015 ±123	52 ±8
	20% + MP	-0.80	3.17 ±0.03	366 ±178	3 ±0
	25% + MP	-0.69	3.36 ±0.01	580 ±1	5 ±1
	30% + MP	-0.50	3.44 ±0.02	462 ±0	7 ±1
10°C/min	10%	-1.87	1.73 ±0.07	411 ±11	78 ±1
	15%	-1.72	1.80 ±0.04	284 ±20	35 ±2
	20%	-1.34	3.06 ±0.01	84 ±1	4 ±0
	25%	-0.98	3.31 ±0.01	46 ±2	4 ±1
	30%	-0.91	3.43 ±0.01	102 ±3	3 ±1
	10% + MP	-1.91	1.30 ±0.05	481 ±12	54 ±4
	15% + MP	-1.46	1.71 ±0.14	258 ±13	30 ±5
	20% + MP	-0.80	3.15 ±0.01	60 ±2	3 ±0
	25% + MP	-0.69	3.34 ±0.00	73 ±2	4 ±1
	30% + MP	-0.50	3.45 ±0.01	60 ±3	3 ±0

Table 2.2 Log-Boltzmann analysis used to determine gel time. Values with asterisks indicate data collected using a smaller gap dimension of approximately 0.6mm. Table reproduced from[55].

2.3.c. Methylparaben influences the gel transition

As previously reported[10,22,45,54,57], the presence of dissolved solutes affects the micellization and gelation behavior of Pluronic solutions. Here the addition of methylparaben influenced both T_{gel} and Δt when compared to neat F127 formulations. Figure 2.6 shows the difference in T_{gel} as determined by power law analysis when saturated MP is added to the F127 formulations. Globally a drop in the gel temperature is seen, with the most pronounced drops occurring at F127 concentrations of 20% and above. The heating rate also had a small effect on the gelation temperature, with the higher heating rates indicating additional lowering of T_{gel} for F127 concentrations of 20% and higher. Table 2.1 shows that for 10% F127, an increase in T_{gel} with added MP was measured, however, it is possible that this is an anomaly due to thermal lag or sample dehydration. The driving force for gel formation at 10% F127 is very low, and while an increase in viscosity can be detected using the rheometer, a self-supporting "gel" phase is never achieved. These measurements agree with those of Sharma *et al*.[45], who also measured a lowering of the gel temperature by roughly 15-20°C for F127 concentrations saturated with MP. Their measurements were carried out using a simpler tube inversion method, however, which allowed the system to come to equilibrium before the measurement was taken. The resolution of their measurements was also limited by the temperature accuracy of their water bath.

The effects of MP on the characteristic gelation time (Δt) were also measured by log-Boltzmann sigmoid analysis. Figure 2.7 shows the change in Δt for F127 solutions both neat and with added MP, at a heating rate of 0.1°C/min. There is a pronounced lowering of Δt, interpreted as a quickening of the gel formation. This difference is again most

pronounced at 20% F127. At concentrations of 25% and above, however, there was no pronounced difference in Δt.

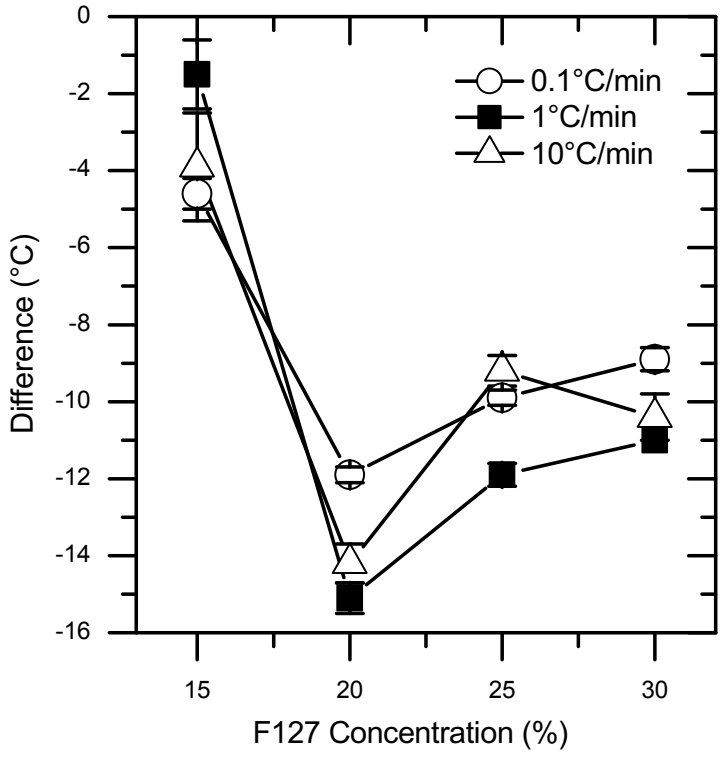

Figure 2.6 Difference in T_{gel} as a result of added methylparaben for 15-30% F127. Figure reproduced from[55]. Absolute values of T_{gel} are listed in Table 2.1.

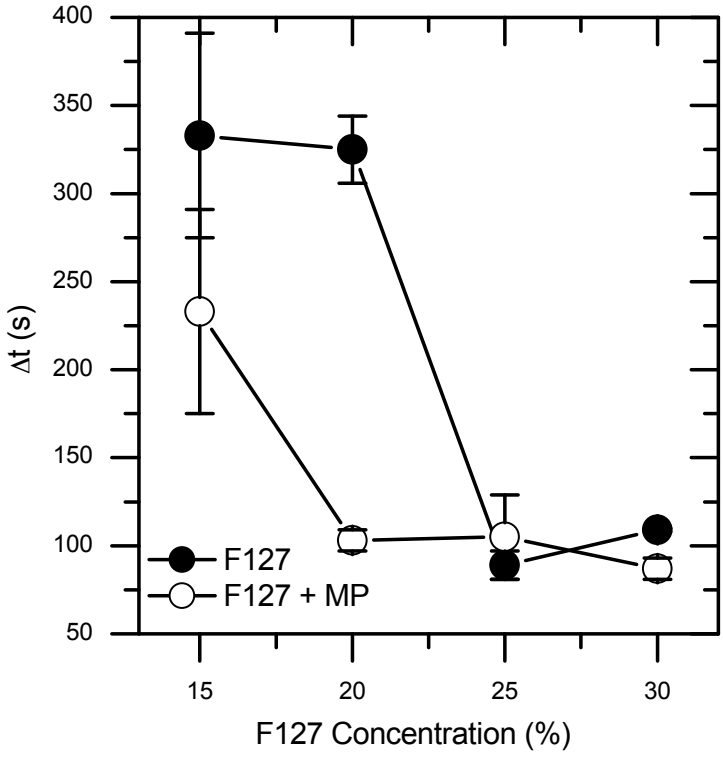

Figure 2.7 Comparison of the characteristic gelation time Δ*t* as a function of F127 concentration under a heating rate of 0.1°C/min. Figure reproduced from[55].

2.4 Discussion

Here the effects of heating rate on the gel properties of aqueous F127 solutions, as well as the effects that the dissolved solute methylparaben has on the system were determined. While previous studies have covered this topic before[4,8,13,22], none have paid particular attention to the effects of heating rate. These results show that there is a kinetic component to the gel formation process as measured by rheometry, and that heating rate affects the gel formation behavior of F127 solutions in a systematic manner between 15 and 30% F127. Higher heating rates correlate with a higher T_{gel} and shorter Δ*t*. At 10% F127, however, the variance in our measurements were notably higher than for the more concentrated F127 solutions. Initially, no gelation event (no change in viscosity) was observed when heating a 10% F127 solution at 1°C/min, whereas gelation was

measurable at 0.1°C and 10°C/min. Repeating these experiments using a smaller gap dimension, in an effort to reduce edge meniscus effects as well as minimize exposed surface area to evaporation, gelation events were recorded with a 1°C/min heating rate. These anomalies are attributed to the fact that at 10%, the driving force for gel formation in F127 is weak, and that systematic changes in the gel behavior are possibly overridden by other factors, such as sample dehydration. As the measured T_{gel} for 10% F127 was the highest of all solutions tested, up to 45°C or higher, any measured rheological response is likely to be dehydrated residues rather than the actual 10% solution. For the higher concentrations of F127, the gelation happens at lower temperatures and thus the rheological responses are recorded before encountering any significant evaporation.

The data illustrate that heating rate has an influence on the gel time. One explanation for this is simply that the gel transition is related to the heating time of the system. In other words, it is obvious that gelation happens more quickly with an increasing temperature as the temperature of the system is being raised more rapidly. If this were the case, however, the measured gel times would scale directly with the heating rate. Thus, Δt for 10°C/min would be simply 10 times higher than that for 1°C/min. The values in Table 2.2, however, indicate that while the heating rate was changed by a factor of 100 between the lowest and highest rates tested, Δt only changes by a factor of 10-30. Therefore, it is reasonable to conclude that there are some kinetic factors present.

Figure 2.6 and Figure 2.7, as well as the data in Table 2.1 and Table 2.2 show that the intermediate concentrations of F127 exhibit the most sensitivity to added MP, in terms of the measured viscoelastic response. This sensitivity is not immediately intuitive given that the trends of T_{gel} and Δt monotonically decrease for increasing F127 concentration

without added MP. One would expect that increasingly higher concentrations of F127 would experience increasingly large modifications in gel behavior, as an already strong driving force for gel formation is amplified by heating rate or added MP. Why then, does added MP affect the gel behavior more profoundly only at the intermediate F127 concentrations? One explanation is if there is some practical upper limit to the driving force to form a gel, which is seen at high concentrations of neat F127 solutions, whereby other limiting factors come in to play (such as the diffusion/aggregation rate of Pluronic micelles). When the driving force is already at or near this maximum, added MP may not enhance gel formation to a significant degree. Another explanation is that the sampling frequency of the rheometer was not sufficient to determine the differences in T_{gel} or Δt. Especially at the highest concentrations, where Δt is only on the order of a few seconds, a 1 Hz maximum sampling rate of the rheometer may not be sufficient to accurately capture and characterize the viscosity profile, thus leading to errors in the fitted model.

Insight into the physical mechanism by which MP affects the gelation behavior can be gained by considering the structure of the molecules involved. To briefly review, the "gelation" event in aqueous F127 solutions is actually the ordering and interaction of F127 micelles into a crystalline-like lattice. This ordering is based on repulsive forces between individual micelles and not physical entanglement or covalent crosslinking common to gel formation in other polymeric systems[58]. Owing to the nonpolar character of MP, which has an octanol/water partition coefficient of 1.96[59], molecules of MP likely segregate into the core of the F127 micelles where they may act as a plasticizer, disturbing the packing of the hydrophobic PPO chains within the micelle core. This plasticizing effect may increase the size of the micelle, which effectively results in

properties similar to solutions at higher temperatures, and the micelles themselves being larger and more numerous. As a result, nearest-neighbor interactions are more likely to occur and cause ordering in solution, culminating with a gelation-like event. Pluronic F127 contains 30% by weight PPO, and the added MP is present at a concentration of approximately 1-2%. Assuming that the MP segregates entirely to the micelle core, given its hydrophobic nature[41], it can be calculated that the weight percentage of MP within the micelle core is between 30% and 10%, for 10% and 30% F127 respectively. Therefore, despite the low total concentration of MP in the solution as a whole, the micelle core contains a considerable amount by weight of MP. Large effects on the properties of micelle formation or ordering are therefore reasonable to expect.

It is also known that the energetics of the micelle system is being affected by the presence of MP, which might ultimately affect the gel behavior of aqueous F127 solutions. Measurements made by Sharma *et al*.[47] indicate a lowering of the critical micelle concentration (*cmc*) for solutions containing dissolved pharmaceutical solutes (including MP). They suggest that this lowering of the *cmc* would facilitate micellar assembly. A more detailed treatment of this topic will be presented in Chapter 3.

2.5 Chapter summary

In this chapter, the viscoelastic response of aqueous F127 solutions was rheologically measured over a range of F127 concentrations. Particular attention was paid to the kinetics of the gel formation, by tracking the viscosity as the solution was heated using a range of heating rates. This aspect of the gel formation had not been previously studied

in detail, so these efforts have culminated in a novel addition to the body of knowledge surrounding gelation behavior in amphiphilic copolymer systems.

It is important to note, however, that the methods used here are mainly observational tools that can only indirectly infer about the structure and evolution of the micelle gel that has formed. In order to more completely understand the nature of the measured response to added solutes, a more in-depth investigation on the structure of these gels is needed. The contents of the following chapter cover an in-depth structural analysis of Pluronic F127 gels and the effect of these ternary additives.

Chapter 3

Structural Study of F127 Gel Formation

3.1 Introduction

In Chapter 2, a viscoelastic characterization of F127 gel formation was presented. While rheometry is useful to study the macroscopic viscoelastic behavior of materials, it does little to explain the physical foundation of the observed changes. In order to better understand the specifics of the changes that added solutes have on the structural evolution of F127 micelle gels, small angle x-ray scattering studies were carried out to more directly observe the ordered cubic phases being formed in heated F127 solutions. As was the case with the phase behavior of F127 gel formation, the structural behavior of micelle gels created by amphiphilic copolymers has been extensively studied in the literature[8,12,16,60,61]. However, a similar lack of attention on the kinetics of gel formation pervades the existing body of structurally focused literature. Additionally, there is a lack of detailed studies on the change in micelle structure as a result of added pharmaceuticals or other solutes.

Scattering methods including SAXS and SANS are typically used to study the structures of polymeric systems[9,10,15,53,54,62-64]. SANS has the advantage where the scattering is due to the nuclei of the sample, which allows for better discrimination between polymeric compounds and their solvents, particularly when deuterated samples are used. However, most neutron sources suffer from low flux and lengthy capture times

are required. SAXS, on the other hand, has the advantage of being available in highly intense beams, allowing for time-resolved capture of transient processes[65].

In this chapter, the results of SAXS studies are presented which set out to explore what structural changes, if any, are present in F127 micelle gels as a result of added ternary solutes. In addition, early attempts have been made to look at these structures in real-time as they are heated. The equipment needed to carry out this type of time-resolved work necessitated high intensity x-ray sources and fast, sensitive detectors. To fulfill these requirements, these scattering studies were carried out at synchrotron facilities.

The methods, results, and discussion presented in this chapter were submitted and published in the journal *Macromolecules*[66].

3.2 Materials and methods

3.2.a. Sample preparation

Solution preparation for the SAXS experiments follows closely the protocol used in Chapter 2, which were based on the descriptions of Schmolka[1]. Deviations from the described procedure involved adding the ternary solutes to a concentration of 1% wt/v instead of saturating the solution. This gave a more controlled testing environment, as the total amount of added solute was kept uniform amongst various additives. Solutes tested were methylparaben (MP) and dexamethasone (DX), which were obtained from Sigma-Aldrich. Three other added compounds, magnesium citrate (MC), *cis*-diamminedichloroplatinum(II) (cisplatin), and propylparaben (PP) were also used in a set of exploratory experiments designed to test the effects of a wider array of additives.

These compounds were also obtained from Sigma-Aldrich and used in a 1% wt/v concentration. In the case of cisplatin and dexamethasone, however, very little of the added solute was actually incorporated into the solution, with the bulk of the additive settling on the bottom of the sample tube. Therefore the solutions measured for cisplatin and dexamethasone were saturated but not at a concentration of 1 wt%.

For sample loading, two different configurations were used according to the heating stages available at the two beamlines used. At Argonne National Labs beamlines 5-ID (shown in Figure 3.1) and 12-BM, samples were loaded into 1.5mm glass capillary tubes (Charles Supper Inc., Natick, MA), which were subsequently sealed using wax to prevent sample evaporation. At Brookhaven National Labs beamline X10A, samples were loaded into custom-made stainless steel sample washers. The sample was pipetted into the annular opening of the washer, and sealed on both sides with Kapton tape. This allowed for an airtight sample housing that was transparent to x-ray transmission, compatible with the heating stage used at the X10A beamline.

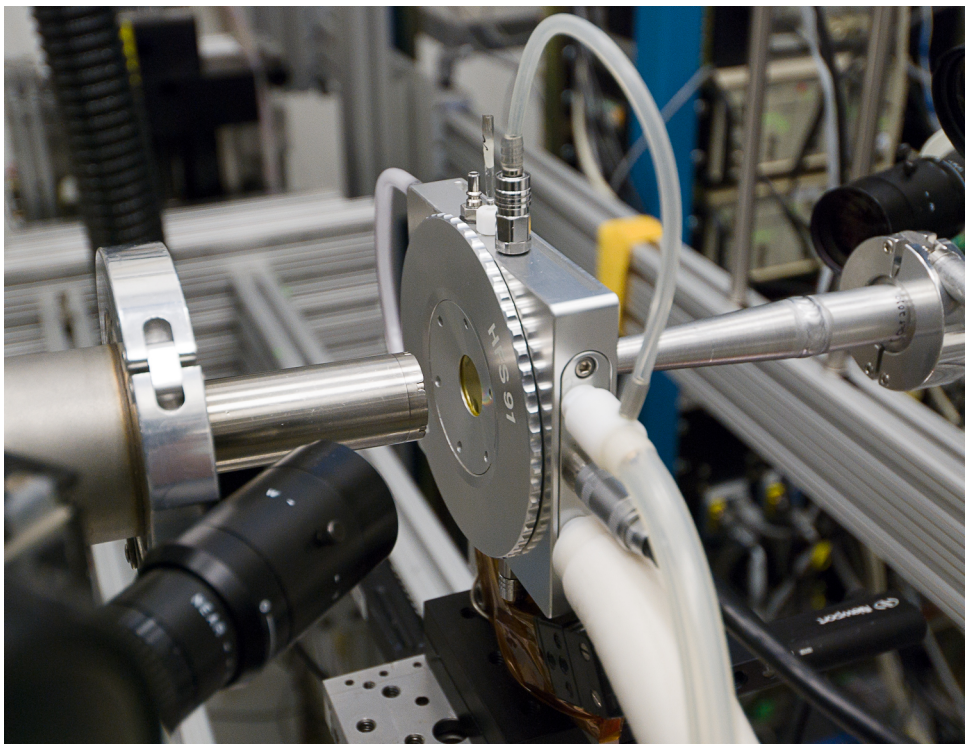

Figure 3.1 Typical transmission SAXS configuration. Focused x-ray beam originates from the left of the image, passes through the sample, and proceed on to the detector (off-screen on the right). Tubes of cooled nitrogen gas (white tubes) enter the sample stage, which also contains a heating element. This image was taken at the Advanced Photon Source 5-ID beamline.

3.2.b. Small-angle x-ray scattering

SAXS experiments were conducted at two facilities, the Advanced Photon Source (APS) at Argonne National Labs in Argonne, IL and the National Synchrotron Light Source (NSLS) at Brookhaven National Labs in Upton, NY.

3.2.b.i NSLS beamline X10A

The beam configuration at the NSLS X10A was as follows. The beam energy used was 11 keV, and the sample to detector distance was approximately 1.8 m. Nominal capture times used were between 1 and 2 minutes. Thermal control of the samples was achieved using either a Mettler-Toledo heating stage, or a Linkham heating stage. 2D data was collected using a Bruker 1500 CCD camera, and initial processing (unwarping

to account for sensor unevenness and background subtraction) was carried out using SAXS software provided by Bruker. Following the unwarping step, the 2D data was integrated around the azimuthal axis and the integrated intensity data exported as spreadsheets. Intensities recorded at the X10A beamline were in the units of detector counts.

3.2.b.ii APS beamline 5-ID

The beam configuration at the APS 5-ID beamline was as follows. A beam energy of 17 keV was used, with a sample to detector distance of approximately 2 m. The detector installed the beamline is a Mar165 made by MarUSA (now Rayonix). A one second capture time was used at this beamline (significantly shorter than that of the other beams owing to its higher photon flux) A Linkham DSC thermal stage allowed for temperature control. Data was collected in 2D and automatically unwarped, background subtracted, and normalized into intensity units of 1/cm. The detector capture routines included automatic integration of the data to 1D format.

3.2.b.iii APS beamline 12-BM

The beam configuration at the APS 12-BM beamline was as follows. The beam energy was 9 keV, with a sample to detector distance of approximately 0.8 m. Like 5-ID, the detector used was also a Mar165 CCD. Capture times of one minute were used on this beamline. Thermal control of the samples was achieved using a Linkham THMS600 heating stage, which was borrowed from the APS Equipment Pool. 2D data was captured and automatically processed into TIFF format images. Background frames were taken automatically to remove sensor noise as part of the capture process. These files were

subsequently batch processed to normalize the intensity to units of 1/cm, and integrated around the azimuthal axis.

3.2.c. Static temperature experimental protocol

A thermal schedule was designed to observe the equilibrium structure of the tested gels at a series of temperatures starting below the critical micelle temperature (*cmt*), to temperatures well above the gel temperature. Samples were loaded into the thermal stage and the temperature was equilibrated at 0°C for 3 minutes. After equilibration, an image was captured and the temperature increased by 10°C, followed by an additional 2-3 minute equilibration period. This process was repeated up to a temperature of nominally 80°C. On some samples, extended incubation at high temperatures was used in order to investigate aging effects of the gel structure with prolonged exposure at high temperatures. For these studies, incubations of 10 or 15 minutes at 80°C were followed by an additional capture. This static temperature testing was conducted at all beamlines used. At least three repetitions of each sample was run to ensure reproducibility of the data, and negative control samples of just the solvent (dH_2O) were also taken to remove the scattering due to the solvent.

3.2.d. Dynamic temperature experimental protocol

The 5-ID beamline at the APS, being an insertion device beamline, had greater photon flux (brightness) than the other beamlines used. Due to this, capture times at the 5-ID beamline were short enough to allow for real-time dynamic capture of SAXS data as the samples were heated. Although the exposure time for each data sample was only one second, sensor readout time and file processing/transfer meant that data was only captured roughly once every 30 seconds.

Samples were loaded into the heating stage and equilibrated at the starting temperature. This temperature was chosen to be roughly 10°C below the known gel temperature of the sample, as was measured or observed prior in both the rheological and the static temperature SAXS experiments. Once the sample was equilibrated at the starting temperature, it was subsequently heated at a controlled rate of 1°C/min to a final temperature 20°C above the starting temperature. Data was collected continuously throughout the duration of the heating.

As the available time at the 5-ID beamline was limited, a heating rate of 1°C/min was chosen because it was high enough to be significantly faster than the quasiequilibrium heating condition (0.1°C/min), yet low enough to allow for reasonable thermal resolution (one sample every 0.5 degrees, assuming 30 seconds minimum between continuous captures). Figure 3.2 illustrates the differences between the two test methods. The temperature of the sample is held constant during the capture event in the static temperature experiments. The short capture times used in the dynamic experiments, however, allowed for continuously increasing sample temperature.

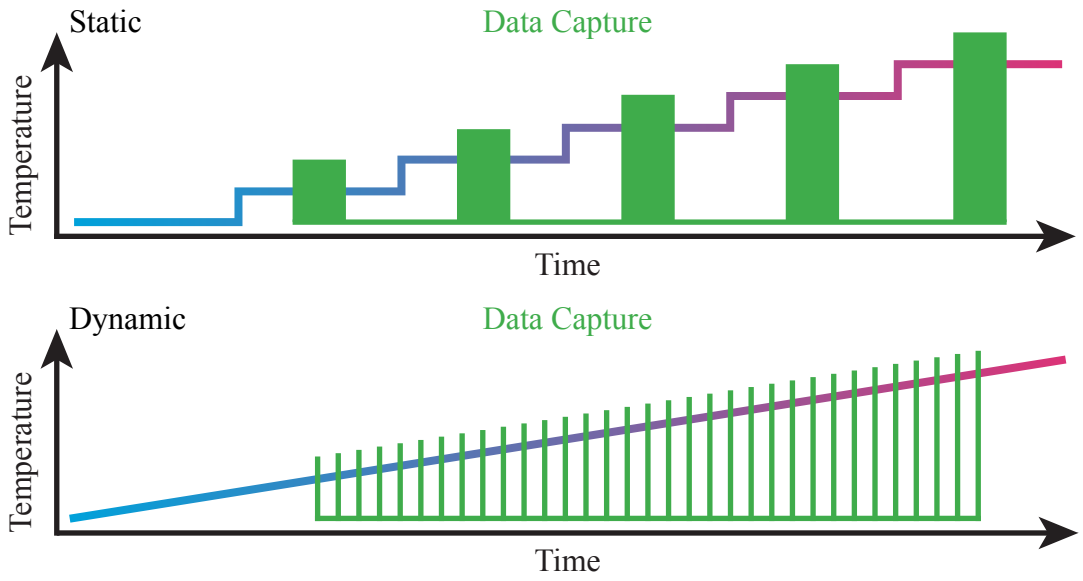

Figure 3.2 Static vs. dynamic SAXS tests. The top plot shows the stepwise temperature increases used in the static temperature experiments. The bottom plot shows the continuously changing temperature in the dynamic experiments. The width of the capture events illustrates that the capture times used in the static experiments were much longer than those used for the dynamic experiments, necessitating the constant temperature.

3.2.e. Quantification and analysis of SAXS data

Integrated 1D SAXS intensity data was plotted as a function of the reciprocal space scattering vector, q. Converting the angular deflections recorded on the imaging sensor to the reciprocal vector q can be achieved by combining Bragg's law (Equation 3.1), with the definition of the reciprocal space scattering vector (Equation 3.2), to relate q to the scattering angle (Equation 3.3). As the x-ray wavelength (λ) and the geometry of the detector are known (giving θ), q can be calculated. Typically, this conversion was automatically carried out in the detector software.

$$\lambda = 2d \sin\theta$$

Equation 3.1

$$q = \frac{2\pi}{d}$$

Equation 3.2

$$q = \frac{4\pi}{\lambda}\sin\theta$$

Equation 3.3

Once the data was plotted as I(q), the peaks were identified and their locations determined using OriginLab's peak analyzer function. The ratios of these peak positions were compared to that of known crystal structures and classifications according to structure could be made. It is known that the structures of Pluronic gels can adopt a variety of ordered phases including hexagonal, lamellar, cubic, and gyroid structures[8,67-69], however F127 gels typically adopt bcc or fcc structures[2,19]. Table 3.1 shows the theoretical peak positions for the fcc and bcc crystal structures, along with their relative positions to the fundamental scattering peak.

fcc Plane	Peak Position	Ratio	bcc Plane:	Peak Position	Ratio
111	q_0	1.000	110	q_0	1.000
200	$\sqrt{4/3}\,q_0$	1.155	200	$\sqrt{2}q_0$	1.414
220	$\sqrt{8/3}\,q_0$	1.633	211	$\sqrt{3}q_0$	1.732
311	$\sqrt{11/3}\,q_0$	1.915	**220**	$\boldsymbol{\sqrt{4}q_0}$	**2.000**
222	$\boldsymbol{\sqrt{12/3}q_0}$	**2.000**	310	$\sqrt{5}q_0$	2.236
400	$\sqrt{16/3}\,q_0$	2.309	222	$\sqrt{6}q_0$	2.449
331	$\sqrt{19/3}\,q_0$	2.517	321	$\sqrt{7}q_0$	2.646
420	$\sqrt{20/3}\,q_0$	2.582	**400**	$\boldsymbol{\sqrt{8}q_0}$	**2.828**
422	$\boldsymbol{\sqrt{24/3}\,q_0}$	**2.828**	**411**	$\boldsymbol{\sqrt{9}q_0}$	**3.000**
333	$\boldsymbol{\sqrt{27/3}\,q_0}$	**3.000**	420	$\sqrt{10}q_0$	3.162

Table 3.1 Summary of expected peaks and relative peak positions for the fcc and bcc crystal structures. Bolded entries are planes with identical ratios in both crystal structures.

3.2.f. Dynamic light scattering

DLS experiments were carried out using an ALV compact goniometer system (Model ALV/SP-125, Langen, Germany) using an ALV/SO-SIPD photon detector. The light source used was an Innova 70C argon ion laser (Coherent, Inc., Santa Clara, CA) with a wavelength of 488 nm and a laser power of 200 mA. 1% solutions of F127 with and without 0.1% MP were carefully prepared from stock solutions and filtered through a 0.22 μm syringe filter and subsequently degassed under vacuum to expunge any particulate impurities and dissolved gasses which may interfere with the measurement.

Approximately 500-1000 μL of sample was loaded into a clean sample tube, and inserted into the DLS system, which was set to a temperature of 30°C. After a 5-minute equilibration period, data was collected for a total of 1 minute per reading at repeated at angles between 40° and 90°, in 10° increments. The resulting correlation time plots were analyzed using a regularized method (CONTIN)[70] to obtain particle size distributions

from the autocorrelation functions. Samples were measured at least three times each at each scattering angle, and the results averaged.

3.3 Results

3.3.a. Static temperature measurements

A typical progression of peak evolution in F127 samples is as follows. At the lowest temperatures, there is typically no scattering. This is because the solution is below the *cmt* and there are no micelles present. As the *cmt* is reached, an amorphous scattering halo develops, indicating the presence of micelles, but no periodic order. As the temperature is increased further, the micelles will arrange into cubic ordered domains, and distinct Bragg peaks will evolve. At the highest temperatures tested, thermal breakdown of the gel occurs and the Bragg peaks give way to an amorphous scattering halo once again. While it is typical to only observe one crystal structure, samples exhibiting peaks from two structures were observed, typically at the higher temperatures.

Static temperature measurements for 20, 25, and 30% F127 is shown in Figure 3.3. The presence of periodic structures (as indicated by the presence of peaks) is more distinct for higher concentrations of F127. This is to be expected, considering the gel forming properties of F127 are positively correlated with increasing concentration[1]. The range of stable micelle gels is also expanded for higher F127 concentrations. Peak formation is first observed at 40°C in 20% F127 and breaks down by 60°C, whereas peak formation in 30% F127 is visible at 30°C and extends all the way to the test maximum of 80°C. For solutions below 20%, Bragg peaks could not be reliably identified from the

amorphous scattering halo. Therefore, the results described from hereafter will focus on concentrations of 20% or greater.

Figure 3.4 shows plots for F127 solutions containing MP. Comparing the MP plots to the neat F127 plots shown in Figure 3.3, it can be seen that the stable range of micelle gels is expanded by the presence of MP. For instance, in the 25% F127 solution, the crystalline lattice breaks down at 70°C, whereas with added MP Bragg reflections are clearly visible at the same temperature.

Based on comparison of the measured peak positions (Table 3.2 and Table 3.3) to the expected positions of Bragg peaks (Table 3.1), most of the identified phases are fcc. Although the expected (200) fcc peak at $(4/3)^{1/2}q_0$ is not seen, the (220) and (311) peaks at $(8/3)^{1/2}q_0$ and $(11/3)^{1/2}q_0$ are clearly identified in all cases. The missing (200) peak could be missing due to defects in the crystalline lattice. The arrangement of micelles is far from the tightly constrained and highly ordered lattices of atomic systems. For example, twinning defects in the lattice, where portions of the structure alternate between the expected ABCABC layering pattern of the fcc lattice to the ABABAB or ACACAC layering of the hcp lattice has been known to suppress individual Bragg peaks[71-73].

The results for samples containing dexamethasone shown in Figure 3.5 are especially noteworthy, exhibiting an unusual scattering behavior where the fundamental scattering peak is suppressed. Starting at concentrations of 25% and greater, the fundamental scattering peak is not visible except for at the higher temperatures tested. It was interesting to note this behavior, and a more comprehensive discussion of its significance is offered in the following section.

Figure 3.4 (a) shows that at 70°C, just before breakdown of the ordered phase, a transition in crystal structure has occurred. This is evident by the appearance of two new peaks that do not align with the peaks seen at 60°C. Further measurement of these peaks indicates that the new peaks are that of the bcc crystal structure (Table 3.3). This behavior, while not seen in every sample, was observed for several F127 concentrations and sample compositions. Figure 3.6 shows a more detailed look at a 30PL solution heated to 80°C, incubated for an additional 10 minutes at 80°C, and then subsequently heated to 90°C. As more time is spent at the high temperatures, the bcc peaks emerge and grow in prominence. Raising the temperature even further to 90°C, the dominant crystal structure in the sample is now bcc.

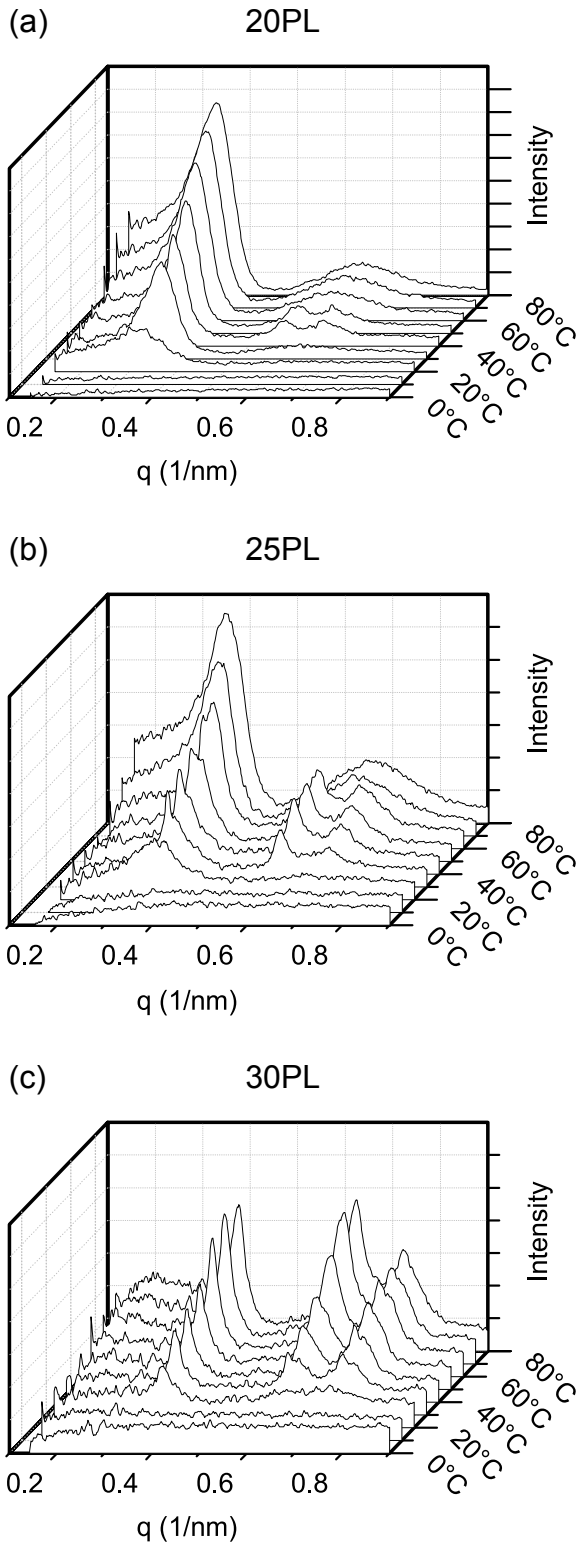

Figure 3.3 Intensity vs. *q* plots for 20-30% F127 solutions. Figure adapted from[66].

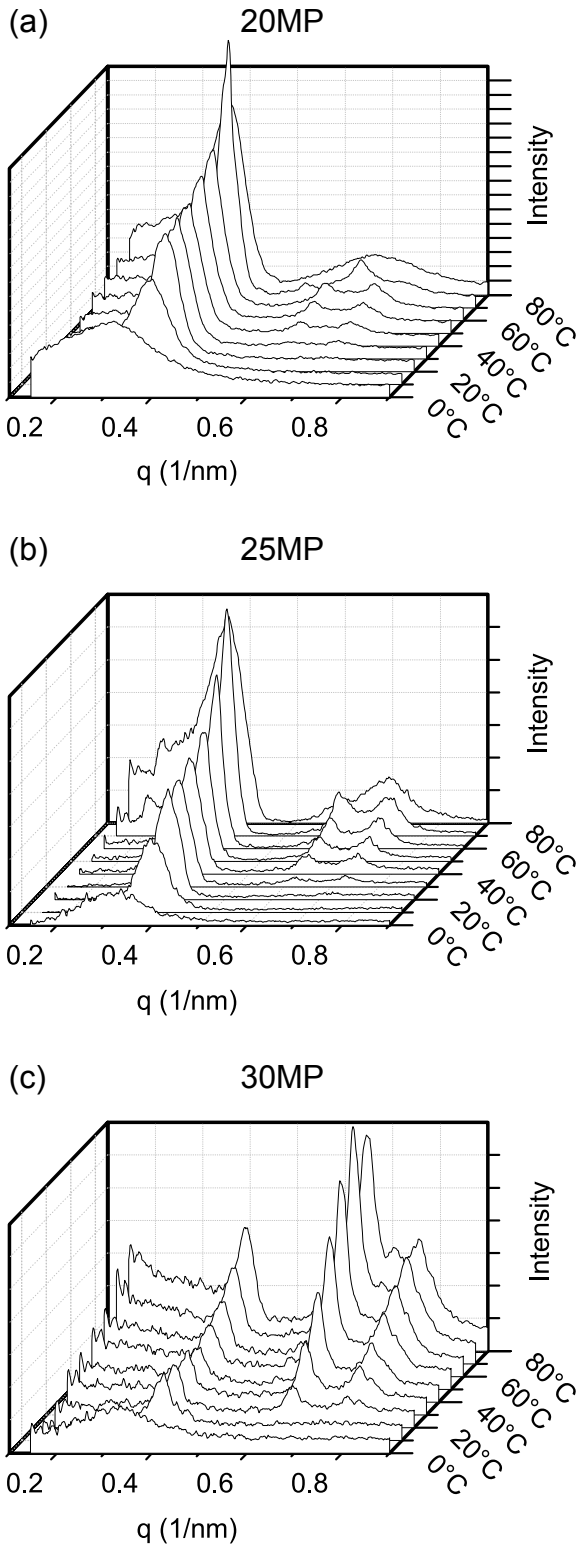

Figure 3.4 Intensity vs. *q* plots for 20-30% F127 solutions containing MP (1% wt/v). Figure adapted from[66].

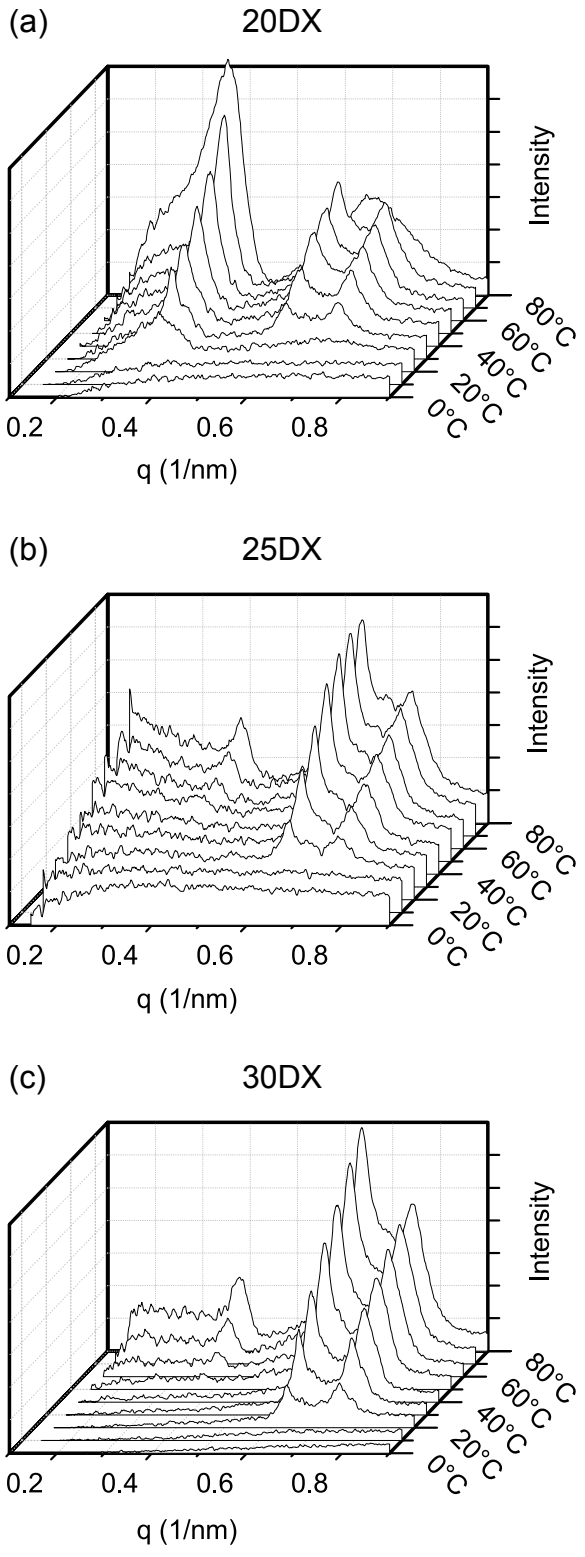

Figure 3.5 Intensity vs. *q* plots for 20-30% F127 solutions containing DX (1% wt/v). Figure adapted from[66].

Sample	q_0	q_1	q_2	Phase
30PL	0.3708	0.6131	0.7233	fcc
30MP	0.3942	0.6465	0.7584	fcc
30DX	*	0.6331	0.7434	likely fcc
25PL	0.3545	0.5952	0.6939	fcc
25MP	0.3775	0.6248	0.7300	fcc
25DX	*	0.6398	0.7467	likely fcc
20PL	0.3408	0.5763	0.6565	fcc
20MP	0.3742	0.6097	0.7150	fcc
20DX	0.3641	0.6097	0.7166	likely fcc

Table 3.2 Identified peak positions (in units of nm^{-1}) and identified phase at 40°C. (*) Indicates that no peak was found at this temperature but visible at higher temperatures. Table reproduced from[66].

Sample	q_0	q_1	q_2	q_3	q_4	Phase
30PL	0.3725	0.6204	0.7233			fcc
30MP	0.3909	0.6431^1	0.7033^2	0.7550^1		fcc+bcc
30DX	0.3792	0.6364^1	0.7400^1			fcc
25PL	0.3578	0.6420				none
25MP	0.3759	0.6114^1	0.7116^1			fcc
25DX	0.3775	0.6364^1	0.7417^1			fcc
20PL	0.3341	0.6231				none
20MP	0.3792	0.5429^2	0.6582^2	0.7367^2		bcc
20DX	0.3692	0.5412^2	0.6114^1	0.6665^2	0.7116^1	fcc+bcc

Table 3.3 Identified peak positions (in units of nm^{-1}) and identified phase at 70°C. Superscripts indicate ^{1}fcc peaks and ^{2}bcc peaks, based on their position relative to the fundamental peak. Table reproduced from[66].

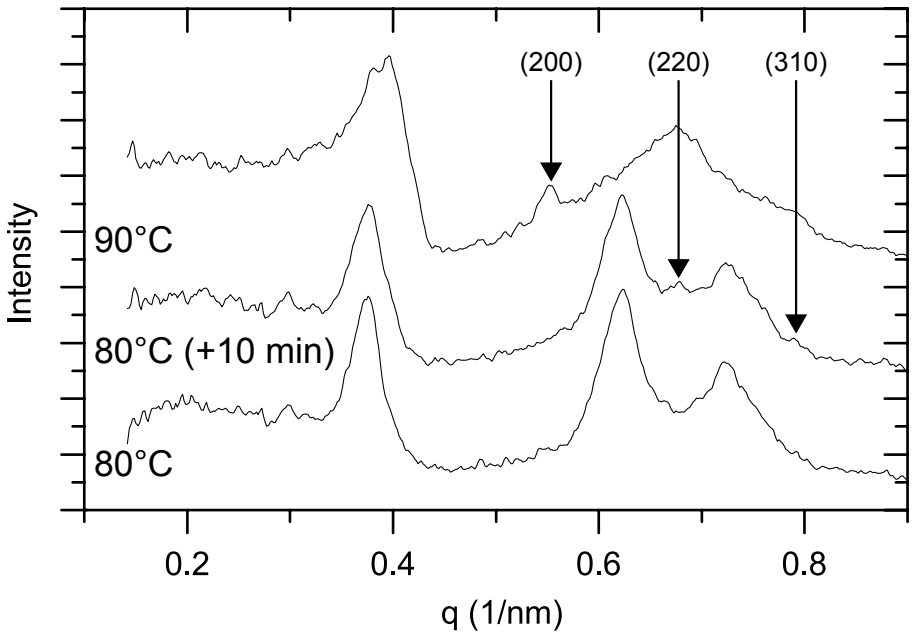

Figure 3.6 Transition from an fcc structure to a bcc structure at high temperatures for a 30% F127 solution. The lines from bottom to top show the sample at 80°C, at 80°C after additional incubation, and finally an increase to 90°C. Arrows indicate the (200), (220), and (310) peaks of the bcc phase. The two large peaks flanking 0.7 nm^{-1} in the 80°C lines are the (220) and (311) peaks of the fcc structure. Figure adapted from[66].

3.3.b. Dynamic temperature measurements

Figure 3.7 compares the results of two dynamic heating experiments. In each graph, the depth scale (going into the page) indicates the system temperature, and the scaling between graphs (a) and (b) is conserved, even though the limits of the temperature ramp have been changed to account for the lowering of T_{gel} with added MP. The graphs clearly illustrate a different behavior in the evolution of the crystalline phase when MP is added to the system. In the case of neat F127, the appearance of Bragg peaks is sudden and abrupt. Peaks form within the span of 2-3°C, whereas peak evolution in the 30MP sample is more subtle and gradual, emerging over the course of the entire ramp. Additionally, inspection of the 2D scattering patterns of heated 30PL and 30MP samples (Figure 3.8) demonstrate different scattering behavior as well. The appearance of the

ring structures in the 30PL case has a nonuniform or "speckled" appearance. Similar descriptions of this behavior have been noted by Wanka *et al*.[8] who noted that patterns of 30% F127 gels observed via SANS exhibited "high intensity spikes superimposed on [a] smooth correlation ring". This is different to what is observed with 30MP, where the ring appearance is comparatively smoother and more uniform.

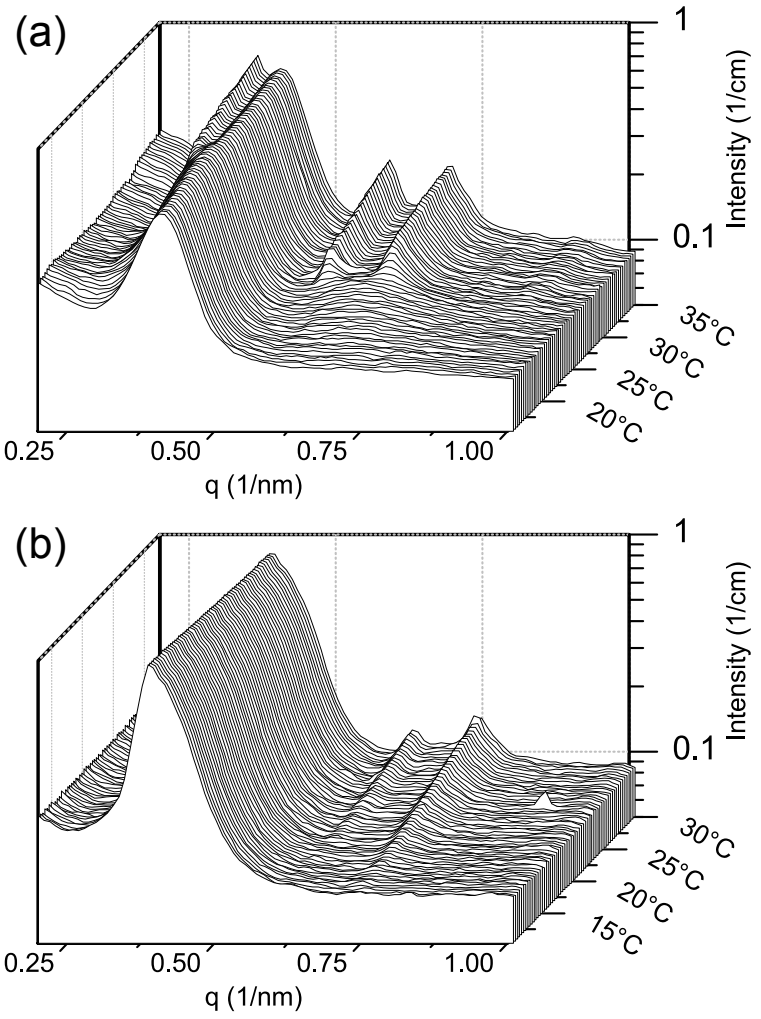

Figure 3.7 Dynamic temperature test of 30PL (a) and 30MP (b) samples heated at a rate of 1°C/min through their gel transition temperatures: 15-35°C for 30PL and 10-30°C for 30MP, respectively. The appearance of the ordered phase is more abrupt in 30PL vs. 30MP. Figure reproduced from[66].

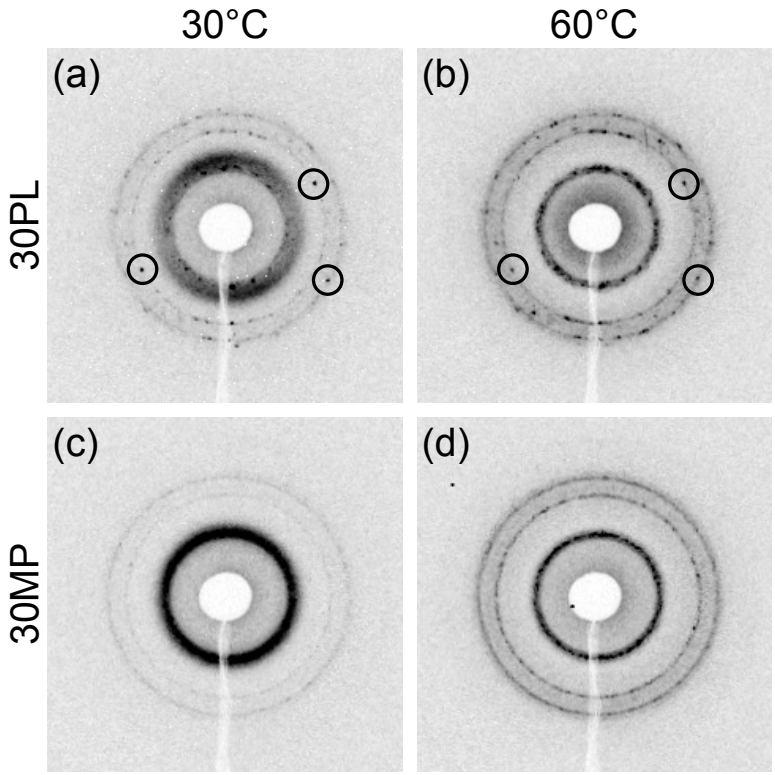

Figure 3.8 2D scattering patterns of 30PL (a, b) and 30MP (c, d) samples at both 30 and 60°C. Diffraction spots that appear (a) do not move as the temperature is further increased (circled examples); however new spots appear as additional crystalline domains are nucleated. Figure reproduced from[66].

3.3.c. Dynamic light scattering

Figure 3.9 shows the distribution of hydrodynamic radii as a function of scattering angle. Higher measured scattering angles resulted in lower reported values of R_h. The greatest variation in R_h was seen at the lower scattering angles. At these lower scattering angles (less than 60°), the samples containing MP demonstrated a lower R_h than the neat F127 samples. At the higher scattering angles, however, these differences vanished. Comparing these results directly to literature suggested that the higher angle values were more accurate, as our results were comparable to the values reported by others using DLS[50,74,75]. However, it is important to note that all of the DLS work previously reported

in literature only reported R_h values collected at a 90° scattering angle. Therefore, it is impossible to tell if the low angle values presented here have any significance.

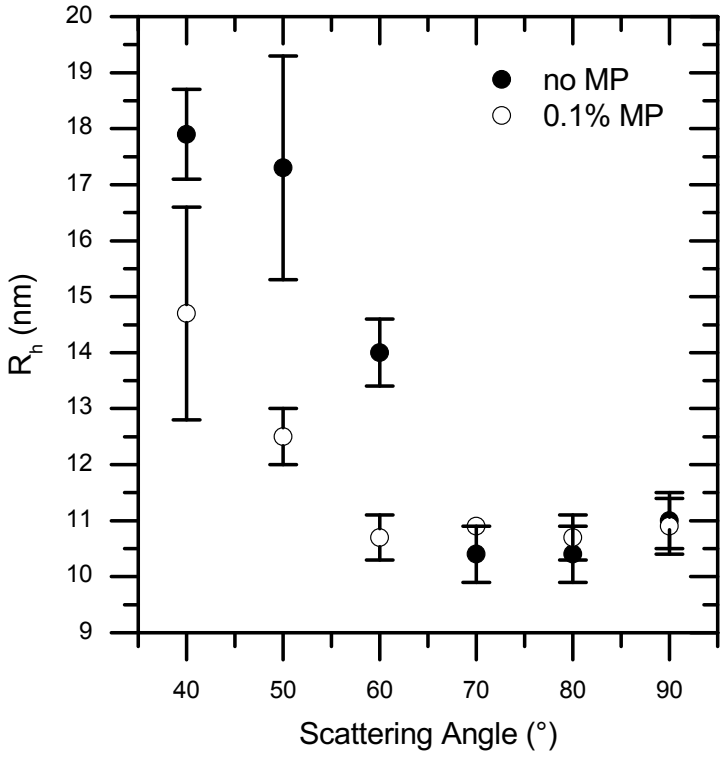

Figure 3.9 Hydrodynamic radius (R_h) as a function of scattering angle. The filled circles indicate neat 1% F127 solutions and the open circles indicate 1% F127 solutions with 0.1% added MP. Figure reproduced from[55].

Using DLS, information regarding the size distribution of micelles in solution can also be obtained. Figure 3.10 compares the distribution of the normalized probability intensity as a function of R_h for a 1% F127 solution both with and without 0.1% added MP. This trend was consistent over all collected scattering angles, but was most pronounced at the presented 70°C scattering angle. Sharma *et al*.[47] noted the same behavior, based on their analysis of SANS data.

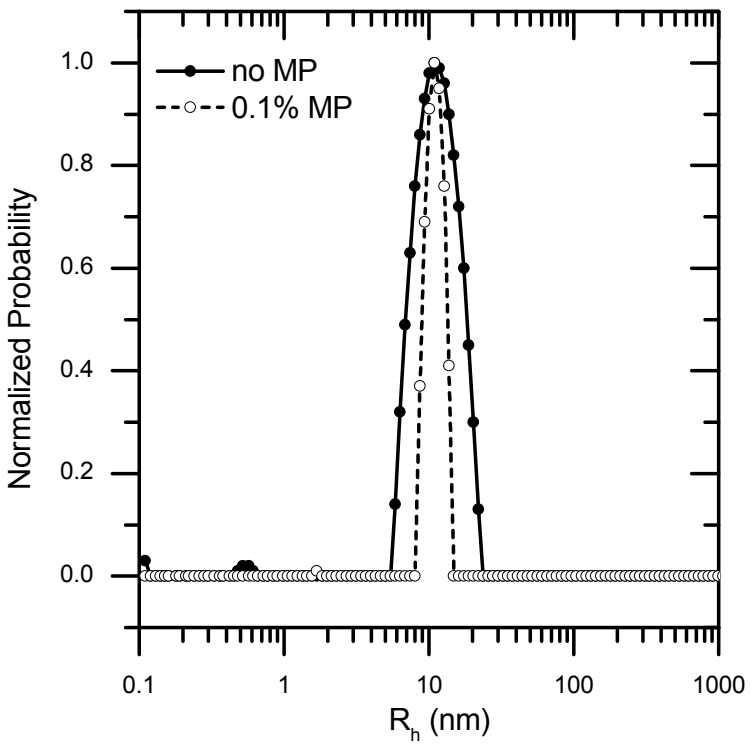

Figure 3.10 Normalized probability intensity as a function of R_h reported for two representative 1% F127 samples, one containing MP (open circles) and one without (filled circles). The sample containing MP has a decreased polydispersity. Figure reproduced from[55].

3.3.d. Scout tests of other additives

In addition to MP and DX, three additional additives were tested, magnesium citrate (MC) and cisplatin (CP). Figure 3.11 shows data collected for magnesium citrate, and Figure 3.12 shows data collected for cisplatin. A control sample of 30% F127 and a test sample of 30% F127 with propylparaben (PP) are shown in Figure 3.13. Peak positions were identified for the 70°C temperature and listed in Table 3.4. The presence of a peak at ratio 1.825 suggests the possibility of the gyroid phase for the 30PL sample, although an expected peak at ratio 1.527 (corresponding to the gyroid (321) phase) is missing[67]. Therefore, a definitive conclusion is difficult to draw. The presence of both fcc and bcc

peaks are indicative of other samples previously run at higher temperatures, where both fcc and bcc peaks were identifiable (Figure 3.6).

Sample	Peak Position	Calculated Ratio	Identified Peak
30PL	0.3501	1.000	fcc (111)
	0.4026	1.150	fcc (200)
	0.5776	1.650	fcc (220)
	0.6389	1.825	gyr (420)[1]
	0.6826	1.950	fcc (311)
30PP	0.3501	1.000	fcc (111)
	0.5864	1.675	fcc (220)
	0.6301	1.800	gyr (420)/bcc (211)*
	0.6826	1.950	fcc (311)
30CP	0.3501	1.000	fcc (111)
	0.4988	1.425	bcc (200)
	0.6301	1.800	gyr (420)/bcc (211)*
	0.6914	1.975	fcc (222)/bcc (220)
20MC	0.3501	1.000	fcc (111)
	0.5864	1.675	fcc (200)
	0.6301	1.800	gyr (420)/bcc (211)*
	0.6914	1.975	fcc (222)/bcc (220)

Table 3.4 Peak positions and calculated ratios for selected datasets at 70°C from the 12-BM beamline. [1]Indicates a possible gyroid phase in the 30PL sample. [2]Possible gyroid phase or bcc (211) peak based on the bcc peak positions listed in Table 3.1.

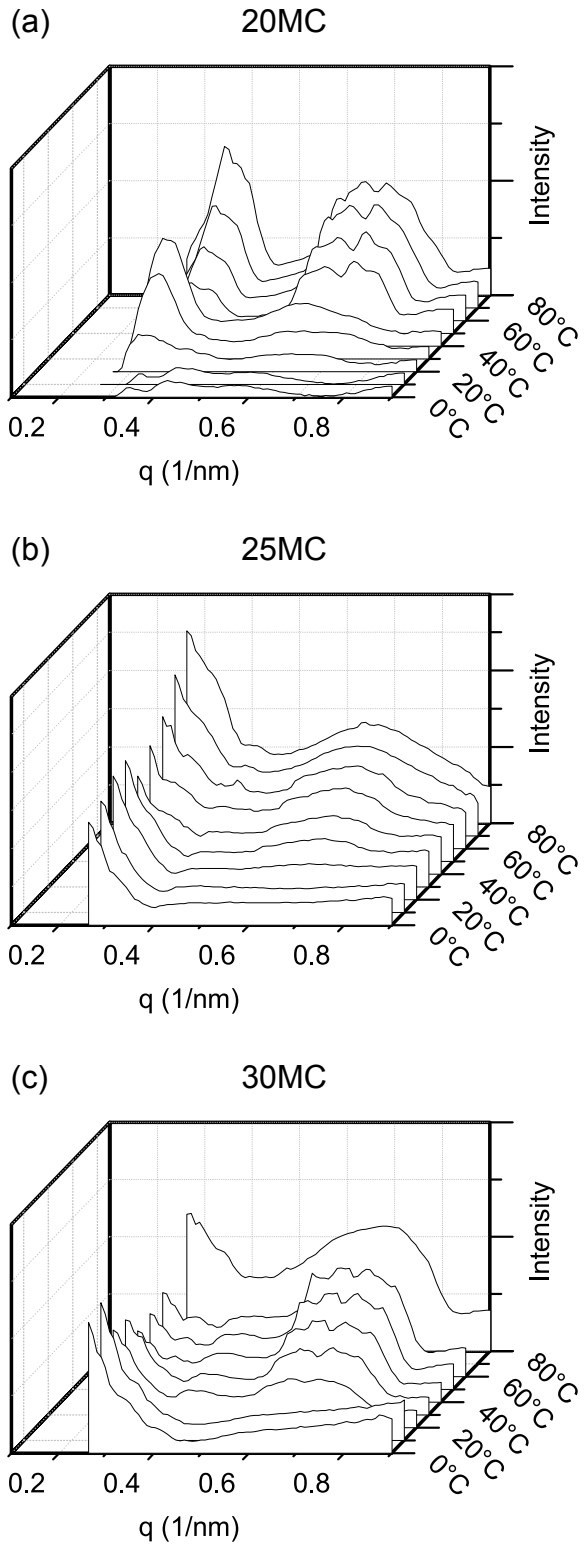

Figure 3.11 Intensity vs. *q* plots for 20-30% F127 solutions containing magnesium citrate (1% wt/v).

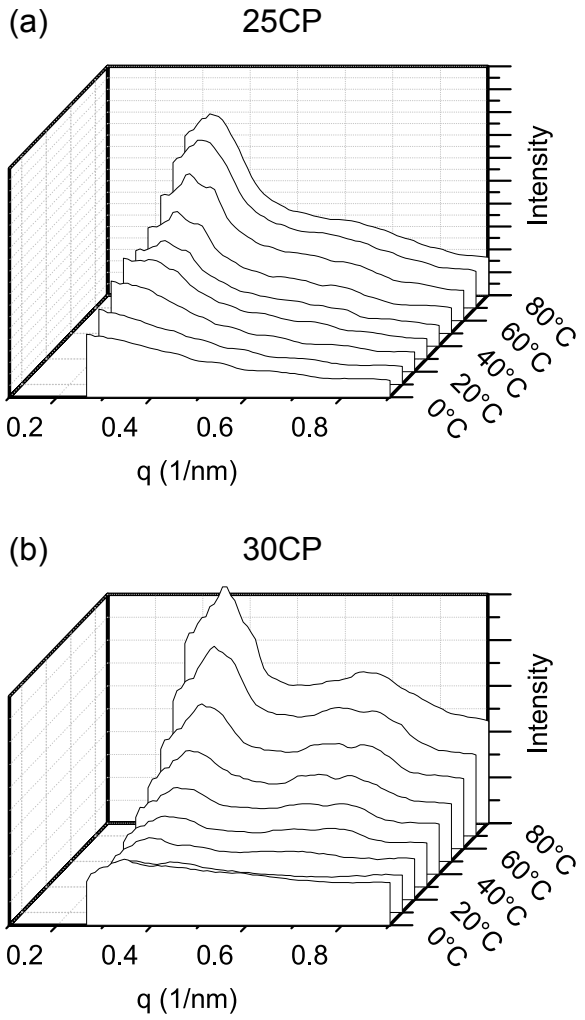

Figure 3.12 Intensity vs. *q* plots for 25-30% F127 solutions containing cisplatin (1% wt/v).

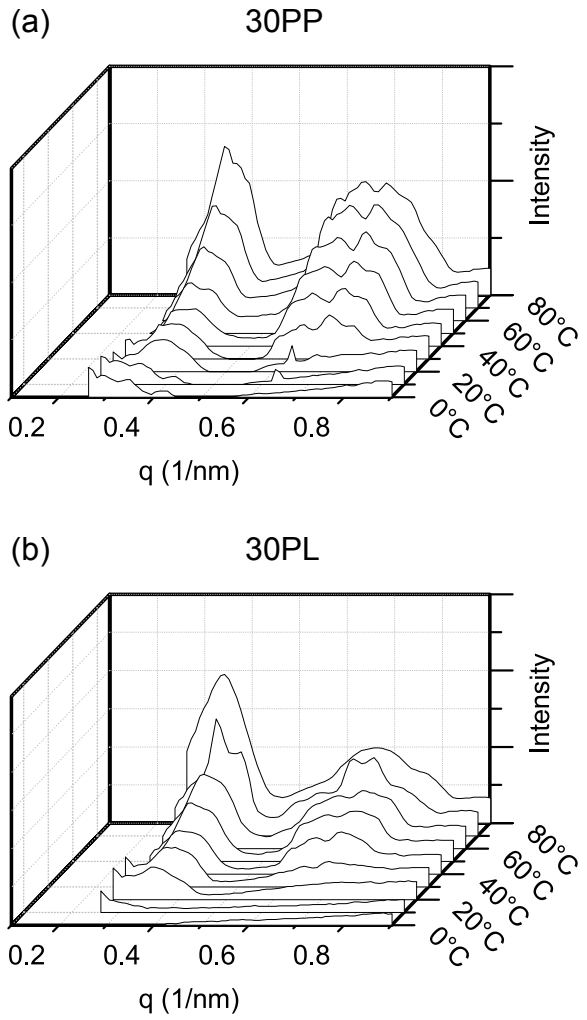

Figure 3.13 Intensity vs. *q* plot for a 30% F127 solution containing propylparaben (1% wt/v). Control solution of 30% F127 is shown in (b).

3.4 Discussion

3.4.a. Evolution of ordered phases in neat and MP-containing solutions

The following process describes the evolution of the ordered phase for 30PL samples, as can be seen in Figure 3.7 (a). At the beginning of the test, a broad amorphous scattering peak indicates the presence of micelles, but no periodic structure. Starting at

around 25°C, three distinct peaks appear. Their positions in reciprocal space (q = 0.367, 0.592, and 0.700 nm^{-1}) can be traced to the fcc lattice structure (having ratios of 1, 1.61, and 1.91, respectively). The amorphous scattering halo is still clearly visible at the onset of the ordered phase, and as the temperature is increased towards the end of the dynamic temperature ramp, the presence of the amorphous halo is still clear. This suggests that "free" micelles are still present in the solution, which have not collected into any ordered phase. Extending this behavior to high temperatures, as can be seen in Figure 3.8, the intensity of the amorphous halo decreases between the 30°C and 60°C images (a, b). A corresponding increase in the intensity and number of scattering centers arranged in rings can also be seen. This indicates that as the temperature of the solution is increased, more and more "free" micelles are incorporated into ordered phases. Furthermore, the distinct scattering spots that appear remain stable throughout the experiment. Once a scattering spot forms, it does not move or disappear for the remainder of the heating ramp (circled examples in Figure 3.8). As the temperature is increased, additional spots form as new ordered domains are created. This data suggest that the mechanism by which the ordered structure develops is that of a heterogeneous nucleation and growth mechanism. Individual domains of ordered phase are created, and grow in size as the temperature is increased.

Comparing the scattering patterns for the 30MP samples shown in Figure 3.7 (b) and Figure 3.8 (c, d), clearly different behavior is observed. The onset of the peaks in Figure 3.7 is more gradual and occurs over the span of 15°C or more, and in fact the peak intensity continually rises through the end of the experiment. The appearance of the rings (Figure 3.8) is much more uniform around the circumferential axis. Fewer discrete spots

are resolved, rather replaced with a continuous scattering ring. This suggests that the evolution of the fcc phase in F127 samples containing MP exhibit a homogenous nucleation and growth behavior.

This conclusion may at first seem contrary to the results presented in Chapter 2, where added MP accelerated the gelation rate and produced a faster rise in viscosity. Further consideration, of the states of each solution, however, might lead to an explanation. In the case of neat F127, large domains of ordered phase are being nucleated in solution. In Callister's review on thermoreversible gels[23], he describes a process in which phase connectivity via adhesion of distinct phases occurs, thus forming ramifying aggregates. Systems like these typically form paste-like gel behavior, which is similar to that observed with F127 micelle gels. In this instance, individual domains of ordered micelles can be considered as the distinct phases. If the number of ordered phases is low but their size large, they may not as readily encounter each other, akin to a "plum pudding" situation, wherein discrete regions of phase (plums) exist in a larger continuum of solution (pudding). In this situation, phase connectivity is delayed as the number of domains is insufficient to form ramifying aggregates. Now consider the behavior of the F127 solutions containing MP. Larger numbers of smaller ordered domains are nucleated, and thus groups of ramifying aggregates develop more easily. So while it may seem that there is less overall order in the solutions containing MP (as evidenced by lower peaks), their distribution amongst the bulk of the solution cause macroscopic gel-like behavior more readily than that of the neat F127 solutions[23].

3.4.b. Addition of MP causes a shift in peak positions

Table 3.2 and Table 3.3 summarize the positions of identified peaks in representative samples of 30PL and 30MP at 40°C and 70°C, respectively. Comparing the measured peak positions in both tables, a small shift towards slightly higher *q* values (roughly 0.03 nm^{-1}) were observed. The addition of MP reduces the d_{111} spacing in 30% solutions of F127 from 29.35 to 27.61 nm, indicating a slightly more compact lattice. DLS results shown in Figure 3.10 corroborate this observation, as an increase in micelle monodispersity was detected as a result of added MP. A lattice comprised of spherical micelles of greater monodispersity would result in a slightly tighter lattice as fewer sizing defects need to be accommodated for, thus producing the observed shift in peak position. Another explanation for the shift in peak position is found in Figure 3.9. A decrease in micelle size as a result of added MP is observed at low scattering angles, which yields a smaller lattice spacing. However, the discrepancy in the observed results between low and high scattering angles was unexpected. In theory, DLS measurements should be independent of scattering angle. It is not clear why the reported size varies with scattering angle, although it suggests that the needed assumptions to apply in DLS theory did not hold under the experimental circumstances, thus making the mathematical analysis incorrect. A search of the literature revealed that there were no experiments measuring F127 micelle hydrodynamic radius using different scattering angles. However, as noted previously, comparisons to DLS data taken by others at 90° revealed similar reported R_h values[1-3].

3.4.c. The presence of additives stabilizes the gel phase

Looking at Figure 3.3, Figure 3.4, and Figure 3.5, it is seen that the presence of the ternary constituents MP or DX result in a stabilization or expansion of the gel phase over a wider temperature range. The onset of ordered phase formation occurred at lower temperatures for the samples including dissolved pharmaceuticals, which corroborate the measurements recorded in the previous chapter concerning the temperature-dependent viscoelastic properties of these formulations. Additionally, the work by Sharma *et al*.[45], who suggested that the *cmt* was reduced due to added pharmaceuticals, is confirmed here, as amorphous scattering halos can be identified at lower temperatures when compared to neat F127 samples (Figure 3.3 and Figure 3.4). At the high temperature regime, the ordered lattice structures persist at higher temperatures as a result of added MP or DX, further broadening the phase space over which F127 gels exist. Considering the DLS observations in Figure 3.10, the observed decrease in polydispersity is likely contributing to the enhanced thermal stability of the gels. Prior work by Yang *et al*.[76] modeling hard-sphere colloidal crystals suggest that increasing polydispersity works to lower the stability of crystalline lattices. Consequently, that the solutions with added MP exhibit lower polydispersity, does serve to explain the increased stability encountered at high temperatures.

3.4.d. Suppression of the primary peak in DX samples

The behavior seen in Figure 3.5 where the primary scattering peak was suppressed over most of the tested temperatures for solutions containing DX was unexpected. The immediate explanation for this observation is that the primary scattering peak is not suppressed at all; rather the first observable peak is the fundamental peak of a different

crystal phase and/or lattice spacing. However, this explanation does not address the fact that at high temperatures, a "new" fundamental scattering peak appears at concentrations of 25% F127 or higher. Furthermore, it would be a remarkable coincidence for the primary and first higher-order scattering peak in these samples to line up so closely with the higher-order scattering peaks of similar F127 samples. Table 3.2 and Table 3.3 show that the measured peak positions of the DX samples line up almost exactly with that the PL and MP samples. Lastly, assuming the first visible peak in each reading is indeed the fundamental peak, the positional ratios of the higher-order peaks would not correspond to any known crystal structure. When taking these considerations into account, it is ultimately more plausible to conclude, however unexpectedly, that the fundamental scattering peak is indeed being suppressed.

A review of previously published literature resulted in only a single reported case of a similar phenomenon, where fundamental scattering peak suppression was seen in thin films of poly(alkoxyphenylevevinylene-*b*-isoprene) rod-coil copolymers arranged into lamellar structures[77]. The authors of that study were also unable to explain the cause of this effect. Some possible explanations of this behavior may emerge after consideration of where the ternary solutes (in this case dexamethasone) segregate within the micelle system. Previously, Nagarajan[41,42] measured the solubility of hydrocarbon chains ("guest" molecules) in PEO-PPO-PEO micelles. As is to be expected, the amphiphilic polymer chains serve to increase the solubility of these guest molecules in aqueous solution. Considering the hydrophobicity of the hydrocarbon chains, it is likely that the guest molecules segregate to the micelle core, which is (relatively) more hydrophobic than the micelle shell, or than the interstitial spaces between micelles. Nagarajan

proposed two situations, one where the guest molecules distribute themselves evenly throughout the micelle core, or one where the increased hydrophobicity of the molecules creates an additional segregated phase, forming a central "core within a core" or "inner core" of highly hydrophobic guest molecules, surrounded by an "outer core" of PPO center blocks, and finally the micelle shell. Similar studies conducted to measure the interaction of solubilized additives within PEO-PPO-PEO micelles also revealed that these additives tended to segregate to within the micelle cores[78-80], although it was not determined whether the additives formed a segregated phase within the micelle cores.

Based on this prior work, and considering the fact that the *n*-octanol/water partition coefficient of DX is ~1.95[81], it is reasonable to assume that the dissolved DX in the solutions tested here also preferentially segregate into the micelle cores. Whether the DX molecules segregate further to form their own "inner core" of DX molecules or whether they remain evenly distributed within the micelle core is unknown, however, if a secondary inner core of DX was forming, it is possible that core-shell interactions between the DX inner core and the PPO outer core could result in peak suppression. One criticism of this explanation is why similar behavior was not observed for MP containing solutions. Although the octanol-water partition coefficients of DX and MP are very similar (1.95 and 1.96, respectively[59,81]), the size of the DX molecule is much larger than that of MP. This might suggest that steric hindrance or other intermolecular interactions may affect each solute differently, owing to their different sizes. Thus, while it may be more feasible for the smaller MP molecule to work its way around the PPO core of the F127 micelle, the larger DX molecule may be more constrained owing to its larger size, and thus preferentially segregates into an additional inner phase.

Finally, it is possible that the primary peak is still present, just reduced in intensity such that it is not resolvable from the background noise of the detector. During the experiments, minimal capture times were used in order to maximize the number of samples or repetitions to be measured during the allotted beam time. This may have resulted in capture times that may not have been high enough to resolve fine or weak features in the data. While this is true, and likely the case, it does not address the fact that the difference in intensity between the first and second peaks is so great. As evidenced by the high temperature, high F127 concentration samples in Figure 3.5, even when the primary scattering peak does appear, its intensity is greatly reduced compared to that of the first higher-order peak. This relationship holds constant for all DX samples observed. Peak fitting routines were attempted on the collected data, using theoretical curves from the NIST Center for Neutron Research (NCRC)'s SANS analysis package. While the fitting routines could match the positions of the peaks (confirming the fcc structure), they failed to produce a definitive match for the intensity ratios. It is currently unknown as to why a match could not be found, or the root cause of this observation. Further study in this area would be merited, as it may shed new understanding on the effects that added DX have on the micelle lattice in F127 gels.

3.4.e. Emergence of bcc phases at high temperatures

At the highest temperatures tested, 80-90°C, peaks from multiple crystal systems were occasionally identified. Mortensen *et al*.[2] also reported a fcc to bcc transition at roughly 25°C in F127 samples that had been purified of diblock impurities. The lower temperature at which the transition occurs is attributable to the purified F127 used in their study. Others have reported similar fcc to bcc transitions in polystyrene-polyisoprene

and poly(oxyethylene)-poly(oxybutylene) diblock copolymer systems[82,83]. Figure 3.6 illustrates a more detailed study into this phenomenon. At 80°C, analysis of the visible peaks results in the structure being classified as being in the fcc phase. After incubating the sample for an additional 10 minutes at 80°C, however, new peaks begin to emerge which correspond with the bcc crystal system. Finally, increasing the temperature further to 90°C results in the bcc phase becoming dominant with fcc peaks no longer being distinguishable in the sample. Softer or thicker micelle coronae tend to favor a bcc packing arrangement whereas harder, thinner coronae tend to favor the fcc packing arrangement[2]. At high temperatures, a softening of the micelle corona could conceivably result in a transition to the bcc-favored condition. Such a transition was also predicted in theoretical calculations by Semenov[84]. While the identification of bcc phases was seen in a wider variety of samples and compositions, it was not regularly identified in any one concentration or formulation, indicating that the presence of pharmaceutical additives did not have an appreciable effect on the observation of this phenomenon.

3.4.f. Scout tests of other additives

The data in Figure 3.11, Figure 3.12, and Figure 3.13 show the result of preliminary studies to testing the additional solutes MC, CP, and PP respectively. Overall, the quality of data from this experiment was relatively poor, with low signal to noise ratio and possible instrument smearing. Additionally, the sample to detector distance at the APS 12-BM beamline was rather less than at other beamlines (roughly 0.8 m as opposed to almost 2 m for the APS 5-ID and BNL X10A), meaning that q resolution of the collected data suffered as well. However, peak positions were determined and indexed as presented in Table 3.4.

The presence of a peak at a ratio of 1.825 for the 30PL sample indicates the possible presence of the gyroid phase, the peak at 1.825 corresponding to the (420) peak of the gyroid structure[67]. However, there should also be a peak at a ratio of 1.527, which was not seen. Lattice defects could be responsible for the suppression of the peak at 1.527, however considering the quality of the data a definitive conclusion cannot be made. Other Pluronic systems have exhibited gyroid structures, particularly surfactants with a lower PEO-PPO ratio or when studied in a mixture of both aqueous and nonpolar solvents[67]. However, for Pluronic F127 the consensus of the literature is that the micelles arrange into cubic domains.

Other concerns with the interpretation of these results include the low solubility of the tested additives in the solution. Cisplatin, for example, is practically insoluble in water. When 1% wt/v CP Was added to F127 solutions, virtually none of it solubilized, even after prolonged sonication and incubation. Therefore, the I(q) plots shown in Figure 3.12 may simply reflect the scattering pattern of neat F127, as the vast majority of CP in the solution simply serves as a particulate contaminant. At high temperatures, interesting behavior was also observed for the CP samples. Typically, solutions containing CP are yellowish orange in color, owing to the color of dry CP. In one instance, the CP solution turned very dark brown after the heating experiment had been completed. It is currently not known why the color of the solution changed, but in addition to the color change, a very large increase in scattering intensity was observed. So large was this increase that the detector was saturated by the end of the one-minute capture period. A second run of the CP samples did not result in the large scattering intensity increase, but a darkening of

the solution was also observed. It is possible that the heat has denatured or damaged the CP molecules.

Added magnesium citrate (MC) also produced inconsistent results. While scattering peaks were visible in the 20 and 30% F127 solutions, the 25% did not exhibit the same prominent scattering behavior. It is possible that more repetitions of this sample would have resulted in more consistent data, but time constraints limited the number of experimental studies that were performed with additional additives.

3.5 Chapter summary

This chapter covers a detailed study into the structure of the micelle gels that solutions of Pluronic F127 surfactants create as they are heated. The effects of added pharmaceutically relevant constituents such as methylparaben and dexamethasone were also investigated. Both static and dynamic tests were conducted to determine both the thermodynamic phase behavior of these systems, as well as the transient kinetics involved with the formation and growth of the crystalline phases.

Novel behaviors were observed as a result of these investigations. It was determined that the presence of added MP alters the appearance of ordered phase behavior from a heterogeneous to a homogeneous nucleation and growth. This observation can be correlated with the observed viscoelastic response discussed in Chapter 2, as well as experimental observations made by previous researchers[47].

The suppression of the primary scattering peak for samples containing dexamethasone are an indication that the interactions between F127 and DX are different than those of F127 and MP, despite the fact that both are hydrophobic small-molecule

additives added to an amphiphilic copolymer system. This topic warrants further investigation as the observed results were consistent across many samples and even multiple beamlines and setups, and observations which have thus far not been reported on in the literature. However, in order to further study this phenomenon, considerable effort is likely required to determine the cause of this scattering behavior. An ideal follow-up to these experiments is to use SANS in a series of similar experimental protocols. The ability to selectively deuterate portions of the polymer chain, pharmaceutical additive, or solvent will extend considerably one's ability to better resolve where within the micelles these added molecules reside, and perhaps the manner in which they interact with the Pluronic copolymer chain.

Chapter 4

Thermophysical Properties of Pluronic Micellization

4.1 Introduction

In Chapters 2 and 3, the viscoelastic and structural characterization of F127 gel formation was carried out. In addition to these tests, experiments were carried out using differential scanning calorimetry (DSC) to measure the thermophysical properties of F127 gel formation. It is important to remember the mechanism by which gelation occurs in aqueous solutions of Pluronic surfactants. Gelation in Pluronic surfactants is achieved by cubic ordered lattices of micelles, otherwise known as "micelle gels"[19,61,85]. There is no chemical crosslinking or physical entanglement that occurs, giving rise to the reversible nature of the gel transition.

Two distinct stages in the phase behavior of the solution are encountered as the temperature is raised. First, at the lowest temperatures, there are no micelles present in the solution. When heated through the *cmt*, micelles spontaneously form. The solution at this stage is in a two-phase regime, consisting of disordered micelles and dispersed polymer chains. Heating the solution further causes more micelles to form, and for each micelle to increase in size. Eventually the micelles will arrange into cubic ordered domains[8,12,13]. This disorder to order transition is what gives rise to the gel behavior in Pluronic solutions.

In this chapter, the results of an overview study are presented which looks at the formation of the micelles themselves, prior to any gelation. Some relatively unexpected and new behaviors were observed where the micellization endotherm was suppressed by the presence of added methylparaben. A qualitative analysis of the data was conducted, and several explanations proposed to describe the behavior and trends that are observed in the data. The ultimate product of this study would be to produce a model that can describe the observed behavior and account for the effects of added compounds.

4.2 Materials and methods

4.2.a. Sample preparation

Pluronic solutions used in these experiments were prepared in a similar manner to that described in Chapter 2. In addition to Pluronic F127, the following Pluronic surfactants were tested: F127, P123, L121, F108, P105, P104, L101, P85, F68, P65, L61, F38, and L35. Pluronic F127 and F68 were obtained from Sigma-Aldrich, and the remainder of the Pluronic surfactants was obtained via a generous gift from BASF corp. (Wyandotte, MI). Figure 4.1 shows the positions of these tested Pluronic surfactants (circled) on the Pluronic grid. Table 4.1 lists By testing a variety of samples across the Pluronic grid, factors such as total molecular weight, PEO arm length or PPO block length could be kept constant and systematic trends in the micellization behavior as a function of these factors could be studied. For Pluronic F127, concentrations between 10% and 30% wt/v were tested. The rest of the Pluronic surfactants were tested only at a concentration of 10% wt/v. This concentration was chosen because it allowed for sufficiently easy dissolution of the Pluronic surfactants into aqueous solution, the

micellization endotherms were still sufficiently large to be easily observable via DSC, and the *cmt* of the solution was maximized, so that issues pertaining to operating near the freezing of the solutions were avoided as much as possible.

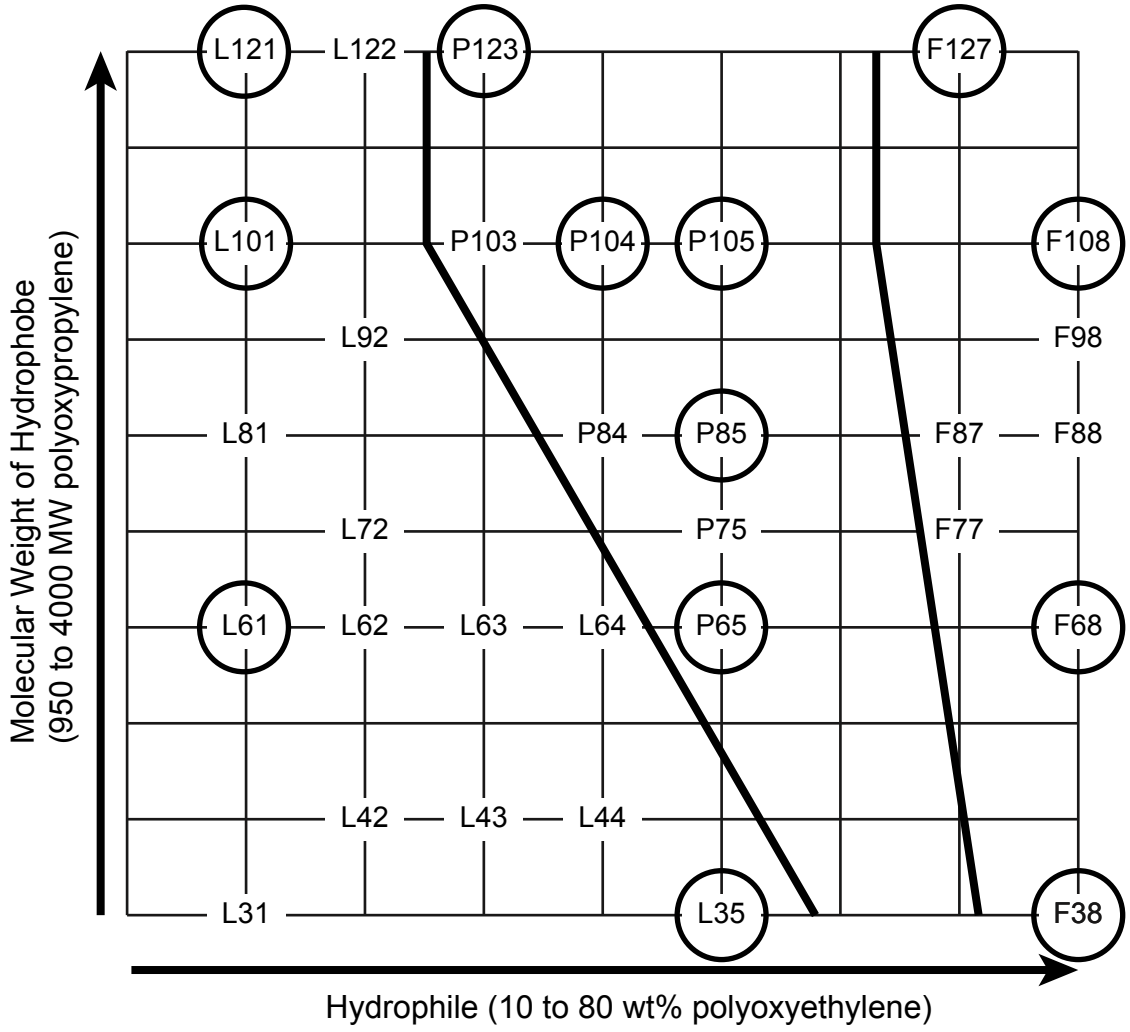

Figure 4.1 Pluronic grid showing commercially available varieties of Pluronic surfactants. Circled items indicate surfactants used in this study.

Pluronic surfactant	$(PEO)_x$	$(PPO)_y$	Approx. molar weight (g/mol)	Percent PEO by weight
F127	99	65	12600	70%
P123	20	70	5750	30%
L121	5	68	4400	10%
F108	132	50	14600	80%
P105	37	56	6500	50%
P104	27	61	5900	40%
L101	4	59	3800	10%
P85	26	40	4600	50%
F68	75	30	8350	80%
P65	19	29	3400	50%
L61	3	30	2000	10%
F38	43	16	4700	80%
L35	11	16	1900	50%

Table 4.1 List of Pluronic surfactants used. Nominal chemical formulae for each are $(PEO)_x(PPO)_y(PEO)_x$. Data compiled from[12,86-91].

To prepare samples for analysis, an empty aluminum TZero™ sample pan was placed onto a microbalance and the weight reading tared to zero. Approximately 10 μL of sample (giving a sample mass of 10 μg) were pipetted into the pan. Care was taken to ensure any bubbles were removed from the solution and that the dispensed solution had wetted the entire bottom surface of the sample pan. The mass of the pipetted solution was recorded and a mechanical press was then used to seal the sample with a TZero™ hermetic sample lid. Completed sample pans were loaded into the Q2000 autosampling tray. As micellization in Pluronic surfactants is a reversible process, one sample could be run through multiple heating ramps, but typically samples were only used for one set of experimental runs.

4.2.b. Differential scanning calorimetry

All DSC experiments were conducted on a TA Instruments (New Castle, DE) Q2000 series DSC with an RCS90 refrigerating unit for cooling. Typical experiments included a single heating ramp starting at a temperature below the *cmt* of the solution, up to typical ending temperature of 95°C. Because the *cmt* of the different formulations can differ significantly from one another, no single universal starting temperature was used. Instead, the starting temperature for each solution was aimed to be as near the freezing point of the solution as possible, without freezing the sample. Higher concentration solutions were started at lower temperatures, owing to a greater freezing point depression. Typical starting temperatures were between -15°C and -5°C. Samples were heated at a constant rate of 10°C/min from the initial to the final temperature. Samples were run a minimum of three times to ensure repeatability.

4.2.c. Data analysis

Data generated by the Q2000 is saved in individual files, which were then opened using the TA Instruments Universal Analysis software. This program allowed for quantitative analysis of the thermogram curves. Typical experiments resulted in a single endothermic peak being detected during each experiment. Three main values were extracted from this peak: the onset temperature (intersection between the baseline and the tangent of the maximum slope in the initial region of the peak), the peak temperature (temperature at which maximum deviation from the baseline is achieved), and the enthalpy of the transition (integrated area between the baseline and the experimental data). Figure 4.2 shows an ideal DSC curve with these values depicted.

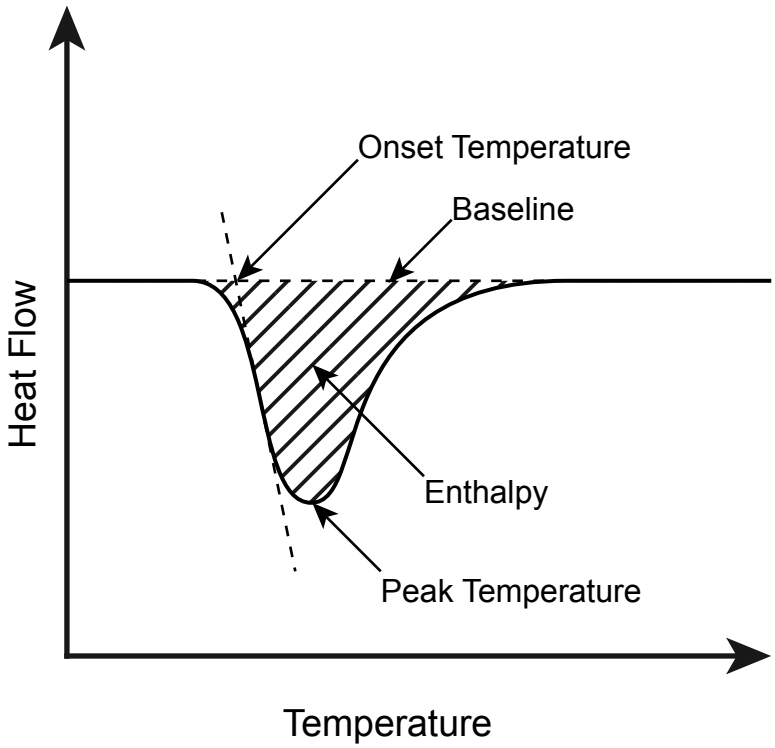

Figure 4.2 Representative DSC micellization endotherm. The labels depict the values measured from each thermogram. The onset temperature is the intersection of the baseline and the maximum slope of the initial portion of the peak. The peak temperature is the maximum deflection from the baseline, and the enthalpy is the total area between the curve and the baseline (shaded).

4.3 Results

4.3.a. Effect of increasing F127 concentration

Figure 4.3 shows a series of DSC thermograms for neat F127 solutions of increasing concentration, ranging from 10 wt% to 50% wt/v. As the concentration increases, the micellization endotherm gets larger, and the peak moves towards lower temperatures. A small secondary endotherm (circles in Figure 4.3) can be seen in the higher concentration solutions. This small secondary peak is associated with F127 gelation, indicating the small endothermic transition associated with micelles ordering into crystal lattices. It is

likely that this peak exists for F127 concentrations that exhibit gelation. However, owing to its small magnitude, it is below the resolving limit for lower concentrations of F127.

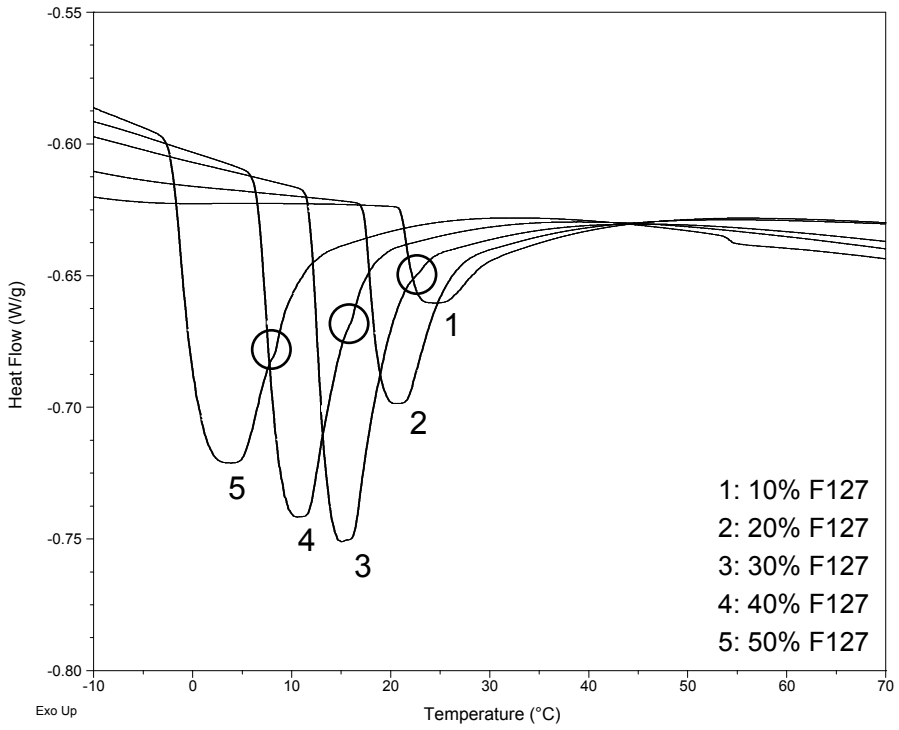

Figure 4.3 DSC thermograms for F127 concentrations ranging from 10 to 50 wt%, in increments of 10%. The numbers 1-5 indicate the curves associated with 10, 20, 30, 40, and 50% F127, respectively. The three circles indicate small secondary endothermic peaks visible for 30, 40 and 50% F127, this is associated with F127 gelation, where the micelles have arranged into crystalline lattices.

4.3.b. Trends in the micellization endotherm for different Pluronic surfactants

Figure 4.4 through Figure 4.9 compare the thermophysical behavior of several different Pluronic surfactants as they were heated. Moving across the Pluronic grid (Figure 4.4 and Figure 4.5), increasing the weight percentage of the PEO block while keeping the PPO core block length constant, leads to smaller and smaller micellization endotherms. The enthalpy of micellization is reduced, while the onset and peak temperatures are increased.

Traversing the Pluronic grid vertically (Figure 4.6, Figure 4.7, and Figure 4.8), keeping the weight percentage of PEO content constant while decreasing PPO core block length, produces a similar. Higher PPO block lengths result in larger micellization endotherms, and the onset and peak temperatures are decreased. The conclusion to draw is that greater PEO content and smaller PPO block length both reduce the enthalpy of micellization, and increase the onset and peak temperatures.

Figure 4.9 compares three Pluronic surfactants with a similar molecular mass. L121 (MW ~4400g/mol), P85 (MW ~4600 g/mol), and F38 (MW ~4700 g/mol) have very different micellization temperatures and enthalpies. Again the general trend is preserved where increasing PPO block length and lower PEO content produces the largest micellization endotherms while decreasing PPO block length and higher PEO content produce the smallest micellization endotherms.

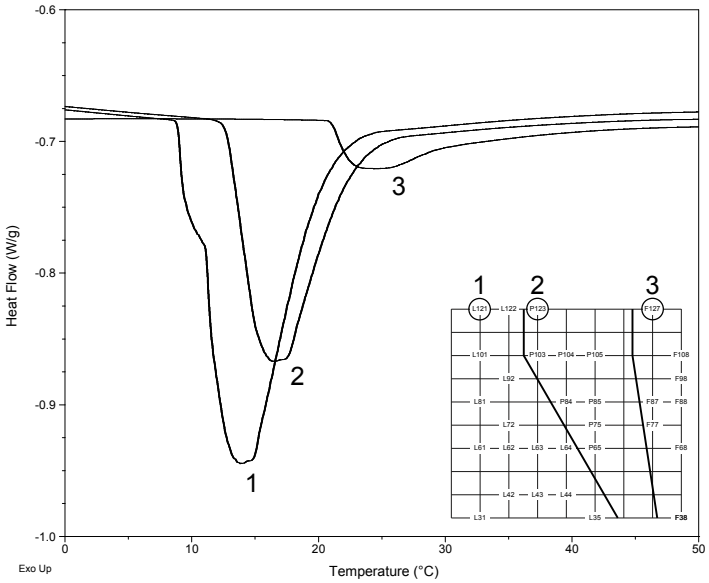

Figure 4.4 10% wt/v Pluronic surfactant series comparing increasing PEO content while keeping PPO block length constant. From numbers 1-3 the surfactants used are L121, P123 and F127, respectively. The curves have been aligned so the initial baseline is consistent for all samples.

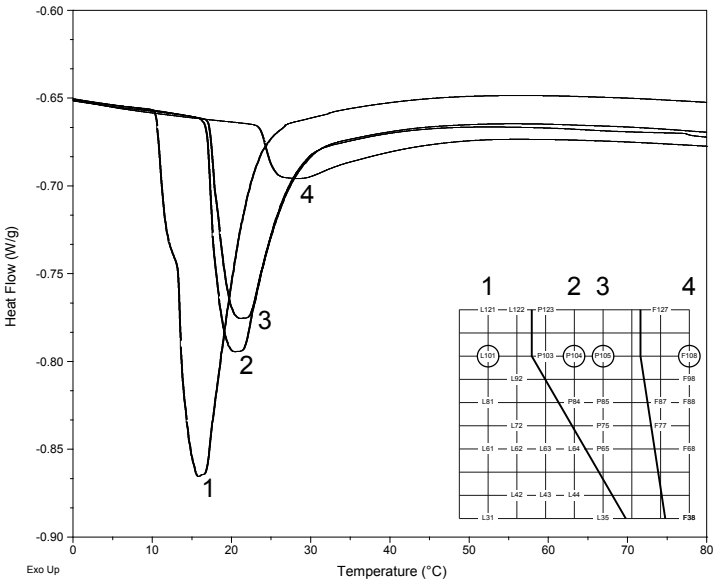

Figure 4.5 10% wt/v Pluronic surfactant series comparing increasing PEO content while keeping PPO block length constant. From numbers 1-4 the surfactants used are L101, P104, P105 and F108, respectively. The curves have been aligned so the initial baseline is consistent for all samples.

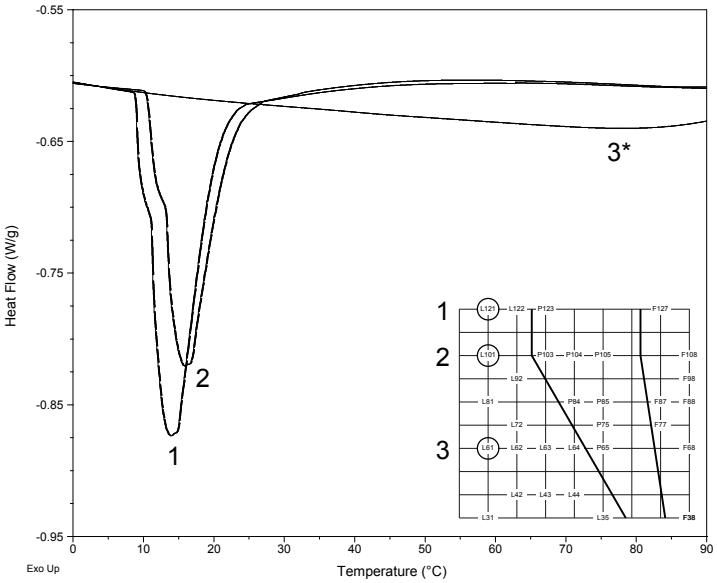

Figure 4.6 10% wt/v Pluronic Surfactant series comparing increasing PPO central block length, while keeping a proportionally constant amount of PEO. From numbers 1-3 the surfactants used are L121, L101, and L61, respectively. (*) It is not entirely clear if surfactant 3 has a resolvable peak. The curves have been aligned so the initial baseline is consistent for all samples.

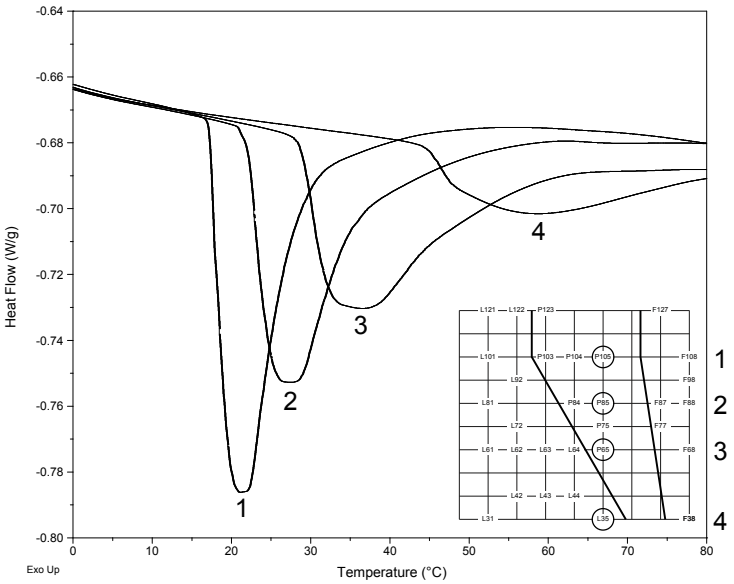

Figure 4.7 10% wt/v Pluronic surfactant series comparing increasing PPO central block length, while keeping a proportionally constant amount of PEO. From numbers 1-4 the surfactants used are P105, P85, P65 and L35, respectively. The curves have been aligned so the initial baseline is consistent for all samples.

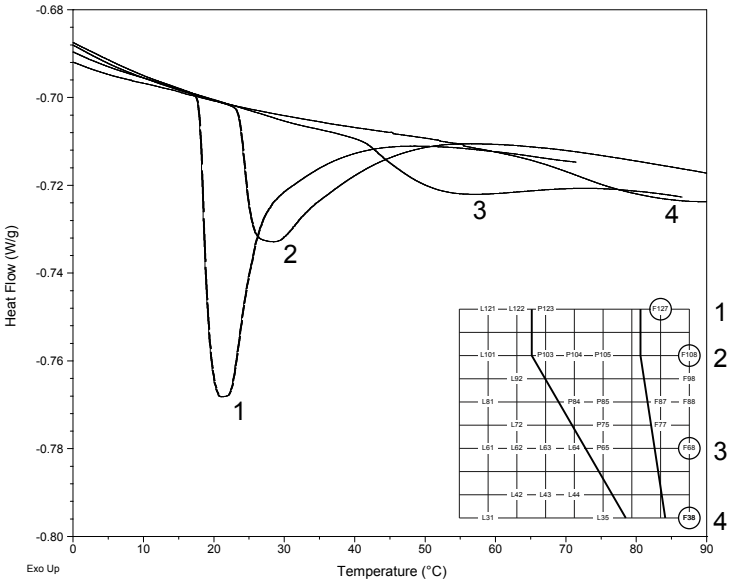

Figure 4.8 10% wt/v Pluronic surfactant series comparing increasing PPO central block length, while keeping a proportionally constant amount of PEO. From numbers 1-4 the surfactants used are F127, F108, F68 and F38, respectively. The curves have been aligned so the initial baseline is consistent for all samples.

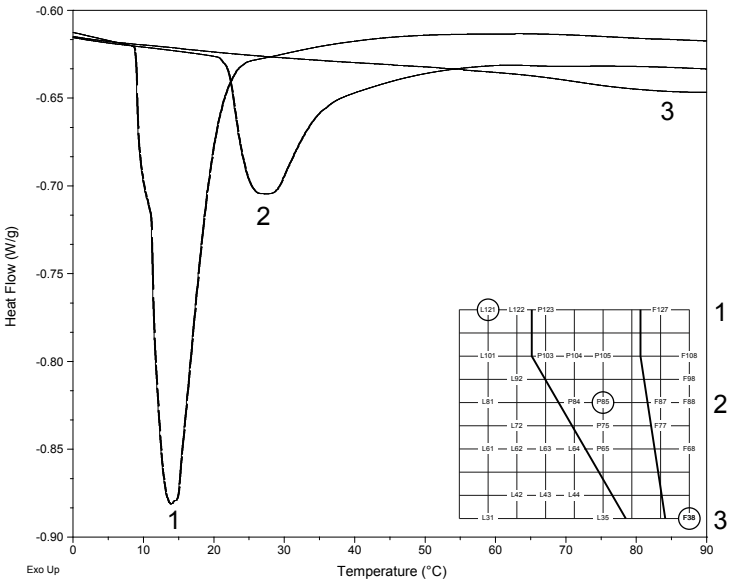

Figure 4.9 10% wt/v Pluronic surfactant series comparing constant molecular weight, while varying the PEO/PPO ratio. From numbers 1-3 the surfactants used are L121, P85 and F38, respectively. The curves have been aligned so the initial baseline is consistent for all samples.

4.3.c. Addition of methylparaben suppresses micellization endotherm

Figure 4.10 depicts a series of DSC thermograms for a solution of 10% F127 with increasing amounts of added MP. Each curve has an additional 0.1% added MP, so the bottom most curve is a neat 10% solution, followed by a 10% F127 solution with 0.1% MP, then 0.2% MP, and so on. As the amount of added MP is increased, the micellization endotherm is increasingly suppressed, resulting in its nearly complete disappearance at 1.0% added MP. In addition, the peak temperature decreases from about 22°C to about 11°C with increasing amounts of added MP.

Figure 4.11 plots the onset and peak temperatures measured from the DSC thermograms in Figure 4.10. Enthalpy values are also plotted using the right *y*-axis. There is a linear dependence on the size of the suppression effect for increasing amounts of added MP. At saturation, the concentration of added MP is roughly 1.5% wt/v, which explains the change in slope from the 1.0% added measurements and the saturated measurements.

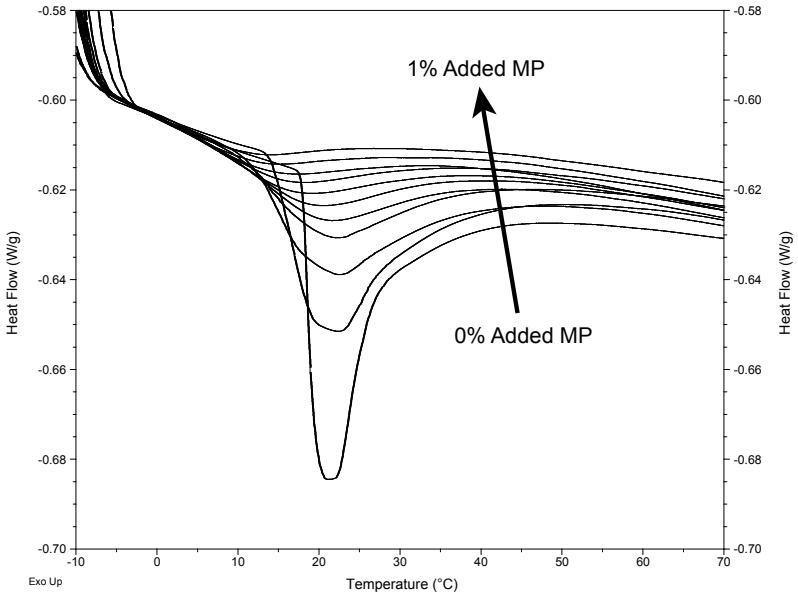

Figure 4.10 10% F127 with progressively increasing amounts (from 0 to 1%) of added MP. The arrow indicates the direction of increasing MP concentration. Each overlaid curve has an additional 0.1% MP added. As increasing amounts of MP are added to the solution, the micellization endotherm is progressively suppressed, and the peak shifts slightly lower in temperature. The curves have been aligned so the initial baseline is consistent for all samples.

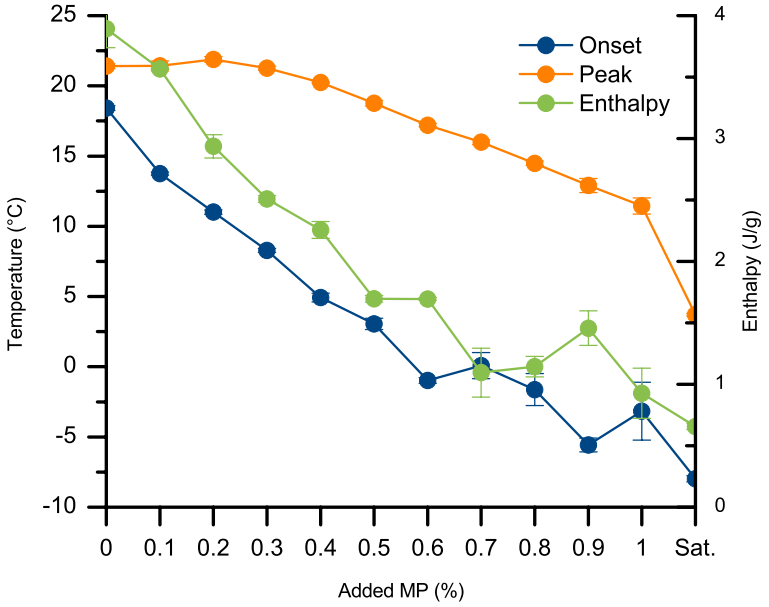

Figure 4.11 Onset temperature, peak temperature, and enthalpy measured for a series of 10% F127 solutions containing increasing amounts of MP.

4.3.d. Added propylparaben produces the same effect as added methylparaben

Figure 4.12 shows a similar experiment as to the one described in 4.3.c, except the additive was propylparaben instead of methylparaben. Again, a similar suppression of the micellization endotherm is observed.

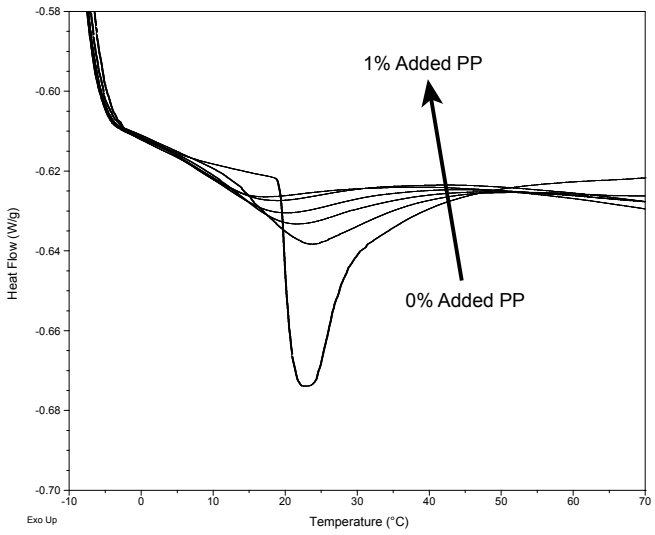

Figure 4.12 10% F127 with progressively increasing amounts (from 0 to 1%) of added PP. The arrow indicates the direction of increasing PP. Each overlaid curve has an additional 0.2% PP added. As increasing amounts of PP are added, the micellization endotherm is again similarly suppressed, as was the case for added MP. The curves have been aligned so the initial baseline is consistent for all samples.

4.3.e. MP also suppresses the micellization endotherms in different Pluronic surfactants

Figure 4.13, Figure 4.14 and Figure 4.15 show the results of similar experiments to that shown in Figure 4.10, performed on solutions of Pluronic P123, F108, and F68. This was done in order to show if different Pluronic surfactants have different suppression characteristics when MP is added. A similar experiment was also attempted for Pluronic L121, however, upon adding MP, white precipitate (presumed to be L121) fell out of solution, and could not be re-solubilized. These specific surfactants were chosen in order

to investigate the effect of decreasing PEO content while keeping a similar PPO block length (F127>P123>L121), or keeping a similar PPO/PEO ratio while decreasing the PPO block length (F127>F108>F68).

Suppression of the micellization endotherm was seen in all cases; however, the magnitude of the suppression varies with the tested surfactant. For F68 and F108 (Figure 4.13 and Figure 4.14, respectively), the micellization endotherm is nearly completely suppressed, as was for F127. P123 (Figure 4.15), however, did not exhibit suppression to the same degree; rather a smaller but still clearly distinguishable micellization endotherm was visible.

Figure 4.16 plots the onset and peak temperatures for the three surfactants F127, P123, and F68 for increasing amounts of added MP. In each case, the distance between the onset and the peak temperatures increases with higher amounts of added MP (a broadening of the peak). The total change in the onset/peak temperature is greater for F68 due to added MP than F127 or P123, indicating that the addition of MP is most sensitive to PPO block length.

Figure 4.17 plots the enthalpy of micellization for F127, P123, and F68 for increasing amounts of added MP. For Pluronic P123, there is a linear relationship between the decrease in the enthalpy of micellization and the amount of added MP. For F127, the enthalpy approaches an asymptotic limit as the MP concentration increases. F68 experiences both the smallest absolute and relative change in the enthalpy. The suggestion of an absolute "minimum" enthalpy is seen (about 1 J/g) as added MP was not able to suppress the enthalpy values further.

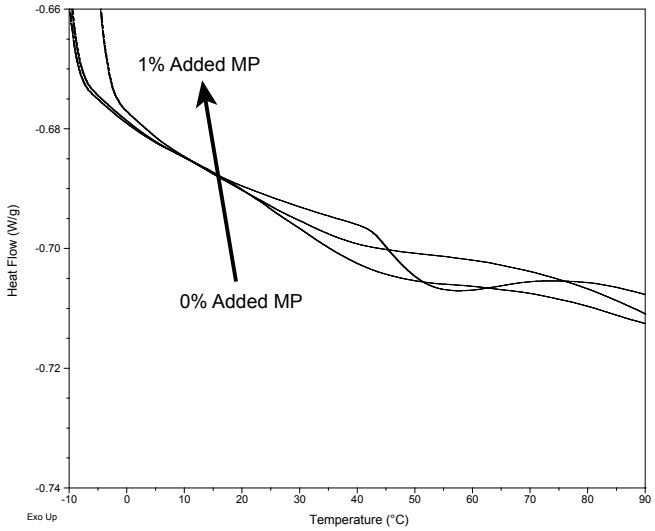

Figure 4.13 10% wt/v Pluronic F68 with progressively increasing amounts (from 0 to 1%) of added MP. The arrow indicates the direction of increasing MP. Each overlaid curve has an additional 0.5% MP added. As increasing amounts of MP are added, the micellization endotherm is suppressed, as was the case for F127. It should be noted, however, that for the 1% added MP curve, the solution was already saturated with MP and thus the actual concentration was somewhere between 0.5% and 1% MP. The curves have been aligned so the initial baseline is consistent for all samples.

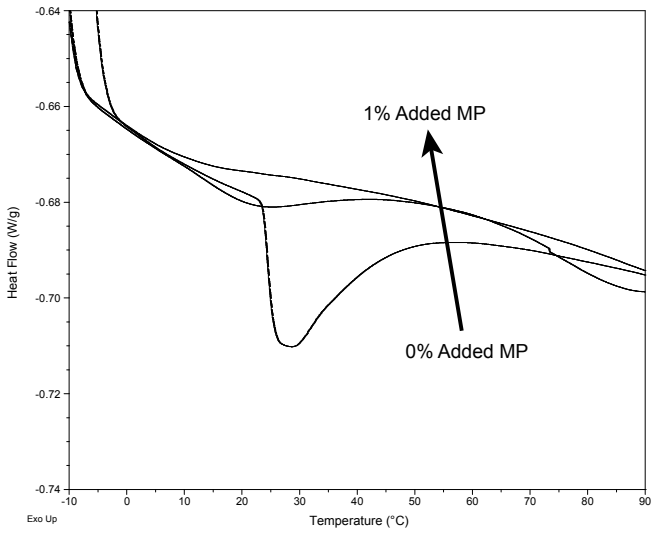

Figure 4.14 10% wt/v Pluronic F108 with progressively increasing amounts (from 0 to 1%) of added MP. The arrow indicates the direction of increasing MP. Each overlaid curve has an additional 0.5% MP added. As increasing amounts of MP are added, the micellization endotherm is suppressed, as was the case for F127. The curves have been aligned so the initial baseline is consistent for all samples.

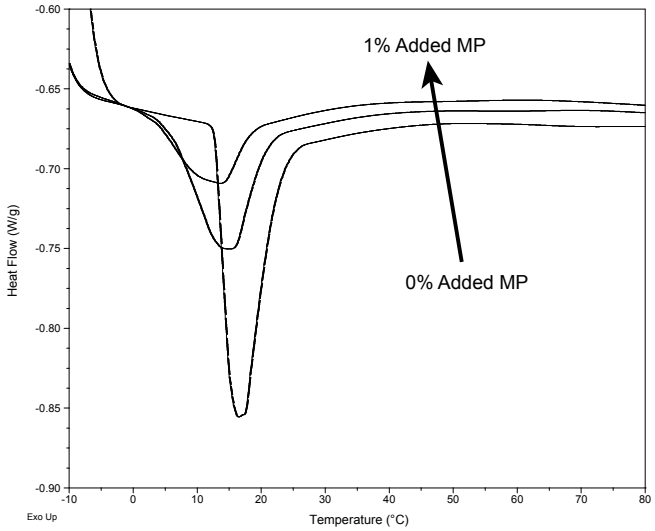

Figure 4.15 10% wt/v Pluronic P123 with progressively increasing amounts (from 0 to 1%) of added MP. The arrow indicates the direction of increasing MP. Each overlaid curve has an additional 0.5% MP added. As increasing amounts of MP are added, the micellization endotherm is suppressed, as was the case for F127. The curves have been aligned so the initial baseline is consistent for all samples.

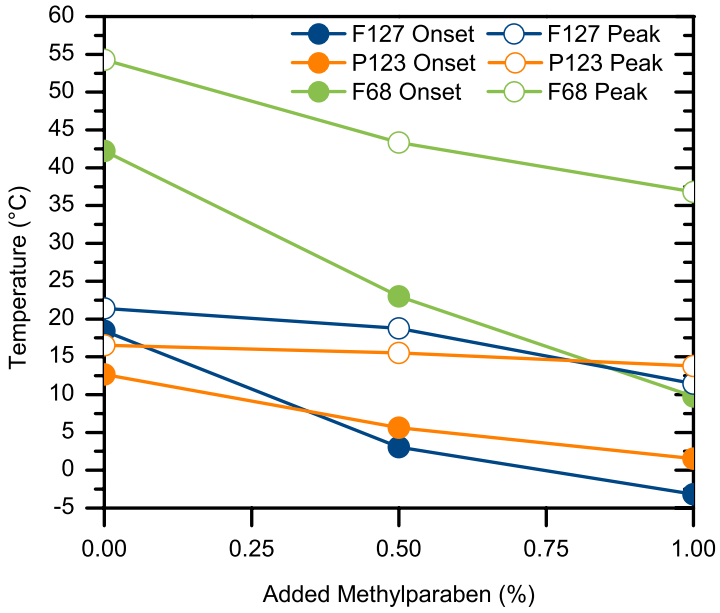

Figure 4.16 Onset and peak temperatures for Pluronic F127, P123, and F68 with increasing amounts of added methylparaben. The F68 solution was already saturated prior to 1% added MP.

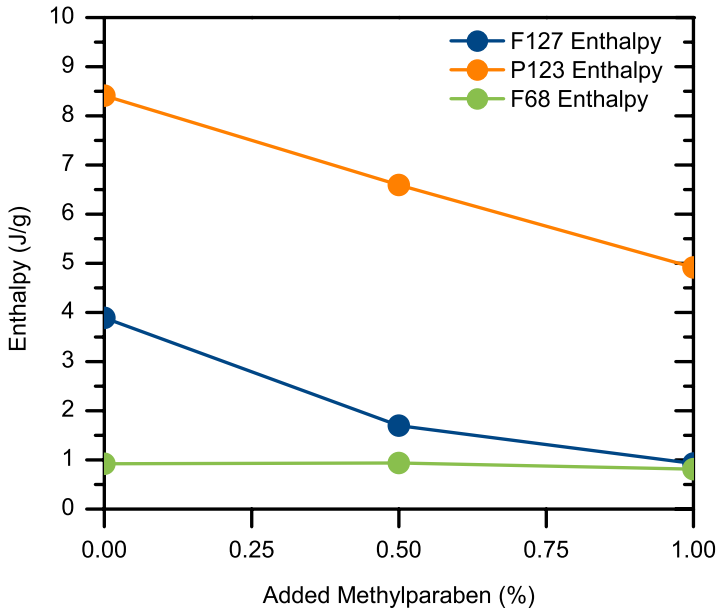

Figure 4.17 Enthalpy of micellization for Pluronic F127, P123, and F68 with increasing amounts of added methylparaben. The F68 solution was already saturated prior to 1% added MP.

4.4 Discussion

4.4.a. Micelle formation vs. gel formation in F127 solutions

Figure 4.3 illustrates the typical thermophysical behavior of F127 solutions over a range of concentrations. Here it is clearly illustrated the presence of two distinct phenomena. As the temperature of an F127 solution is increased from below to above its *cmt*, micelles form as their formation becomes energetically favorable. As mentioned previously, the primary driving force for this change is entropically-driven[7], as the formation of micelles breaks down the structured hydrophobic bonding of water molecules around the PPO block segments ("water cages"), resulting in a large increase in entropy. This process is what gives rise to the large endothermic peak seen in the DSC thermograms. It is important to note, however, that this (relatively) large endothermic

peak is not associated with F127 gelation as was measured in the previous chapters. Micelle formation can be most directly seen in the I(q) SAXS plots in Chapter 3, where an amorphous scatting halo becomes visible at temperatures above the *cmt* but below the critical gel temperature.

As the temperature of each solution continues to rise, a second process occurs in which the micelles arrange into quasicrystalline lattices. For higher concentrations of F127, a secondary process can be detected via DSC (circle in Figure 4.3), as the magnitude of the peak is sufficient to resolve within the sensitivity of the measuring apparatus. This second event is associated with the actual formation of viscous gel, corresponding with Bragg scattering seen in SAXS and a large rise in complex viscosity measured via rheometry. The circled secondary peak for 30% F127 in Figure 4.3 occurs between approximately 20 and 25°C. Comparing that value to Figure 3.3, where Bragg peaks appear between the 20 and 30°C readings for 30% F127 demonstrate that the secondary DSC endotherm correlates with the onset of micelle ordering. Additionally, the critical gel temperature for 30% F127 solutions is reported as 17°C in Table 2.1. Considering that the critical gel temperature is defined as the onset of gel formation, and that the gel transition can take several degrees to complete, the small discrepancy between the rheometry data and the DSC/SAXS data can be accounted for.

4.4.b. Trends in the micellization endotherm across the Pluronic grid

The series of figures between Figure 4.4 and Figure 4.9 show the trends in micelle formation as the Pluronic grid is traversed. Higher PEO/PPO ratios result in smaller endotherms, as do smaller PPO block lengths. It therefore follows that the majority of the energetic contributions to the total enthalpy of micellization comes from the

hydrophobic PPO block if the molecule, and not the hydrophilic PEO arms. These observations are consistent with current theory on micelle formation in amphiphilic copolymers[53,92,93]. Additionally, the longer the PEO arms are, the smaller the total micellization endotherm. This is due to an increasingly positive enthalpy from the formation of the micellar core-shell interface[42].

Pluronic surfactants with high PPO content and low PEO content (L121, L101) exhibited a unique double-hump micellization endotherm. This is due to the phase behavior of Pluronic L121 (Figure 1.4) and the presence of a two-phase liquid crystal region of lamellar aggregates[94,95].

4.4.c. Added methylparaben suppresses the micellization endotherm

Added methylparaben (and added propylparaben) suppressed the micellization endotherm. An initial explanation for this observation would be that micelles do not form in solutions containing MP, however, it has already been clearly demonstrated that micelle formation and ordering still occurs, as the previous rheometer, DLS, and SAXS data (Chapters 2 and 3) show.

Previously, Kelarakis *et al*.[96,97] reported athermal or near athermal micellization in ethylene oxide/1,2-butylene oxide (EO/BO) diblock copolymers. Their conclusion was that a balance of positive and negative contributions to the enthalpy of micellization that very nearly cancel each other out. For EO/BO copolymers, Kelarakis determined that the positive enthalpy of micellization due the hydrophobic effect balanced with the negative enthalpy of micellization from dispersion interactions within the micelle core, resulting in a net near-zero enthalpy of micellization.

In the case of methylparaben, it is likely that a similar effect is happening. As was mentioned before, MP and other hydrophobic additives localize or preferentially associate themselves with the PPO core block in Pluronic surfactants[41]. This would result in specific enthalpic contributions (for example, the hydrophobic effect of dehydrating PPO regions) being modified by the presence of MP, whereas others are left unmodified (such as the formation of the PEO shell).

Relating the lowered enthalpy of micellization to other work, this observation also correlates with the results obtained by Sharma *et al*.[47] who noted a reduction in *cmt*, and the rheometry and SAXS data presented earlier in previous chapters, which demonstrate gel formation at lower temperatures. With the enthalpic cost associated with micelle formation significantly reduced, it would stand to reason that micelles form earlier and more easily than in neat F127 solutions. As such, gelation is allowed to occur more easily and at lower temperatures as well.

Studies of Pluronic surfactant micellization in the presence of small amounts of ionic surfactants have been previously carried out. Jansson *et al*.[89] also observed a suppression in the micellization endotherm of P123 upon the addition of the ionic surfactants sodium dodecylsulfate (SDS) and hexadecyltrimethylammonium chloride (CTAC). In their measurements, however, the peak position was shifted to higher temperatures and not lower temperatures, as is reported here for added MP. The explanation given was that the ionic surfactant forms small complexes with the Pluronic surfactants in solution, thus sequestering them and making them unavailable for incorporation into micelles- thereby reducing the magnitude of the micellization endotherm.

4.4.d. Effect of added methylparaben on different Pluronic surfactants

Comparing the results in Figure 4.13, Figure 4.14, and Figure 4.15 to Figure 4.10 reveal the differences in behavior when MP is added to other Pluronics. Moving laterally across the Pluronic grid, the magnitudes of the endotherms increases as the PEO/PPO ratio decreases, and the absolute suppression from MP is reduced. Moving vertically up and down the grid, the endotherms get smaller as the PPO block length is reduced, and a greater suppression of the endotherm is seen.

Pluronic F68 experienced the least change in the enthalpy of micellization. The addition of MP did not affect the size of the endothermic peak to a significant extent. The shape and position of the peak (with respect to temperature), however, changed more than the other two Pluronic surfactants tested. The peak temperature lowered by almost 20°C and the difference between the onset and the peak temperatures increased from approximately 10°C to 30°C. This suggests a distinct broadening of the transition, which can be visualized in Figure 4.13.

A solution of 10% Pluronic F68 could not fully dissolute 1% added MP, which both F127 and P123 could at equal concentrations. This indicates that the "carrying capacity" of F68 is reduced compared to that of the other two surfactants. F127 could solubilize more MP than F68, although it reaches saturation somewhere between 1 and 2 wt% added MP[47]. Pluronic P123 was also able to completely dissolute 1% added MP, however when MP was added to a solution of 10% L121, a white precipitate immediately began to fall out of solution. When MP is added, it is possible that the MP molecules act as "glue", binding the PPO cores from multiple polymer chains together, as they preferentially associate with each other and the added MP molecules. However, because

this large hydrophobic aggregate is not sufficiently "protected" by a thick PEO corona, the aggregates cannot remain in solution and precipitate.

The amount of relative peak suppression due to added MP in Pluronic F127 was greater than that of F68 or P123. The absolute magnitude of the suppression was similar to that of P123, however, the enthalpy value approached an asymptotic minimum as the concentration of MP was increased to 1%. F127 also experienced significant peak broadening with the addition of MP (Figure 4.12), the difference between the onset and the peak temperature values increasing from 5°C to about 15°C at 1% added MP. For the two Pluronic surfactants with high PEO content, significant broadening of the endothermic peak was observed.

Pluronic P123 experienced the largest absolute suppression in the enthalpy of micellization, but owing to its large endothermic peak in neat solutions, the amount of relative change was comparatively less than F127 (a 40% reduction compared to a 75% reduction for Pluronic F127). A linear response in the suppression is observed, unlike F127 where increasingly higher amounts of MP resulted in less additional suppression. P123 experienced the least sensitivity in peak shifting and broadening as a result of added MP.

These results show that the absolute amount of enthalpic suppression from added MP is most sensitive to the length of the PPO center block, with longer PPO blocks experiencing greater suppression. The amount of temperature shift and peak broadening is most sensitive to the PEO/PPO ratio, with Pluronic surfactants that have the highest amount of PPO by weight experiencing the largest shifts in peak position and peak broadening due to added MP.

4.5 Chapter Summary

In this chapter, the thermophysical driving force of micellization for a variety of Pluronic surfactants was investigated. The notable observation of the suppression of the micellization endotherm that occurs in the presence of added pharmaceuticals such as MP was investigated, and this behavior was probed for other Pluronic surfactants as well, in order to understand the mechanism by which this occurs. Additionally, global trends in the micellization behavior were probed as a function of the two molecular parameters PEO content and PPO center block length.

The data presented suggest that the MP is modifying the energetic contributions to the micelle core formation. The discussion covers a mostly qualitative explanation of the observed behavior. A logical follow up to this initial overview would be to conduct more detailed, quantitative studies of the specific molecular interactions that take place between MP (or other ternary additives) and the micelle core. Techniques such as SANS or NMR would allow more detailed investigations into the intermolecular interactions that are taking place, which would ultimately lead to the development of a model that would describe this behavior. Currently, models do exist which cover the energetics of micelle formation[7], however, they do not account for the contributions of dissolved solutes and their effect on the overall energetic balance.

Chapter 5

Summary and Future Work

5.1 Summary

The aim of this dissertation work was to provide a comprehensive study of the effect that the added pharmaceutical methylparaben had on the thermogelling system of aqueous solutions of Pluronic 127. Investigations into the changes in both the micellization and gelation transitions were completed, as well as a structural characterization of the micelle gels.

The viscoelastic properties of Pluronic F127 gels were studied both as a function of heating rate and added methylparaben. It was found that T_{gel} (the critical gel temperature) increased slightly (~2-3°C) with increasing heating rate. The gel time, Δt, decreased with increased heating rate, but not in direct proportion to the heating rate. This indicates some dependence on kinetic effects.

Adding methylparaben to F127 solutions also resulted in pronounced changes in F127 gelation. T_{gel} dropped significantly, up to 15°C for a 20% F127 solution. These values matched those previously measured by Sharma *et al.*[45]. Gel time was also substantially affected by the addition of MP. An almost four-fold decrease in the gel time was observed at 20% F127, with the acceleration being less pronounced for other concentrations. These results suggest that the presence of MP has an effect on the

formation and organization of Pluronic micelles, which manifest in observable changes in the gel transition.

Structural evaluation of F127 solutions provided insight into the effects of added MP on the formation and ordering of the F127 micelles. Evidence of periodic scattering, present above the critical gel temperature, could be seen using SAXS. The range of temperatures over which periodic scattering could be observed was expanded upon the addition of methylparaben and dexamethasone. This indicates that the range of temperatures where stable gels exist is expanded because of these added pharmaceuticals. If the presence of periodic scattering in the SAXS data suggests the presence of the gel phase, then the lowering of T_{gel} as measured by rheometry is reflected in the SAXS patterns, with corresponding periodic scattering observed at lower temperatures. In the rheometry experiments presented in Chapter 2, a decrease in T_{gel} on the order of 15°C was observed upon adding MP to a 20% solution of F127. This lowering is similarly observed in the SAXS data, where peaks can be seen in the data collected at 10°C lower than the neat F127 solutions (periodic scattering at 40°C in Figure 3.3 versus periodic scattering at 30°C in Figure 3.4).

Additionally, a small change in the lattice spacing was measured, with an approximate 5% decrease in the lattice parameter for added methylparaben. This finding correlated with DLS results that indicated a decrease in the polydispersity of F127 micelles with added MP. A more uniform size distribution of micelles means that the cubic lattice does not need to accommodate as many sizing defects, and thus can arrange itself with a slightly tighter packing configuration as a result.

Time-resolved SAXS studies on the effects of heating rate and added MP result in a change in the evolution of the ordered micelle lattices. For solutions of Pluronic F127, ordered domains of micelles packed in a cubic lattice grow via heterogeneous nucleation and growth, with relatively few domains being nucleated. Upon the addition of MP, however, the nucleation and growth changes to homogeneous nucleation and growth, with a larger number of domains.

The energetics of micelle formation was also probed for various Pluronic surfactants. Trends in the magnitude and position of the micellization endotherm were observed for several surfactants located across the Pluronic grid. Pluronic surfactants with higher PEO content resulted in smaller micellization endotherms, and the position of the endothermic peaks was shifted to higher temperatures. Pluronic surfactants with larger PPO center blocks also resulted in larger micellization endotherms, and the peak positions were shifted to lower temperatures. The largest endotherms were observed for Pluronic surfactants with long PPO centers and short PEO arms (i.e. L121, P123) and the smallest endotherms were observed in surfactants containing short PPO centers and long PEO arms (i.e. F68).

These observed trends demonstrate how changes in the relative lengths of the PPO and PEO blocks in the Pluronic surfactant alter the total magnitude of the micellization endotherm. There are several separate processes that contribute to the total enthalpy of the micellization endotherm in Pluronic surfactants. These contributions can be summarized in Equation 5.1, where *HP* stands for the hydrophobic effect, *IF* for the formation of the core-shell micellar interface, *disp* for dispersion forces within the micelle core, and *conc* for the concentrating effect of PEO chains within the micelle

shell[95,97]. These terms vary in relative magnitude and sign. The hydrophobic effect is the dominant contributor and is negative (endothermic)[97]. The core-shell interface is positive (exothermic) and relatively small compared to the other contributions[97]. The dispersion forces that develop in the micelle core are positive and roughly one third to one fourth that of the hydrophobic effect[95], and the concentration of PEO into the micelle shell is also positive, being essentially the opposite of the heat of dilution for PEO into aqueous solution[95].

$$\Delta H_{total} = \Delta H_{HP} + \Delta H_{IF} + \Delta H_{disp} + \Delta H_{conc}$$

Equation 5.1

As the trends in Chapter 4 show, varying the lengths of the PEO or PPO blocks in the Pluronic surfactant will alter the relative magnitudes of these contributions relative to one another. Increasing the PEO arm length, for example, will increase the magnitude of ΔH_{conc}, and make the total enthalpy more positive (or closer to zero, as the enthalpy is a negative endothermic value). This can be seen in Figure 4.4 and Figure 4.5, where increasing the PEO content but keeping a constant PPO block length reduces the magnitude of the micellization endotherm. Similarly, decreasing the PPO core block while keeping the amount of PPO constant (Figure 4.6, Figure 4.7, and Figure 4.8) produces a similar decrease in the magnitude of the endotherm. The reason for this is because the shorter PPO block produces a smaller ΔH_{HP}, which in turn decreases the overall magnitude of the transition.

The effect of added methylparaben suppressed the magnitude of the micellization endotherm, as well as shifted the location of the endothermic peak to lower temperatures.

For Pluronic surfactants that had a large micellization endotherm (Pluronic P123), the relative amount of suppression per unit of added MP was less, however the total magnitude of the suppression was greater. A linear relationship between added MP and the degree of suppression was observed in these cases. For Pluronic surfactants with relatively small micellization endotherms (such as those for F127, F68), the relative amount of suppression was greater, in some cases lowering the enthalpy of micellization to nearly zero, but the magnitude of the change was less than that of P123, since the size of the micellization endotherms was much less to begin with.

Again considering the individual contributions to the total enthalpy of micellization in Equation 5.1, the effect of added MP can be seen by studying the relative amount of suppression for Pluronic surfactants with different PPO and PEO block lengths. As mentioned earlier, it is very likely that the MP localizes to the micelle core, as previous work by Nagarajan *et al*.[41] examining the behavior of hydrophobic guest molecules in Pluronic micelles shows. Therefore, the added MP acts upon the micelle core, where a suppression of the hydrophobic effect may be taking place, which would then reduce the negative enthalpic contribution of the ΔH_{HP} term. Similarly, enhanced dispersion interactions within the micelle core could increase the positive magnitude of the ΔH_{disp} term, again pushing ΔH_{total} towards zero.

Interpreting the observed experimental results as a whole, a clearer picture of the effect of added methylparaben on the micelle formation and ordering process is revealed. Due to the specific interactions between added MP molecules and the Pluronic surfactant, the energetic barrier for micelle formation is lowered, which in turn causes micelles to form more readily at lower temperatures. This was measured using DSC, and the

resultant consequences seen in the SAXS data (appearance of the amorphous scattering halo at lower temperatures for added MP). With a greater number of micelles formed for a given temperature as compared to solutions devoid of MP, ordering will also occur at lower temperatures. This is again seen in the SAXS data, where periodic scattering peaks are observed at lower temperatures for solutions containing MP. The rheometry data also suggest enhanced ordering at lower temperatures, as T_{gel} was measured to decrease as well. Finally, the high-temperature stability of the micelle lattices was increased by the presence of methylparaben.

5.2 Future work

The data presented in this dissertation presents a more complete picture of the specific interactions of methylparaben and Pluronic F127. In certain situations, other additives produced markedly different behavior in the resulting F127 gels. Added dexamethasone changed the scattering behavior of F127 gels as compared to F127 gels with added methylparaben. This suggests that differences in the molecular interactions between Pluronic surfactants and ternary additives can lead to markedly different resulting behavior. DSC experiments of solutions containing dexamethasone may shed more light on how dissolved dexamethasone affects the energetics of micellization of Pluronic F127. Overall, a more detailed investigation into the specific interactions that take place between ternary additives and Pluronic surfactants is warranted, to come up with a molecular explanation for the observed changes. Nuclear magnetic resonance (NMR) may prove useful in determining the types of intermolecular interactions that are being formed between molecules of Pluronic surfactant and ternary solutes.

Although the scattering studies presented here shed light on the structural changes in the micelle lattice, further avenues for study are still available. Most notably, employing neutron scattering as opposed to x-ray scattering may optimize the scattering contrast between the micelle core and the micelle shell, which would allow one to better determine if changes in the micelle lattice were a result of changing core size, or if the micelle shell was similarly being affected by added MP.

Efforts to apply these characterization techniques to a broader class of additives or amphiphilic polymers are also worthy objectives for further study. By generalizing these results to classes of additives (for example hydrophobic or hydrophilic molecules, low molecular weight or high molecular weight, etc.), refinements can be made to the current models of the micellization and gelation behavior of Pluronic surfactants. These models can be updated to account for the presence of ternary additives, which would allow for more accurate prediction of modifications in the micellization and aggregation behavior of amphiphilic copolymers in complex formulations.

Regarding the kinetics of gel formation, while the results from the rheometry portion of this study revealed that kinetic limitations were present in the system, the subsequent SAXS and DSC studies did not thoroughly examine the kinetics of gel formation in Pluronic solutions. An expanded set of scattering studies targeting the kinetics of the gel transition at different heating rates would produce useful information on the process of gel formation itself, to determine whether micelle assembly is largely regulated by diffusion, or if some other process is the rate-limiting factor.

References

(1) Schmolka, I. Artificial Skin .1. Preparation and Properties of Pluronic F-127 Gels for Treatment of Burns. *J Biomed Mater Res* **1972**, *6*, 571–&.

(2) Mortensen, K.; Batsberg, W.; Hvidt, S. Effects of PEO-PPO diblock impurities on the cubic structure of aqueous PEO-PPO-PEO pluronics micelles: fcc and bcc ordered structures in F127. *Macromolecules* **2008**, *41*, 1720–1727.

(3) Kabanov, A. V.; Lemieux, P.; Vinogradov, S.; Alakhov, V. Pluronic block copolymers: novel functional molecules for gene therapy. *Adv. Drug Deliv. Rev.* **2002**, *54*, 223–233.

(4) Yu, G. E.; Deng, Y. L.; Dalton, S.; Wang, Q. G.; Attwood, D.; Price, C.; Booth, C. Micellisation and Gelation of Triblock Copoly(oxyethylene/oxypropylene/oxyethylene), F127. *J Chem Soc Faraday T* **1992**, *88*, 2537–2544.

(5) Mortensen, K.; Pedersen, J. Structural Study on the Micelle Formation of Poly(ethylene oxide) Poly(propylene oxide) Poly(ethylene oxide) Triblock Copolymer in Aqueous-solution. *Macromolecules* **1993**, *26*, 805–812.

(6) Lau, B.; Wang, Q.; Sun, W.; Li, L. Micellization to gelation of a triblock copolymer in water: Thermoreversibility and scaling. *J Polym Sci Pol Phys* **2004**, *42*, 2014–2025.

(7) Vadnere, M.; Amidon, G.; Lindenbaum, S.; Haslam, J. Thermodynamic Studies on the Gel Sol Transition of Some Pluronic Polyols. *Int J Pharm* **1984**, *22*, 207–218.

(8) Wanka, G.; Hoffmann, H.; Ulbricht, W. Phase Diagrams and Aggregation Behavior of Poly(oxyethylene)-Poly(oxypropylene)-Poly(oxyethylene) Triblock Copolymers in Aqueous Solutions. *Macromolecules* **1994**, *27*, 4145–4159.

(9) Prudhomme, R.; Wu, G.; Schneider, D. Structure and rheology studies of poly(oxyethylene-oxypropylene-oxyethylene) aqueous solution. *Langmuir* **1996**, *12*, 4651–4659.

(10) Chaibundit, C.; Ricardo, N. M. P. S.; Ricardo, N. M. P. S.; de M L L Costa, F.; Wong, M. G. P.; Hermida-Merino, D.; Rodriguez-Perez, J.; Hamley, I. W.; Yeates, S. G.; Booth, C. Effect of ethanol on the micellization and gelation of pluronic p123. *Langmuir* **2008**, *24*, 12260–12266.

(11) Castelletto, V.; Parras, P.; Hamley, I. W.; Bäverbäck, P.; Pedersen, J. S.; Panine, P. Wormlike micelle formation and flow alignment of a pluronic block copolymer in aqueous solution. *Langmuir* **2007**, *23*, 6896–6902.

(12) Alexandridis, P.; Hatton, T. A. Poly(ethylene oxide)-poly(propylene oxide)-poly(ethylene oxide) block copolymer surfactants in aqueous solutions and at interfaces: thermodynamics, structure, dynamics, and modeling. *Colloid Surface A* **1995**, *96*, 1–46.

(13) Wanka, G.; Hoffmann, H.; Ulbricht, W. The aggregation behavior of poly-

(oxyethylene)-poly-(oxypropylene)-poly-(oxyethylene)-block-copolymers in aqueous solution. *Colloid Polym Sci* **1990**, *268*, 101–117.
(14) Lam, Y.; Goldbeck-Wood, G. Mesoscale simulation of block copolymers in aqueous solution: parameterisation, micelle growth kinetics and the effect of temperature and concentration morphology. *Polymer* **2003**, *44*, 3593–3605.
(15) Pozzo, D. C.; Walker, L. M. Small-angle neutron scattering of silica nanoparticles templated in PEO-PPO-PEO cubic crystals. *Colloid Surface A* **2007**, *294*, 117–129.
(16) Mortensen, K. Structural studies of aqueous solutions of PEO - PPO - PEO triblock copolymers, their micellar aggregates and mesophases; a small-angle neutron scattering study. *J Phys-Condens Mat* **1999**, *8*, A103–A124.
(17) Walz, M.; Magerl, A.; Wolff, M.; Zabel, H. Structure and texture of micelles under shear. *Superlattice Microst* **2007**, *41*, 185–189.
(18) Wolff, M.; Magerl, A.; Zabel, H. NS-SANS for the investigation of micellar systems. *Thin Solid Films* **2007**, *515*, 5724–5727.
(19) Jiang, J.; Burger, C.; Li, C.; Li, J.; Lin, M. Y.; Colby, R. H.; Rafailovich, M. H.; Sokolov, J. C. Shear-induced layered structure of polymeric micelles by SANS. *Macromolecules* **2007**, *40*, 4016–4022.
(20) Reddy, N.; Fordham, P.; Attwood, D.; Booth, C. Association and Surface-Properties of Block-Copoly-(Oxyethylene Oxypropylene Oxyethylene) L64. *J Chem Soc Faraday T* **1990**, *86*, 1569–1572.
(21) Zhou, Z.; Chu, B. Light-Scattering Study on the Association Behavior of Triblock Polymers of Ethylene-Oxide and Propylene-Oxide in Aqueous-Solution. *J Colloid Interf Sci* **1988**, *126*, 171–180.
(22) Malmsten, M.; Lindman, B. Self-Assembly in Aqueous Block Copolymer Solutions. *Macromolecules* **1992**, *25*, 5440–5445.
(23) Callister, S.; Keller, A.; Hikmet, R. On Thermoreversible Gels - Their Classification, Relation to Phase-Transitions and Vitrification, Their Morphology and Properties. *Makromol Chem-M Symp* **1990**, *39*, 19–54.
(24) Hamley, I. W.; Pople, J.; Fairclough, J.; Terrill, N.; Ryan, A.; Booth, C.; Yu, G.; Diat, O.; Almdal, K.; Mortensen, K.; Vigild, M. Effect of shear on cubic phases in gels of a diblock copolymer. *J Chem Phys* **1998**, *108*, 6929–6936.
(25) Schmolka, I. R. A review of block polymer surfactants. *J Am Oil Chem Soc* **1977**, *54*, 110–116.
(26) El-Kattan, A. F.; Asbill, C. S.; Kim, N.; Michniak, B. B. Effect of formulation variables on the percutaneous permeation of ketoprofen from gel formulations. *Drug Delivery* **2000**, *7*, 147–153.
(27) Fang, J.-Y.; Leu, Y.-L.; Wang, Y.-Y.; Tsai, Y.-H. In vitro topical application and in vivo pharmacodynamic evaluation of nonivamide hydrogels using Wistar rat as an animal model. *Eur J Pharm Sci* **2002**, *15*, 417–423.
(28) Liaw, J.; Lin, Y. Evaluation of poly(ethylene oxide)-poly(propylene oxide)-poly(ethylene oxide) (PEO-PPO-PEO) gels as a release vehicle for percutaneous fentanyl. *J Control Release* **2000**, *68*, 273–282.
(29) Morishita, M.; Barichello, J. M.; Takayama, K.; Chiba, Y.; Tokiwa, S.; Nagai, T. Pluronic F-127 gels incorporating highly purified unsaturated fatty acids for buccal delivery of insulin. *Int J Pharm* **2001**, *212*, 289–293.

(30) Shin, S. C.; Kim, J. Y. Enhanced permeation of triamcinolone acetonide through the buccal mucosa. *Eur J Pharm Biopharm* **2000**, *50*, 217–220.
(31) Kim, E. Y.; Gao, Z. G.; Park, J. S.; Li, H.; Han, K. rhEGF/HP-beta-CD complex in poloxamer gel for ophthalmic delivery. *Int J Pharm* **2002**, *233*, 159–167.
(32) Fawaz, F.; Koffi, A.; Guyot, M.; Millet, P. Comparative in vitro-in vivo study of two quinine rectal gel formulations. *Int J Pharm* **2004**, *280*, 151–162.
(33) Miyazaki, S.; Ohkawa, Y.; Takada, M. *Antitumor effect of PF-127 gel containing mytomicin C on sarcoma-180 ascites tumor in mice*; Chem Pharm. Bull, 1986.
(34) Erukova, V. Y.; Krylova, O. O.; Antonenko, Y. N.; Melik-Nubarov, N. S. Effect of ethylene oxide and propylene oxide block copolymers on the permeability of bilayer lipid membranes to small solutes including doxorubicin. *Biochim. Biophys. Acta* **2000**, *1468*, 73–86.
(35) Kabanov, A. V.; Zhu, J.; Alakhov, V. Y. Pluronic block copolymers for gene delivery. *Adv Genet* **2005**, *53*, 231–261.
(36) Nalbandian, R. M.; Henry, R. L.; Wilks, H. S. Artificial Skin II. Pluronic F-127 Silver-Nitrate or Silver Lactate Gel In Treatment of Thermal Burns. *J Biomed Mater Res* **1972**, *6*, 583–590.
(37) Nalbandian, R. M.; Henry, R. L.; Balko, K. W.; Adams, D. V.; Neuman, N. R. Pluronic F-127 Gel Preparation as an Artifical Skin in the Treathemtn of 3rd-Degree Burns in Pigs. *J Biomed Mater Res* **1987**, *21*, 1135–1148.
(38) Ohta, S.; Nitta, N.; Takahashi, M.; Sonoda, A.; Tanaka, T.; Yamasaki, M.; Furukawa, A.; Takazakura, R.; Murata, K.; Sakamoto, T.; Kushibiki, T.; Tabata, Y. Pluronic F127: Application in arterial embolization. *J Vasc Interv Radiol* **2006**, *17*, 533–539.
(39) Kabanov, A. V.; Batrakova, E. V.; Alakhov, V. Y. Pluronic block copolymers for overcoming drug resistance in cancer. *Adv. Drug Deliv. Rev.* **2002**, *54*, 759–779.
(40) Escobar-Chavez, J. J.; Lopez-Cervantes, M.; Naik, A.; Kalia, Y. N.; Quintanar-Guerrero, D.; Ganem-Quintanar, A. Applications of thermoreversible pluronic F-127 gels in pharmaceutical formulations. *J Pharm Pharm Sci* **2006**, *9*, 339–358.
(41) Nagarajan, R. Solubilization of "guest" molecules into polymeric aggregates. *Polym Advan Technol* **2001**, *12*, 23–43.
(42) Nagarajan, R. Solubilization of hydrocarbons and resulting aggregate shape transitions in aqueous solutions of Pluronic (R) (PEO-PPO-PEO) block copolymers. *Colloid Surface B* **1999**, *16*, 55–72.
(43) Bentley, M. V.; Marchetti, J. M.; Ricardo, N.; Ali-Abi, Z.; Collett, J. H. Influence of lecithin on some physical chemical properties of poloxamer gels: rheological, microscopic and in vitro permeation studies. *Int J Pharm* **1999**, *193*, 49–55.
(44) Ricci, E.; Bentley, M.; Farah, M.; Bretas, R.; Marchetti, J. Rheological characterization of Poloxamer 407 lidocaine hydrochloride gels. *Eur J Pharm Sci* **2002**, *17*, 161–167.
(45) Sharma, P. K.; Reilly, M. J.; Bhatia, S. K.; Sakhitab, N.; Archambault, J. D.; Bhatia, S. R. Effect of pharmaceuticals on thermoreversible gelation of PEO-PPO-PEO copolymers. *Colloid Surface B* **2008**, *63*, 229–235.
(46) Sharma, P. K.; Bhatia, S. R. Effect of anti-inflammatories on Pluronic (R) F127: micellar assembly, gelation and partitioning. *Int J Pharm* **2004**, *278*, 361–377.

(47) Sharma, P. K.; Reilly, M. J.; Jones, D. N.; Robinson, P. M.; Bhatia, S. R. The effect of pharmaceuticals on the nanoscale structure of PEO-PPO-PEO micelles. *Colloid Surface B* **2008**, *61*, 53–60.
(48) Aalto, T. R.; Firman, M. C.; Rigler, N. E. p-hydroxybenzoic acid esters as preservatives. I. Uses, antibacterial and antifungal studies, properties and determination. *J Pharm Sci* **2006**, *42*, 449–457.
(49) Barba, A. A.; d'Amore, M.; Grassi, M.; Chirico, S.; Lamberti, G.; Titomanlio, G. Investigation of Pluronic (c) F127-Water Solutions Phase Transitions by DSC and Dielectric Spectroscopy. *J Appl Polym Sci* **2009**, *114*, 688–695.
(50) Gentile, L.; De Luca, G.; Antunes, F. E.; Rossi, C. O.; Ranieri, G. A. Thermogelation analysis of F127-water mixtures by physical chemistry techniques. *Appl Rheol* **2010**, *20*, U10–U18.
(51) Trong, L. C. P.; Djabourov, M.; Ponton, A. Mechanisms of micellization and rheology of PEO-PPO-PEO triblock copolymers with various architectures. *J Colloid Interf Sci* **2008**, *328*, 278–287.
(52) Artzner, F.; Geiger, S.; Olivier, A.; Allais, C.; Finet, S.; Agnely, F. Interactions between poloxamers in aqueous solutions: Micellization and gelation studied by differential scanning calorimetry, small angle X-ray scattering, and rheology. *Langmuir* **2007**, *23*, 5085–5092.
(53) Chaibundit, C.; Ricardo, N. M. P. S.; Ricardo, N. M. P. S.; O'Driscoll, B. M. D.; Hamley, I. W.; Yeates, S. G.; Booth, C. Aqueous gels of mixtures of ionic surfactant SDS with pluronic copolymers P123 or F127. *Langmuir* **2009**, *25*, 13776–13783.
(54) Wu, Y.; Sprik, R.; Poon, W.; Eiser, E. Effect of salt on the phase behaviour of F68 triblock PEO/PPO/PEO copolymer. *J Phys-Condens Mat* **2006**, *18*, 4461–4470.
(55) Meznarich, N. A. K.; Love, B. J. The Kinetics of Gel Formation for PEO-PPO-PEO Triblock Copolymer Solutions and the Effects of Added Methylparaben. *Macromolecules* **2011**, *44*, 3548–3555.
(56) Norman, A.; Fairclough, J.; Mai, S.; Ryan, A. Poly(oxyalkylene) block copolymers in aqueous solution - Phase behavior and transition kinetics. *J Macromol Sci Phys* **2004**, *B43*, 71–93.
(57) Scherlund, M.; Brodin, A.; Malmsten, M. Micellization and gelation in block copolymer systems containing local anesthetics. *Int J Pharm* **2000**, *211*, 37–49.
(58) Jeon, S.; Granick, S.; Kwon, K.; Char, K. Microviscosity in poly(ethylene oxide)-polypropylene oxide-poly(ethylene oxide) block copolymers probed by fluorescenece depolarization kinetics. *J Polym Sci Pol Phys* **2002**, *40*, 2883–2888.
(59) Yalkowsky, S. H.; Valvani, S. C.; Roseman, T. J. Solubility and partitioning VI: octanol solubility and octanol-water partition coefficients. *J Pharm Sci* **1983**, *72*, 866–870.
(60) Hamley, I. W. The effect of shear on ordered block copolymer solutions. *Curr Opin Colloid In* **2000**, *5*, 342–350.
(61) Jiang, J.; Li, C.; Lombardi, J.; Colby, R. H.; Rigas, B.; Rafailovich, M. H.; Sokolov, J. C. The effect of physiologically relevant additives on the rheological properties of concentrated Pluronic copolymer gels. *Polymer* **2008**, *49*, 3561–

3567.
(62) Nolan, S.; Phillips, R.; Cotts, P.; Dungan, S. Light scattering study on the effect of polymer composition on the structural properties of PEO-PPO-PEO micelles. *J Colloid Interf Sci* **1997**, *191*, 291–302.
(63) Park, M.; Bang, J.; Harada, T.; Char, K.; Lodge, T. Epitaxial transitions among FCC, HCP, BCC, and cylinder phases in a block copolymer solution. *Macromolecules* **2004**, *37*, 9064–9075.
(64) Taboada, P.; Velasquez, G.; Barbosa, S.; Castelletto, V.; Nixon, S.; Yang, Z.; Heatley, F.; Hamley, I. W.; Ashford, M.; Mosquera, V.; Attwood, D.; Booth, C. Block copolymers of ethylene oxide and phenyl glycidyl ether: Micellization, gelation, and drug solubilization. *Langmuir* **2005**, *21*, 5263–5271.
(65) Hammouda, B. A tutorial on small-angle neutron scattering from polymers. *NIST* **1995**.
(66) Meznarich, N. A. K.; Juggernauth, K. A.; Batzli, K. M.; Love, B. J. Structural Changes in PEO-PPO-PEO Gels Induced by Methylparaben and Dexamethasone Observed Using Time-Resolved SAXS. *Macromolecules* **2011**, *44*, 7792–7798.
(67) Alexandridis, P.; Olsson, U.; Lindman, B. A record nine different phases (four cubic, two hexagonal, and one lamellar lyotropic liquid crystalline and two micellar solutions) in a ternary isothermal system of an amphiphilic block copolymer and selective solvents (water and oil). *Langmuir* **1998**, *14*, 2627–2638.
(68) Newby, G. E.; Hamley, I. W.; King, S. M.; Martin, C. M.; Terrill, N. J. Structure, rheology and shear alignment of Pluronic block copolymer mixtures. *J Colloid Interf Sci* **2009**, *329*, 54–61.
(69) Zhou, S.; Su, J.; Chu, B. Water-induced micellar structure change in pluronic P103/water/o-xylene ternary system. *J Polym Sci Pol Phys* **1998**, *36*, 889–900.
(70) Provencher, S. CONTIN - A General-Purpose Constrained Regularization Program for Inverting Noisy Linear Algebraic and Integral-Equations. *Comput Phys Commun* **1982**, *27*, 229–242.
(71) Loose, W.; Ackerson, B. J. Model-Calculations for the Analysis of Scattering Data From Layered Structures. *J Chem Phys* **1994**, *101*, 7211–7220.
(72) Castelletto, V.; Hamley, I. W.; Holmqvist, P.; Rekatas, C.; Booth, C.; Grossmann, J. Small-angle X-ray scattering study of a poly(oxyphenylethylene)-poly(oxyethylene) diblock copolymer gel under shear flow. *Colloid Polym Sci* **2001**, *279*, 621–628.
(73) McConnell, G. A.; Lin, M. Y.; Gast, A. P. Long-Range Order in Polymeric Micelles Under Steady Shear. *Macromolecules* **1995**, *28*, 6754–6764.
(74) Chaibundit, C.; Ricardo, N. M. P. S.; Costa, V. de M. L. L.; Yeates, S. G.; Booth, C. Micellization and gelation of mixed copolymers P123 and F127 in aqueous solution. *Langmuir* **2007**, *23*, 9229–9236.
(75) Wu, C.; Liu, T.; Chu, B.; Schneider, D.; Graziano, V. Characterization of the PEO-PPO-PEO triblock copolymer and its application as a separation medium in capillary electrophoresis. *Macromolecules* **1997**, *30*, 4574–4583.
(76) Yang, M.; Ma, H. Effect of polydispersity on the relative stability of hard-sphere crystals. *J Chem Phys* **2008**, *128*, 134510.
(77) Olsen, B. D.; Li, X.; Wang, J.; Segalman, R. A. Near-surface and internal

lamellar structure and orientation in thin films of rod–coil block copolymers. *Soft Matter* **2009**.

(78) Ruthstein, S.; Raitsimring, A. M.; Bitton, R.; Frydman, V.; Godt, A.; Goldfarb, D. Distribution of guest molecules in Pluronic micelles studied by double electron electron spin resonance and small angle X-ray scattering. *Phys Chem Chem Phys* **2009**, *11*, 148–160.

(79) Steinbeck, C.; Hedin, N.; Chmelka, B. Interactions of charged porphyrins with nonionic triblock copolymer hosts in aqueous solutions. *Langmuir* **2004**, *20*, 10399–10412.

(80) Jia, L.; Guo, C.; Yang, L.; Xiang, J.; Tang, Y.; Liu, H. Interaction between Reduced Glutathione and PEO−PPO−PEO Copolymers in Aqueous Solutions: Studied by 1H NMR and Spin−Lattice Relaxation. *J Phys Chem B* **2011**, *115*, 2228–2233.

(81) Caron, J.; Shroot, B. Determination of Partition-Coefficients of Glucocorticosteroids by High-Performance Liquid-Chromatography. *J Pharm Sci* **1984**, *73*, 1703–1706.

(82) Lodge, T.; Bang, J.; Park, M.; Char, K. Origin of the thermoreversible fcc-bcc transition in block copolymer solutions. *Phys Rev Lett* **2004**, *92*, –.

(83) Hamley, I. W.; Daniel, C.; Mingvanish, W.; Mai, S.; Booth, C.; Messe, L.; Ryan, A. From hard spheres to soft spheres: The effect of copolymer composition on the structure of micellar cubic phases formed by diblock copolymers in aqueous solution. *Langmuir* **2000**, *16*, 2508–2514.

(84) Semenov, A. Microphase Separation in Diblock Copolymer Melts - Ordering of Micelles. *Macromolecules* **1989**, *22*, 2849–2851.

(85) Yang, Y.; Wang, J.; Zhang, X.; Lu, W.; Zhang, Q. A novel mixed micelle gel with thermo-sensitive property for the local delivery of docetaxel. *J Control Release* **2009**, *135*, 175–182.

(86) Flodstrom, K.; Alfredsson, V. Influence of the block length of triblock copolymers on the formation of mesoporous silica. *Micropor Mesopor Mat* **2003**, *59*, 167–176.

(87) Bomqvistt, B.; Warnheim, T.; Claesson, P. Surface rheology of PEO-PPO-PEO triblock copolymers at the air-water interface: Comparison of spread and adsorbed layers. *Langmuir* **2005**, *21*, 6373–6384.

(88) Al-Saden, A. A.; Florence, A. T.; Morrison, H.; Whateley, T. L. Association of poloxamer block copolymers in aqueous solution [proceedings]. *J. Pharm. Pharmacol.* **1979**, *31 Suppl*, 81P.

(89) Jansson, J.; Schillen, K.; Olofsson, G.; da Silva, R.; Loh, W. The interaction between PEO-PPO-PEO triblock copolymers and ionic surfactants in aqueous solution studied using light scattering and calorimetry. *J Phys Chem B* **2004**, *108*, 82–92.

(90) Bromberg, L.; Alakhov, V. Effects of polyether-modified poly(acrylic acid) microgels on doxorubicin transport in human intestinal epithelial Caco-2 cell layers. *J Control Release* **2003**, *88*, 11–22.

(91) Cardoso, M. B.; Smolensky, D.; Heller, W. T.; Hong, K.; O'Neill, H. Supramolecular assembly of biohybrid photoconversion systems. *Energy Environ. Sci.* **2010**, *4*, 181.

(92) Grant, C. D.; DeRitter, M. R.; Steege, K. E.; Fadeeva, T. A.; Castner, E. W. Fluorescence probing of interior, interfacial, and exterior regions in solution aggregates of poly(ethylene oxide)- poly(propylene oxide)-poly(ethylene oxide) triblock copolymers. *Langmuir* **2005**, *21*, 1745–1752.
(93) Alexandridis, P.; Holzwarth, J.; Hatton, T. A. Micellization of Poly(Ethylene Oxide)-Poly(Propylene Oxide)-Poly(Ethylene Oxide) Triblock Copolymers in Aqueous-Solutions - Thermodynamics of Copolymer Association. *Macromolecules* **1994**, *27*, 2414–2425.
(94) Cardoso da Silva, R.; Olofsson, G.; Schillen, K.; Loh, W. Influence of Ionic Surfactants on the Aggregation of Poly(Ethylene Oxide)−Poly(Propylene Oxide)−Poly(Ethylene Oxide) Block Copolymers Studied by Differential Scanning and Isothermal Titration Calorimetry. *J Phys Chem B* **2002**, *106*, 1239–1246.
(95) Rodriguez-Abreu, C.; Sanchez-Dominguez, M.; Sarac, B.; Rogac, M. B.; Shrestha, R. G.; Shrestha, L. K.; Varade, D.; Ghosh, G.; Aswal, V. K. Solution behavior of aqueous mixtures of low and high molecular weight hydrophobic amphiphiles. *Colloid Polym Sci* **2010**, *288*, 739–751.
(96) Kelarakis, A.; Havredaki, V.; Yu, G. E.; Derici, L.; Booth, C. Temperature dependences of the critical micelle concentrations of diblock oxyethylene/oxybutylene copolymers. A case of athermal micellization. *Macromolecules* **1998**, *31*, 944–946.
(97) Kelarakis, A.; Havredaki, V.; Rekatas, C.; Booth, C. Thermodynamics of micellisation of a diblock copolymer of ethylene oxide and styrene oxide in water. *Phys Chem Chem Phys* **2001**, *3*, 5550–5552.